Mass Transport in Fractured Media

Transition to anomalous transport

Dissertation
zur Erlangung des Grades eines Doktors der Naturwissenschaften

der Geowissenschaftlichen Fakultät
der Eberhard-Karls-Universität Tübingen

vorgelegt von
Ralph Mettier
aus Langwies

2007

Tag der mündlichen Prüfung: 25.06.2007

Dekan: Prof. Dr. Peter Grathwohl

1. Berichterstatter :	Prof. Dr. Olaf Kolditz
2. Berichterstatter :	PD Dr. Christopher Ian McDermott

Abstract

Substantial understanding of the processes involved in fluid flow and tracer transport in geological systems can be gained from the use of numerical simulations. Regardless of the nature or scale of a geological system, the probability of encountering fractures in hard rock units is high. Therefore, modelling flow and transport in fractures and fracture networks is a key component of almost any complex hydrogeological simulation. Over the last few decades, with the increase in computational power and the availability of increasingly sophisticated and powerful specialized modelling software, numerical models have become increasingly commonplace, and are meanwhile regarded as vital tools in the wide field of geoscience.

This work portrays the development of a series of numerical models, with discrete fracture network geometry, based on the knowledge of an actual fracture network gained through prior experiments performed at the Grimsel Test Site (GTS) in the Swiss Alps. A three dimensional reconstruction of the actual fracture network geometry is developed from the extensive photographic data set provided by the Excavation Project (EP) and used as the basis for purely advective particle tracking models, as well as for fully advective-dispersive transport models. Realistic fracture apertures based on actual fracture measurements are generated through a geostatistical method and their influence upon flow and transport is studied. Various degrees of heterogeneity with regard to aperture distributions are generated and used in a Monte Carlo approach to examine their influence. Further, the retardation effects of matrix diffusion are also considered and incorporated into the models by means of a new semi-analytical method included in the FEM code Rockflow/Geosys V4. The resulting breakthrough curves are analysed and fitted with several analytical solutions, including advective dispersive transport with matrix diffusion and continuous time random walks (CTRW). It is shown that the standard advection dispersion equation (ADE) is not suitable for approximating or predicting breakthrough curves from heterogeneous models.

The development of the various models portrayed herein depended strongly on the ongoing advances made in the available modelling codes and in new and dedicated preprocessing tools. Several newly developed methods and tools were tested and applied during the project.

For the first time, a group of numerical simulations is presented, that incorporates complex fracture network geometry based on actual field data, geostatistically generated realistic apertures and the effect of matrix diffusion. This new level of realism provides the basis for new insights into the role of heterogeneity, matrix diffusion and the combination of both in the transition toward anomalous transport.

Zusammenfassung

Das Wissen über die an Fluss- und Transportprozessen beteiligten Mechanismen kann durch die Verwendung von numerischen Simulationen deutlich erweitert werden. Unabhängig der Natur oder der Grössenordnung des untersuchten Systems ist das Auftreten von Klüften und Spalten in Felsstrukturen sehr wahrscheinlich. Daher stellt das Modellieren von Fluss- und Transport in geklüfteten Medien eine wesentliche Komponente der meisten komplexen hydrogeologischen Simulationen dar. Mit der andauernden Entwicklung von immer Leistungsfähigeren Computern und dem Aufkommen von spezialisierter und leistungsfähiger Software zur numerischen Modellierung haben sich numerische Simulationen in den letzten Jahren und Jahrzehnten etabliert, und sind nun als wichtiges Werkzeug im weiten Feld der Geowissenschaften anerkannt.

Diese Arbeit stellt die Entwicklung und Anwendung einer Reihe solcher numerischer Modelle dar. Die Modelle basieren auf dem bestehenden Wissen über ein natürliches Kluftsystem in den Schweizer Alpen, welches durch frühere Experimente am Felslabor Grimsel untersucht wurde. Eine dreidimensionale Rekonstruktion der Kluftgeometrie wird entwickelt und als Basis für sowohl rein advective 'Particle Tracking' Modelle, als auch für advektiv-dispersive Transportmodelle verwendet. Realistische Kluftöffnungsweiten, basierend auf gemessenen Weiten von untersuchten Klüften, werden mittels einer Geostatistischen Methode für die Modelle generiert. Der Einfluss dieser Heterogenität auf Fluss und Transport wird untersucht. Vergleichbare Öffnungsweitenverteilungen mit unterschiedlich starker Heterogenität werden generiert und deren Einfluss im Rahmen eines Monte Carlo Ansatzes Untersucht. Ebenso wird der retardierende Einfluss von Matrix Diffusion in den Modellen berücksichtigt und untersucht. Die resultierenden Durchbruchskurven werden mittels einer Auswahl an analytischen Methoden, unter anderem mit Matrix Diffusion und 'Continuous Time Random Walks' (CTRW), angepasst und interpretiert. Es wird dabei gezeigt, dass die herkömliche Advektions-Dispersions Gleichung (ADE) nicht geeignet ist um Durchbrüche von heterogenen Modellen anzunähern oder vorauszusagen.

Die Entwicklung der vorgestellten Modelle wird ermöglicht durch die fortwährende Entwicklung im Bereich von numerischen Modellierungscodes, sowie durch neue und verbesserte Werkzeugen zur Erstellung und Verwaltung der Modellgeometrie. Etliche neue Methoden und Werkzeuge wurden im Rahmen der Arbeit getestet und verwendet.

Erstmals wird eine Gruppe von numerischen Simulationen vorgestellt, welche complexe, auf Felddaten beruhende Kluftnetzwerkgeometrien beinhalten, sowie geostatistisch generierte Öffnungsweiten und Matrix Diffusion. Dieser neue Grad an Realitätsnähe bildet die Basis für neue Erkenntnisse bezüglich der Rolle von Heterogenitäten, Matrix Diffusion und deren Kombination im Übergangsbereich zum anormalen Transport.

Table of Contents

1. Introduction

The conceptual ideal of a large homogeneous rock body is rarely found in the field. Across almost all scales, from sub-mm to km lengths, rock volumes contain disturbances and heterogeneities. In crystalline rock, these heterogeneities are, among others, often present in the form of fractures, or fracture networks. It seems obvious that such features will change the hydraulic properties of a rock volume, but to which degree they can impact the flow and transport behaviour in such a system is less clear. Various approaches to numerically modelling the behaviour of hydrogeological systems in fractured crystalline rocks are in common use, the simplest of which is the representation of the entire fractured rock volume as a single block of equivalent porous media (EPM). These models are however rarely sufficient to describe the system acurately. Several other approaches to modelling such systems exist, and are continuously being developed and advanced. Among these methods, are i.e. dual- and multiporosity models, pipe models, and various continuum and hybrid model approaches(National Research Council, 1996). Analytical approaches to understanding and describing flow and transport in fractures and fracture networks also exist, but are limited to single fractures with homogeneous aperture, fracture networks which can be approximated by isotopic porous media, or fractures and fracture networks with statistically describable heterogeneities, both in aperture and geometry.

An alternative, and often superior, approach is the use of a numerical model incorporating a discrete fracture network. Such models are often generated based on statistics of fracture location, shape, size and clustering, obtained from surrounding geological outcrops, borehole logs, or estimated from geological knowledge of similar systems. This type of approach to generating seemingly realistic fracture networks is made necessary by the fact that detailed information about actual fracture locations and extent is rarely available.

A unique 'treasure trove' of information about a natural fracture network is provided in the Nagra/JNC EP (Excavation Project, Alexander et al., 2003) data set, in which actual information about the size, number and position of the fractures in a complex natural fracture network is contained. This extraordinary dataset forms the basis for the models used in this study.

1.1. Excavation Project data set and background

1.1.1. Geological background of the Grimsel Test Site and the studied shear zone

The host rock surrounding the Grimsel Test Site (GTS) consists of granodioritic rock, which stems from a granitoid intrusion into the surrounding Devonian and older sediments roughly 300Ma ago. It was followed by further intrusions of lamprophyric and apilitic material. Roughly 20Ma ago, the geologic volume was subject to metamorphosis of the greenschist facies, resulting in the granodiorite seen today. Also during the involved ductile deformation, several NE-SW running shear zones were caused, which can be seen as mylonitic structures penetrating the granodiorite. During the following cooling and uplift period, these shear zones were reactivated, and deformed in a ductile manner, creating the general appearance of the shear zone fracture networks, one of which is studied within this project. The overall geology of the region is well studied, and has been described in detail in the relevant literature(i.e. Bossart & Mazurek, 1991). Figure 1 shows a conceptual profile through the Grimsel area and surrounding region.

Today, the major structural elements, such as the main fractures, can be seen to strike at roughly 240°, and dip sub vertically at 80°. Three roughly parallel major shear structures can be identified over a distance of roughly 100m, which together make up the main Grimsel shear zone. This study deals with a 2.6 m subsection of one of these shear structures. As with the large scale shear zone, each of the individual shear structures can be considered as a one dimensional structure on a scale of several meters upward. On the smaller, single meter to sub-meter scale, the shear structure can be seen to consist of a complex network of individual fractures. Studying the detailed geometric nature of such a network was the goal of the Excavation Project .

1.1.2. History of the Excavation Project and data set

The Excavation Project (Alexander et al., 2003), henceforth EP, was performed as a follow-up project after the Migration (MI) project (Frick et al., 1992, Hadermann & Heer, 1996 and Smith et al., 2001). During MI a

number of tracer tests, using various tracers, such as the non-sorbing Uranine Dye, ^{82}Br, ^{123}I, ^{3}He and ^{3}H, as well as weakly sorbing ^{22}Na, ^{24}Na, ^{85}Sr and ^{86}Rb and the strongly sorbing ^{137}Cs were performed along a number of dipoles in the fracture network of a pronounced shear zone at the Grimsel Test Site.
After termination of MI, one of the dipoles, was injected with fluorescent resin, which at injection temperature has hydraulic properties very similar to those of water. Once the rock volume containing the assumed fracture network was saturated with resin, the entire volume was heated, causing the resin to solidify, thus stabilizing the rock volume. Large diameter (~30cm) cores were then taken roughly parallel to the shear zone, thereby extracting the major part of the rock volume containing the flow field that had been studied with the MI dipole pumping tests.
The extracted cores were cut into slices of thickness between two and four cm, and both faces of each slice were photographed in visible and ultraviolet (UV) lighting. The UV light causes the fluorescent resin to show up in the photographs, exposing the impregnated fractures which are often hard to identify in the visible light images. The combined set of all 304 images are provided on a CD-ROM by Nagra/JNC and shall henceforth be referred to in this project as the EP data set.
Related to EP, further transport experiments with various tracers have been performed in other parts of the same shear zone within the framework of the Radionuclide Retardation Programme (RRP) Project (Hadermann & Heer, 1996; Smith et al., 2001, Alexander et al. 2003, Biggin et al., 2003) and Colloid Retention and Retardation (CRR) Project (Möri, 2003, Geckeis et al. 2004).

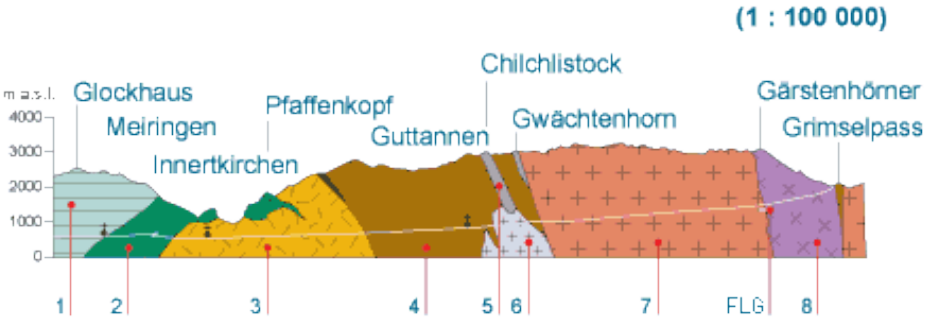

Figure 1: *Conceptual profile (roughly N/S) through the Grimsel area.*

1 - Sediments of the Wildhorn nappe (Jurassic, Cretaceous)
2 - Autochthonous and parautochthonous sediments (Triassic to Lower Tertiary)
3 - Innertkirchen Crystalline
4 - „Altkristallin" (predominantly light gneisses and dark biotite schists, partly amphibolites and lime silicate rocks)
5 - Vulcanoclastites (pyroclastites and metasediments)
6 - Mittagfluh Granite
7 - Central and Southern Aare Granite
8 - Grimsel Granodiorite. Image courtesy of Nagra, Wettingen, Switzerland (www.nagra.ch)

1.2. Scientific goals and methods

The aim of this project is to build on the knowledge obtained from EP and related projects, and investigate the influence of heterogeneities on the overall flow and transport behaviour in a complex network of fractures in a volume of crystalline rock, both with and without considering the influence of matrix diffusion. This objective is approached primarily in four steps:

* Reconstructing the geometry of the fracture network (Chapter 2)

The first step of the project is to reconstruct a convincing digital 3D model of the geometry of the fracture network segment contained in the cores excavated during the EP project. A certain degree of simplification is inevitable, but capturing the characteristic properties of the structure is key. The extracted fracture network model shall consist of two dimensional planar irregular polygonal fractures in 3D space. Additionally, the

extent of individual fractures in their third dimension, namely the fracture thickness, or aperture shall be determined.

* Conservative transport, modelled using a particle tracker (Chapter 3)

Once a convincing representation of the actual fracture network geometry is obtained, a FEM method can be used to calculated the hydraulic flow field in the system. The influence of the network geometry is studied by comparing to models representing a single fracture. A particle tracker will serve to model conservative, purely advective transport in the obtained hydraulic system.

* Fully advective dispersive transport, with matrix diffusion (Chapter 4)

A more advanced system of FEM tools, including powerful dedicated preprocessing software is used to construct a number of models portraying advective dispersive transport in single fracture models with realistic aperture distributions derived from the apertures used in the earlier steps. In addition, the influence of matrix diffusion (MD) is studied by running the same models with and without the use of a new and powerful semi-analytical hybrid method for including MD.

* Analysis and interpretation of the obtained breakthrough curves (Chapter 5)

Each set of numerical models described in the above sets will produce characteristic breakthrough curves. Comparing these curves to known analytical solutions, such as the standard advection-dispersion equation (ADE), advective-dispersive transport with matrix diffusion (ADE + MD) and continuous time random walks (CTRW), attempting to fit them, and if successful, comparing the obtained values for flow velocity, dispersivity and other crucial values to the actual values used in the numerical models, promises to give important insight into the shortcomings of representing hydrogeological systems with oversimplified analytical models.

1.3. Differences to previous work

Fracture networks have been studied and modelled extensively throughout the literature. A number of different approaches are discernible, all with their own unique advantages and limitations. In this work a discrete fracture network approach, based on actual geometric data, is used. In addition, integration of a new semi-analytical hybrid approach allows a system complexity to be considered, which is beyond previous comparable work. The combination and interaction of reality-based fracture network geometry, realistic variable fracture apertures, and matrix diffusion provide an opportunity for gaining advanced insight into complex near-realistic hydrogeological systems. This section shall offer an overview of the existing standard techniques used to model flow and/or transport in fractured media, together with a few examples from the relevant literature.

1.3.1. Equivalent porous media

From a hydraulic point of view, and strongly simplified, a rock volume containing a network of fractures can be described by observing the in- and outflow characteristics at given points on defined boundary surfaces. What happens in the volume in between can be considered basically a black box. The whole system can thus be represented by a block of homogeneous porous media with the same hydraulic behaviour Obvious advantages to this method are the simplicity of the approach, and consequently, low or negligible need for computational power or processing time. This approach is strongly coupled to the concept of the 'representative elementary volume' REV (Bachmat & Bear, 1986). The REV can be defined as the smallest volume at which a system can be considered to be homogeneous. Below the level of the REV, individual pores and corn boundaries introduce heterogeneities that cannot be ignored. Typically, for sandstones, REVs are on the scale several hundred to several thousand grain diameters. If the studied example volume happens to qualify as a REV for the whole system, then this approach offers a degree of scalability. However, there is no straightforward way of determining this, short of comparing predictions to actual field measurements. Pure EPM models are rarely used today, as the field has progressed to more complex and detail approaches. A typical example of this method can be found in (Long et al., 1982).

1.3.2. Dual-/Multiporosity

By extending the EPM approach to a model consisting of two or more systems of blocks of porous material, overlaying each other in space, and coupled by a temporally and spatially dependent exchange function, heterogeneities such as fractures can be accommodated into the model. Typically, for a dual porosity model, the porous rock matrix will be represented by one system, while the fracture network will be represented by another. Interaction between liquid and solid phases can be incorporated into the exchange function. The dual porosity method is well documented in the literature, i.e. Douglas & Arbogast (1990) or Pfingsten & Soler (2003).

1.3.3. Pipes /Tubes

Representing the individual fractures, groups of fractures or strongly fractured regions of the system with cylindrical pipes has a number of advantages. Heterogeneity is easily represented by variable numbers of pipes per cross section area. Flow directions are not fixed to the shortest distance between in- and outflow boundaries, and variable conductivities can be approximated by changing the pipe diameters. In addition, flow through a cylindrical pipe allows the use of simple analytical formulations, which make the overall computational load easy to handle.
The most glaring downside to this approach is that fractures are very obviously not tubes in reality. While macropores and connected pores may be somewhat similar to the concept of a tube, there is now way to fit the hydraulic character of a large roughly planar fracture with tubes.
Pipe analogue network models have found widespread use over the years, an example of which can be found in i.e. Dershowitz & Fidelibus (1999).

1.3.4 Single fracture models

Approximating flow and transport through a fractured medium by modelling the relevant processes in a single well defined fracture is another widespread method. Studies of flow and transport in a single fracture are widespread, and well documented (i.e. Moreno et al., 1988; Maloszewski & Zuber, 1993; Oron & Berkowitz, 1998; Lunati et al., 2003). However, reducing a complex fracture network to a single representative fracture will invariably lead to a mismatch between flow velocities, flow volumes and interactive surface area. Often, several parallel fractures can provide a better approximation (Hadermann & Heer, 1996), but the influence of geometric heterogeneities, such as intersections between fractures remain beyond the reach of this approach.

1.3.5. Discrete fracture networks based on statistical and regional data

If no information on the actual position, extent and orientation of fractures within the studied volume is directly available, a statistically generated fracture network is often used. This approach has become increasingly widepsread with the increased availability of computational resources (Cacas et. al, 1990, Berkowitz & Scher, 1997, de Dreuzy, 2001 and Park et al., 2003, among others). The involved generation algorithms, such as Warzone or Enhanced Baecher (Dershowitz et al. 1995) are usually tuned to reproduce characteristics observed in outcrops near the studied area, or known similar fracture networks. Nonetheless, the generated fracture network cannot be guaranteed to show any geometric similarity with the actual system. A recent example of such an approach is the work by Maryska et al. (2004), in which hydraulic flow in a highly complex fracture network is modelled, based on geometric data from small diameter borehole logs. Fractures are simplified as circular planar structures, the diameter of which is again estimated from the knowledge of fractures detected in the borehole logs. The regular shape of the fractures allows for an excellent discretization.

1.3.6. Discrete fracture networks based on actual fracture geometry

If detailed information of the actual fracture network structure is available, a discrete fracture network which reflects the actual networks characteristics, provides a promising opportunity to study the influence of heterogeneities on the hydrogeological system. Kalbacher et al. (2005) present such a model to describe a potential geothermal reservoir in the deep continental borehole (KTB) program. Despite the relatively small number of fractures however, the realistic geometry presented the authors with substantial difficulties where the discretization and meshing of fractures intersecting at inconvenient angles was concerned. In addition,

the degree of detail obtainable from the available data was limited to the few largest fractures. Nonetheless, the results are convincing, and appear to point the way such studies will take in the near future. The work presented here can be considered to belong in this category, albeit taken to a higher degree of complexity, and incorporating additional effects such as heterogeneous fracture apertures, and matrix diffusion.

1.3.7. Realistic fracture apertures

Smooth walled fractures, while known to exist, are fairly rare in actual hydrogeological systems. Recreating realistic fracture apertures is a well known problem, both for laboratory scaled analogue models, and for numerical models. Field measurements of fracture apertures are often interpreted as showing normal (Neuzil & Tracy, 1981) or log-normal (Johns et al. 1993) distributions of fracture apertures. Another widely used approach attempts to recreate realistic aperture distribtuions under the assumption that apertures follow a fractal pattern of distribution (Brown 1987, Wang et. al, 1988) However, if the actual fractures of the system are not accessible, the aperture distributions must be assumed as similar to aperture distributions from surrounding outcrops or other comparable systems.
In contrast, the availability of the EP data set allowed at least limited measuring of actual apertures. Together with the results from pumping tests performed on the same fracture network, a reasonable attempt at reconstructing realistic fracture apertures could be made. The process is described below, and in more detail in Mettier et al. (2006, first enclosed article).

1.3.8. Matrix diffusion

Diffusive transport of tracer material into and back out of 'pores' in the rock matrix bounding the individual fractures has long been known to exert a considerable retardation effect on tracer breakthrough in fracture networks. Analytical solutions are available for simple cases, such as single fractures with smooth walls and homogeneous apertures. For rough walled fractures, and fracture networks, numerical solutions can be used. However, most of the numerical solutions rely on a simplified representation of the porous matrix through line or prism elements, extending from the model element faces or from the vertices. Due to the very slow transport velocities involved in matrix diffusion, discretization of these additional elements must be very fine. This massively increases the size of the numerical model, and can quickly lead to run times several orders of magnitude longer than the same model without matrix diffusion. An extensive overview of the state of the art in understanding and modelling matrix diffusion is presented in the review article by Jakob (2004). An alternative, semi-analytical approach to this task is presented and used below, and in McDermott et al. (2006, third enclosed article).

2. Reconstructing the fracture network

Extracting the relevant geometric characteristics of the fracture network portrayed in the EP data set involves a chain of image processing and sorting steps. Most of these tasks were performed using freely available image processing tools. Where the tasks were more specialized, dedicated Matlab scripts were created. The following is an overview of the performed modifications and processing steps, provided to facilitate an eventual reproduction of the work.

2.1. Position and orientation of major fractures

2.1.1. Image preprocessing

The lower face image of each slice was flipped horizontally to provide a continuous viewing direction along the cylinder axis. Differential rotation between slices, produced by imprecision during the photographing were removed by re-rotating the slice images. The necessary angle of rotation was determined by comparing roughly linear structures (usually fracture sections) in consecutive images, under the assumption that within the small distance between two images (<= 3cm), the fracture traces may have shifted in a translatory fashion, but in all probability will not have changed their angle of orientation by any significant factor. To facilitate the rotation, a circular subtractive mask was applied to the images, after the radius and centre point were determined by selecting and measuring the position of three points on the circumference of each slice.
Determining the z-coordinate (position along cylinder axis) of each image was done by simple interpolation

from the average slice thickness and the known overall length of the cores. The estimated thickness of the saw blade (3mm) was also taken into account, thus providing alternating separations between two neighbouring images of ~3cm (top of slice A to bottom of slice A) and 3mm (bottom of slice A to top of following slice B).

2.1.2. Extraction and approximation of major fractures

After the images from the data set were prepared in this fashion, the basic geometric characteristics could be extracted. This also required a chain of fairly simple operations, mostly performed with additional small Matlab tools developed for the specific tasks.
The significant visible fracture traces were selected and marked by chains of points, thus linearising the intersection lines between fractures and image planes. The selected points in three dimensions were grouped into major fractures, interconnecting fractures between the major fractures, and insignificant minor fractures each represented by a point cloud. A least squares best fitting planar surface was placed through each point cloud, using singular value decomposition to obtain the directional cosines of each plane. Each fracture plane was clipped to encompass the projections of all the points in the respective point cloud onto the plane. This results in a polygonal, planar, two dimensional representation of each major or connecting fracture.

2.1.3. Intersection and discretization of fractures

The 22 resulting fracture representations (henceforth 'fractures') were then combined into a single geometric model of the simplified geometric appearance of the fracture network. Calculating the intersections between the individual planar polygons was performed by applying a robust meshing tool provided by Golder Inc. (Dershowitz et al., 1995; http://fracman.golder.com/). Selecting the mesh nodes on the endpoints of intersection lines, the original polygonal fractures can be separated into smaller polygons, which do not intersect each other. These are essential in order to generated a high quality mesh. The actual mesh is generated by means of Delaunay Triangulation, and the final mesh quality is judged using three criteria (Kalbacher et al., 2006, second enclosed article), known as length, angle and area criteria.

2.2. Fracture apertures

In addition to the size and orientation of a fractures, its extension in the third dimension, namely its aperture is a key parameter in the behaviour of fluid flowing through the fracture, and therefore also for the behaviour of any type of tracer being carried by the fluid. In addition, the aperture of a fracture can have an influence on possible interaction with the fracture surface or with the surrounding rock matrix. In many cases, fracture apertures and especially their variations, are not considered in numerical models, instead being simplified to a smooth constant value. Geological evidence however, and the EP data set is no exception, consistently shows that fracture apertures are very rarely constant over any significant distance.
Measuring apertures for all the identified fractures in the images is impossible due to resolution limits. Within the EP data set images, a large portion of the fractures are not sufficiently wide to allow their apertures to be measured with any reasonable accuracy. At the given image resolution (~0.7mm/pixel), a fracture must have an aperture of >3.5mm (5 pixels) in order for the aperture to be determined directly from the image. Smaller fractures will appear as partially discoloured pixels, or as diffuse lines in the images.

2.2.1. Obtaining apertures from the data set images

An alternative approach to obtaining the aperture distribution was sought, that could produce realistic apertures for a given fracture geometry. As fracture apertures can generally be considered as spatially correlated values a geostatistical approach was chosen for this task: There exists in a section of one core, a fairly large fracture, which shows an aperture of >5mm over a length of 20 images (~40cm), and also an extension at least halfway across the core slice, often more (>15cm). Within this section of a major fracture, the aperture can be measured directly from the image by simple pixel counting. The apertures measured in this section appear to conform to a log-normal type distribution, as shown inset in Figure 2, something which is often seen and described in geological systems (see e.g. Bianchi et al., 1969; Keller, 1998; deDreuzy et al, 2001; Vandersteen et al., 2003). We assume that this distribution should also hold for the smaller fractures. During the experiments conducted on this shear zone at the Grimsel Site, average transmissivities along

several dipoles of varying lengths were measured, and it was concluded that on a scale of up to 35m, the average transmissivity within the plane of the shear zone can be assumed to be 2.2 +/- 0.7 x 10-6 m2 s-1 (Frick et al., 1992). Applying the cubic law to this transmissivity, it is possible to calculate an estimated equivalent mean hydraulic aperture of roughly 10^{-4}m. Thus we can assume that we have a log-normal aperture distribution, of which the median is known, and of which the large aperture flank is at least partially known. If it is assumed that the studied major fracture is representative of all fractures in the network, and that we have detected and measured all points along the fracture at which the aperture is > 5mm, then it is possible to calculate the percentage of apertures which are 5mm or larger, over the characteristic area of the studied fracture. Consulting a quantile table for the underlying normal distribution can provide us with the a standard deviation, which when transformed back to log-normal, yields the intended expectation value of 10^{-4}m and also fits the measured large apertures. The precise procedure is presented in detail in the first enclosed article (Mettier et al., 2006).

2.2.2. Generating realistic aperture distributions

In order to produce apertures for any given geometry, an experimental variogram of the measured apertures is calculated, and fitted with a model variogram. The model variogram is then modified to accommodate the total distribution as determined above, by adjusting the sill value. This model variogram can then be used for a sequential Gaussian simulation (Armstrong, 1998) of any number of aperture distributions over a given mesh. The experimental and theoretical variograms used in Mettier et al. (2006) are shown in Figure 2. It is important to note that the sequential Gaussian simulation (SGS) is performed in 2D, thus the apertures for each fracture must be calculated individually, instead of for the whole fracture network at once. Besides greatly reducing the necessary computational effort, this avoids elements near fracture intersections having closely related apertures, due to their close proximity. The statistical calculations where performed with the free statistics package R (http://www.r-project.org/), and the gstat geostatistics toolbox for R (Pebesma, 2004). Besides reproducing the observed aperture distribution it is possible to generate aperture distributions with higher or lower degrees of heterogeneity, by modifying the variance of the underlying normal distribution before applying the SGS.

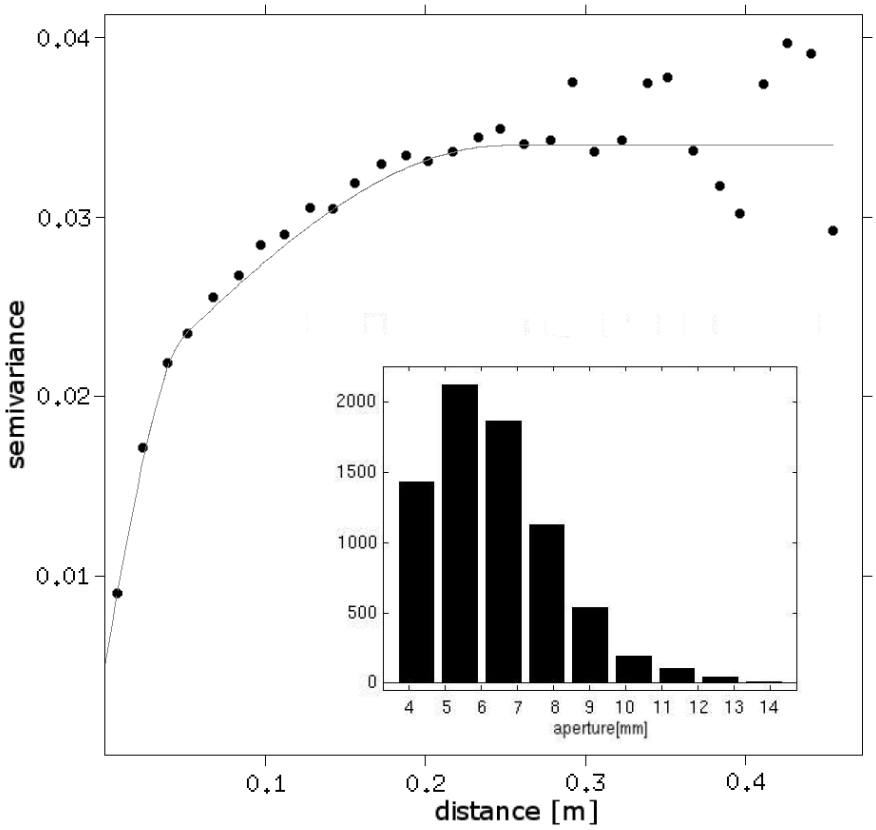

Figure 2: *Experimental (solid circles) and theoretical (line) variograms of the calculated aperture distribution. Inset, the histogram of the measure apertures in a fracture section with consistently large apertures, showing the log-normal behaviour*

3. Modelling conservative transportthrough particle tracking

3.1. Degrees of geometric complexity

By selecting and combining characteristics of the basic geometric model, three models with different degrees of complexity are generated. The dominant feature in the fracture network consists of the three almost parallel major fractures, running roughly parallel to the two extracted core axes. A model describing only one of these major fractures is the simplest possible case. In this model, the influence of the geostatistical aperture distribution alone can be observed, and compared to the behaviour of the same model with a constant aperture, which would be a simple planar fracture, a case for which their exist several analytical solutions, i.e. Ogata-Banks (Agricultural Research Service, 1982).
Within this step, this single fracture model with variable apertures is labelled as case A. A second simplified model consists of the full fracture network, with constant apertures. This model provides some insight into the sole influence of macroscopic geometric heterogeneity on the overall transport behaviour and is labelled as case B. The model with the greatest degree of complexity, labelled case C, with full network geometry and geostatistically generated variable apertures, combines the influence of large and small scale heterogeneity. Figure 3 illustrates the three levels of complexity used in this phase of the project.

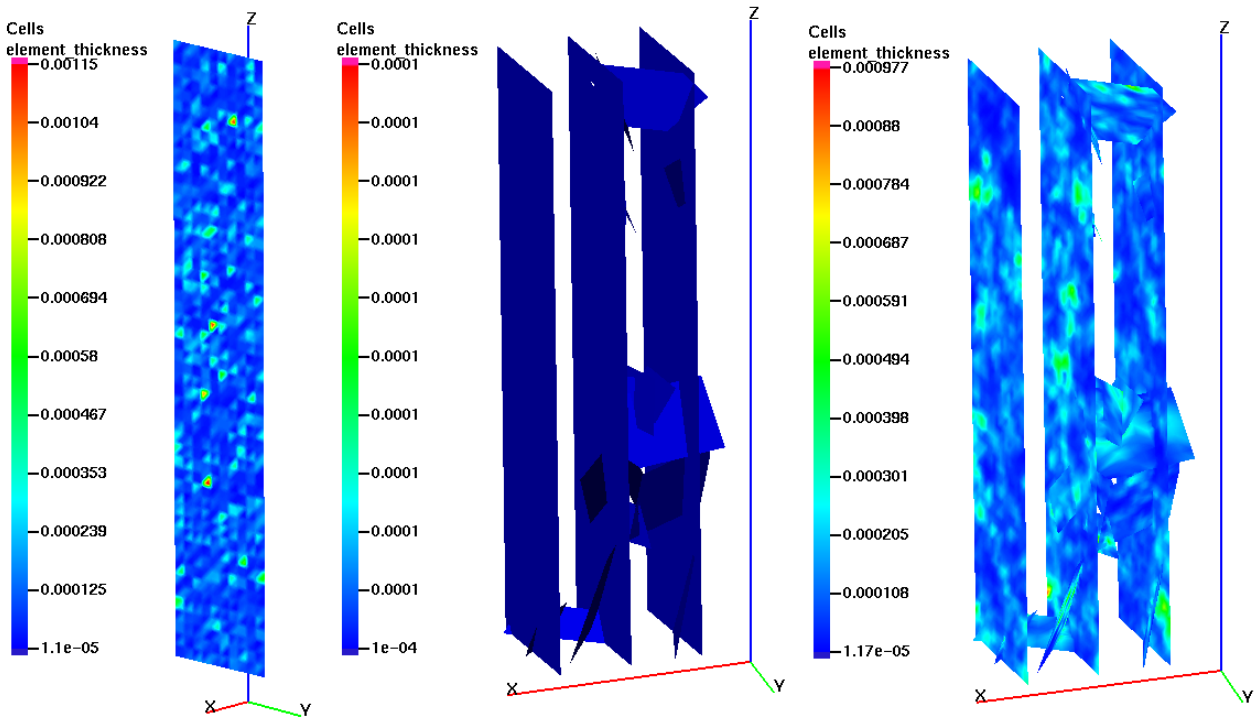

Figure 3: *Illustration of the three degrees of geometric complexity used for the particle tracker models. Left, Case A, a single planar fracture with geostatistically generated heterogeneous apertures; centre, Case B, a network of 23 planar fractures with a homogeneous aperture, and right, Case C, a fracture network with heterogeneous apertures.*

3.2. Hydraulics

The models described above were set up with a hydraulic head difference of 1m over their 2.6m length. The 'lower' boundary (at z=0.2m) was originally set up as an inflow boundary by setting a fixed hydraulic head of 1m. The 'upper' boundary (z=2.8m) was set as an outflow boundary, with a fixed hydraulic head of zero, thus creating a main flow direction along the positive z-axis. As the described hydraulic flow field is static in

time, it was easily calculated by running a single time step of each model variation in the FEM program Rockflow V2 (Kolditz et al., 1999) to solve the hydraulic equations. The total flux over an inflow boundary with the given average aperture of 10^{-4}m was calculated, and distributed equally over the length of each models inflow edge. With these fluxes, the actual boundary condition was then set as a Neumann flux boundary (constant flux, instead of constant head) in the models. The advantages of this unusual choice shall be described in the following section 'Particle Tracking'. An example of the hydraulic fields in the various model geometries is shown in Figure 4

3.3. Particle tracking

One approach to simulating mass transport in a fracture network model, of which the hydraulic field is already known, is to employ a particle tracking tool. For this task, an in-house developed tracker named PTC (Kosakowski, 1998) was used. The program releases one virtual particle for every given unit of tracer flux. The flux boundary conditions described above allow for releasing a particle cloud which was evenly spread along the inflow boundary in all three cases, and is not dependent on the aperture of the fracture elements along the inflow edges.
A possible drawback of this choice of boundary conditions is the fact that a larger than expected number of particles were forced into elements with small apertures, if they happened to occur on the inflow edge.

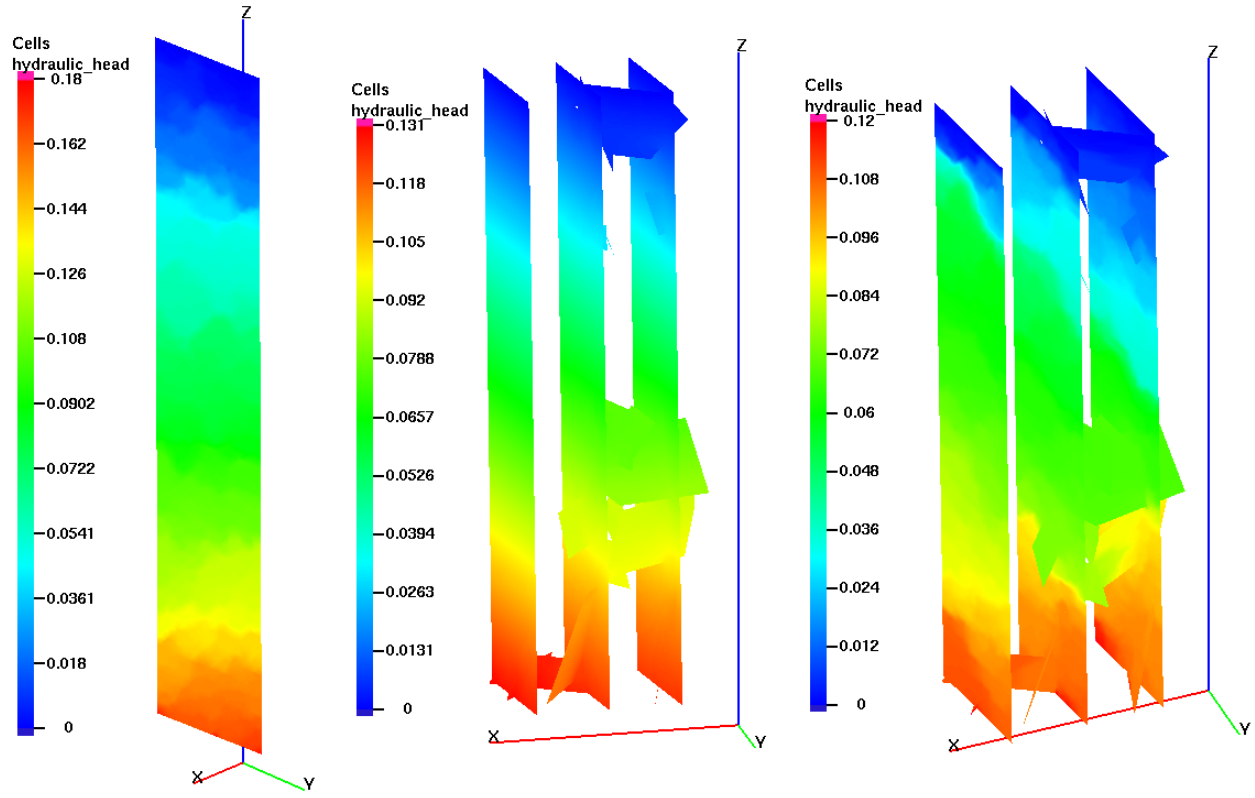

Figure 4: *Hydraulic heads for three model examples. Left: Case A - Single fracture, variable apertures, centre: Case B - fracture network with constant aperture, right: Case C - network with variable apertures.*

However, due to the also abnormally high flux for these small aperture elements, the flow velocity therein was also very high, which caused the particles to move out of these elements very quickly, thus returning to the undisturbed flow field, and not significantly influencing the breakthrough at the outflow boundary.
50 realizations of the models with variable apertures were performed, with equivalent aperture distributions. The passage times of all particles passing the outflow boundaries were logged. Histograms of these particle arrival times provided breakthrough curves for each realization, as well as averaged breakthroughs for the whole model series.

3.4. Preferential flow paths

The particles were injected as a near homogeneous cloud at the inflow boundary. After a short distance (<10cm), the majority of particles was channelled into a few select 'chains' of elements. These preferential flow paths appear similar to preferential flow paths observed in laboratory analogue models and also in naturally occurring systems. They are also in agreement with the findings of Moreno & Neretnieks, 1985; Tsang & Tsang, 1987 and Johns & Roberts, 1991, who postulated that fluid flow should be unevenly distributed in a fracture plane with rough surfaces. The sharp boundaries of these flow paths are clearly due to the absence of dispersion in the particle tracking models. The presence of this heterogeneous distribution of particles must be considered when flow velocities form the model are discussed. Obviously, the models with homogeneous apertures did not display this characteristic behaviour. Some sample illustrations of such preferential flow paths are shown in Figure 5.

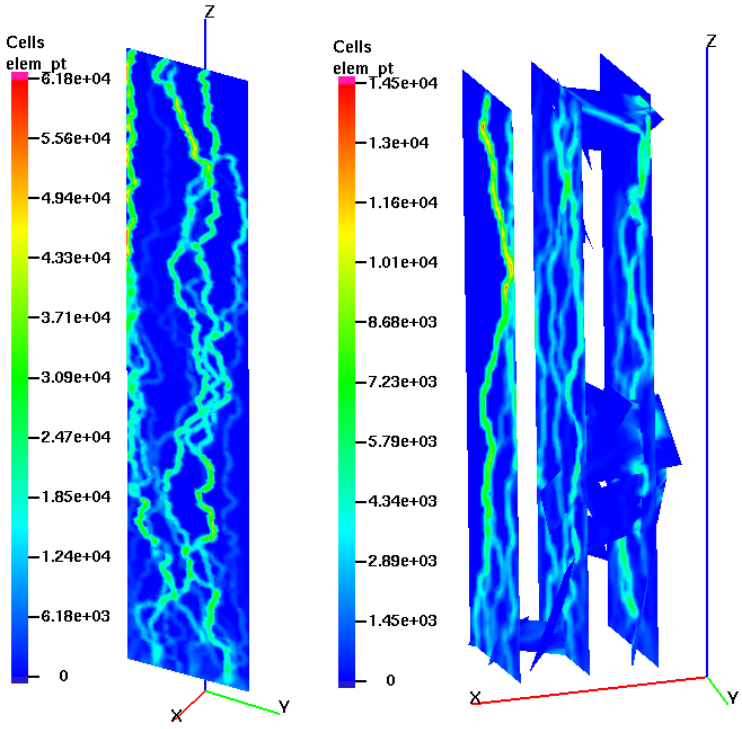

Figure 5: *Two examples of preferential flow paths forming in the particle tracker models, once for a single fracture model, and once for a fracture network model.*

4. Advective-dispersive transport, with matrix diffusion

The second approach to the topic involved the direct numerical solution of the advective dispersive transport equation (ADE) for the network model described above. These models, encompassing fully advective dispersive transport are solved, using the advanced FEM package Rockflow/Geosys Version 4. In addition, a new, fast, semi-analytical method of modelling the influence of Matrix Diffusion was used.

4.1. Model setup

4.1.1. Geometry and apertures

All model realizations in this step were based on the single fracture model with variable apertures, as used in the previous conservative transport models. Basically, a fluid flow scheme from bottom to top was again

chosen. However, in order to achieve agreement with some desire boundary conditions, the in and outflow boundaries were modified as follows:

The tracer inflow boundary was moved away from the edge of the fracture by a few cm (one row of elements), in order to avoid tracer mass to disperse back over the inflow edge. Hydraulic inflow was kept at the edge of the fracture. In order to get a smooth regular hydraulic inflow, the row of elements between hydraulic and tracer inflow boundary were set to a constant aperture equal to the average aperture in the rest of the model.

The hydraulic outflow boundary was set at twice the distance from the inflow boundary as in the conservative transport particle tracking models. The tracer breakthrough curves were however recorded at 2.6m distance from the tracer inflow boundary, the same as in the previous models. The large distance between recorded outflow (breakthrough curves) and the modelled outflow results in behaviour which is comparable to an analytical solution with an outflow boundary "at infinity".

Fracture apertures were again calculated geostatistically, based on the measured apertures as described above. However, the variance of the normal distribution underlying the actual log-normal aperture distributions were modified prior to calculating and mapping the resulting apertures to the model elements. This allowed several model realizations to be considered, with variable degrees of heterogeneity in fracture aperture, as opposed to the single variance used with the conservative transport models.

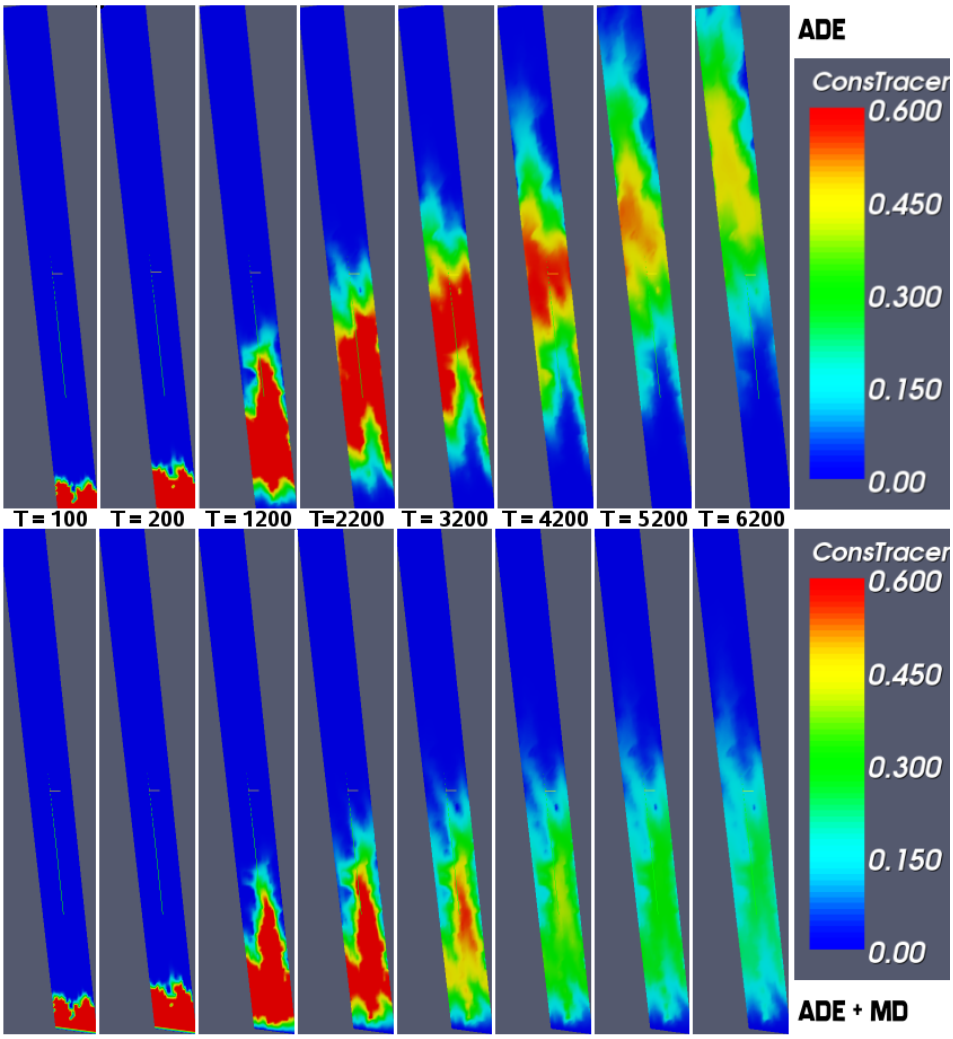

Figure 6: *Time series of an example realization of advective dispersive transport without (to) and with (bottom) matrix diffusion, performed in Rockflow Geosys V4, with the new semi-analytical solution for matrix diffusion. The two model realizations are identical apart from the effect of matrix diffusion. The retardation effect of the matrix diffusion is clearly visible in the later time steps, as is the overall channelling effect of the small scale heterogeneity.*

4.1.2. Matrix diffusion

All model variations were run once with matrix diffusion (MD) being considered, and once without MD. The method used to calculate the effects of matrix diffusion is a semi-analytical method which describes the diffusive transport of tracer mass into the rock matrix and back out as sink and source terms located at each mesh node. The magnitude of the sources and sinks are calculated analytically from the time series of former tracer concentrations at every node. A more detailed explanation, together with the mathematical description of the method, is a major part of McDermott et al. 2006 (third enclosed article).
The parameters chosen were based on the characteristic parameters observed during the CRR experiments (Kosakowski 2004), and the subsequent work by Kosakowski & Smith (2005). This method, while still increasing the necessary computational effort, is massively less resource-intensive than conventional methods such as brush or prism models. The method was tested and verified by Kosakowski (2006), by comparing it to the already widely tested and accepted picnic code (Barten & Robinson, 2001)

4.2. Model realizations

As mentioned, the degree of heterogeneity is modified to study the effect of a gradual change from homogeneous to heterogeneous apertures. The original underlying variance determined from the measure apertures mentioned above, is ~0.9, a value which leads to numerical difficulties when solving for advective dispersive transport. The variances of the underlying normal distributions were therefore systematically modified, to values of [0 (homogeneous case), 0.01, 0.02, 0.04, 0.10, 0.20], and were used to calculate a set of 20 realizations for each variance. These 101 models (20 realizations for each variance + 1 realization for homogeneous) were then run in Rockflow/Geosys, both for conventional ADE, and for ADE + MD with the new semi-analytical method.

4.3. Observations

Visually studying the spread of tracer mass through the models at several selected time steps instantly leads to a number of conclusions. First, and most obvious is the retardation effect of matrix diffusion. Comparing identical models with and without MD, it appears clear that MD can significantly affect the rate at which the tracer is transported and spread through the fractures. With increasing time, as the area of the model in contact with the tracer cloud increases, this effect also becomes stronger.
Second, an increase in the degree of heterogeneity leads to more pronounced channelling This effect is to be expected when recalling the effect seen in the particle tracker models. Due to dispersion being considered in these models, the channels or preferential flow paths are not as pronounced or as sharply bounded as in the particle tracker models.
In combination, it can also be observed that an increase in heterogeneity also impacts the effectiveness of MD as a retarding agent. This would be expected, as the observed increase in channelling with increased heterogeneity also leads to a change in the fracture surface area available for MD to take effect.
A detailed quantitative analysis of these effects may well lead to significant insights on the precise effects of heterogeneity alone, as well as interacting with matrix diffusion. However, a substantially greater number of model runs with much larger variation in parameters would be necessary to create an sufficient base for formulating such conclusions. Creating such a base would exceed not only the scope and time frame of this project, but also the available computational resources and possibly the numerical limits of the available tools.

5. Analysis and interpretation of breakthrough curves

5.1. Purely advective transport - particle tracker

The two particle tracking models with variable apertures (cases A and C) were run 50 times, with individually generated aperture distributions, in order to assure a statistically valid effect of the aperture distribution on the overall flow and transport behaviour Obviously, this is not possible or necessary for case B with the constant aperture. The breakthrough curves for the variable aperture models were calculated to represent a combined curve of the 50 realizations, by concatenating the arrival times of each individual particle from all 50 model realization into a single arrival time file. These times were then binned into 50 logarithmically spaced time periods between the overall earliest and latest arrivals. The number of particles

in each of these bins is representative of the total number of particles passing the 50 respective outflow boundaries over the length of the time bin. This stacking process effectively smoothes the breakthrough curves, and gives us a better idea of the average impact of a variable aperture, rather than the effect of one particular realization, which may not capture the effect of the underlying geostatistically determined distribution.

5.1.1. Local transit time distributions

In these purely advective models, a breakthrough curve can be interpreted as a first arrival time distribution over the length of the entire model. If the entire model is considered as a black box, the inverse of such arrival time distributions can also be displayed as overall transit time distributions multiplied by the overall length of the model. In contrast, local transit time (LTT) distributions are considered on the scale of the individual elements. The flow velocity calculated by the numerical FE model for each triangular mesh element, is inverted, weighted with the size of the element, and then again weighted with the number of particles that the particle tracker recorded as traversing said element. This results in a local transit time distribution, for a standard element and an average particle, or a function which describes the probability of any given particle to traverse a standard element in a given time. As with the breakthrough curves, the 50 realization for the variable aperture models were stacked before calculating the LTT distributions. The LTT distributions for the three model variations are displayed in Figure 7. On a log-log scale, the right hand (low velocity) flank of the curves shows a strong linear tendency. This represents a power law behaviour.

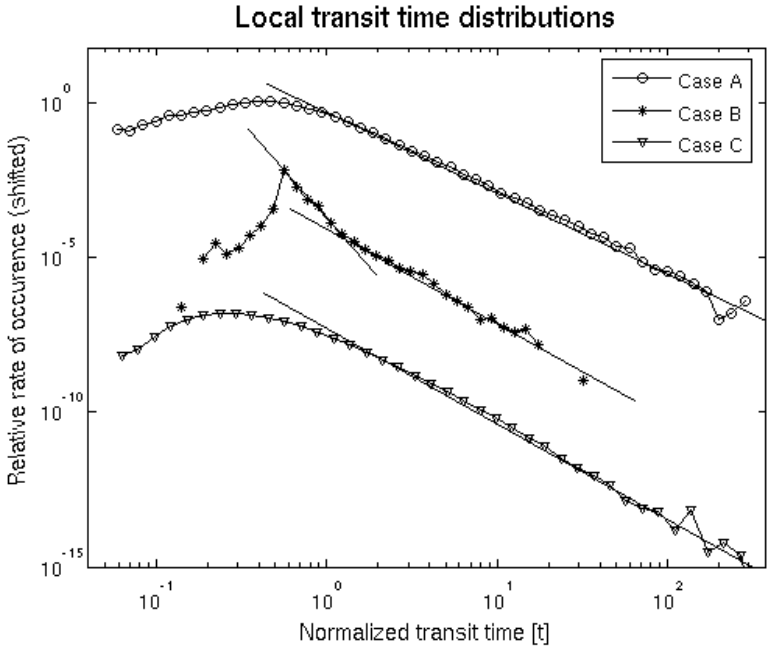

Figure 7: Local transit time distributions for the three particle tracker models. Note the linear (in log-log scale) slope towards the right, indicating a dominant power law behaviour for the low velocity elements. The curves of Cases B and C have been shifted along the y-axis be 3 respectively 6 orders of magnitude in order to facilitate viewing.

5.1.2. Fitting the breakthrough curves with ADE and CTRW

The breakthrough curves generated by the particle tracker, were fitted with two curves obtained from analytical approaches to solving transport in hydrogeological systems. The standard advection dispersion equation (ADE) which was fitted using the Ogata-Banks solution (Bear, 1972) and continuous time random walks (CTRW), an approach that models transport with a series of particle movements on a regular grid (Dentz et al., 2004; Cortis & Berkowitz, 2005). The distance covered in each movement, and the time taken

for each movement is governed by an internal probability density function, usually noted as Ψ(x,t). For an exponential function as Ψ(x,t), CTRW becomes synonymous with ADE. By applying other distributions, statistically describable heterogeneities can be incorporated into CTRW. A the mathematical background and more detailed implications of using this method are discussed in Mettier et al. 2006 (first enclosed article).
In addition to breakthrough curves, transit time distributions play an important role in fitting analytical curves to the particle tracking solutions. While a breakthrough curve can be seen as a macroscopic transit time distribution, a local transit time distribution can be extracted from the flow velocities and number of registered particles for each model element. Once this distribution is normalized for element size, it gives us a general probability density function for the transport velocity a given particle will experience in the model. In the case of the particle tracking models, the use of a truncated power law for Ψ(x,t) in CTRW appears sensible, due to the strong power law components visible in the local transit time distributions. This is a typical example of small scale heterogeneity being describable by a statistical rule, and thus the transport behaviour influenced by the heterogeneity being describable through CTRW. Note that the larger scale heterogeneity given by the intersection and connection of major fracture is not easily captured statistically, at least not on the scale of the model, and thus CTRW does not provide a convincing fit to the breakthrough curves. ADE, which cannot account for any type of heterogeneity consistently fails to fit anything except the peak of each breakthrough curve.

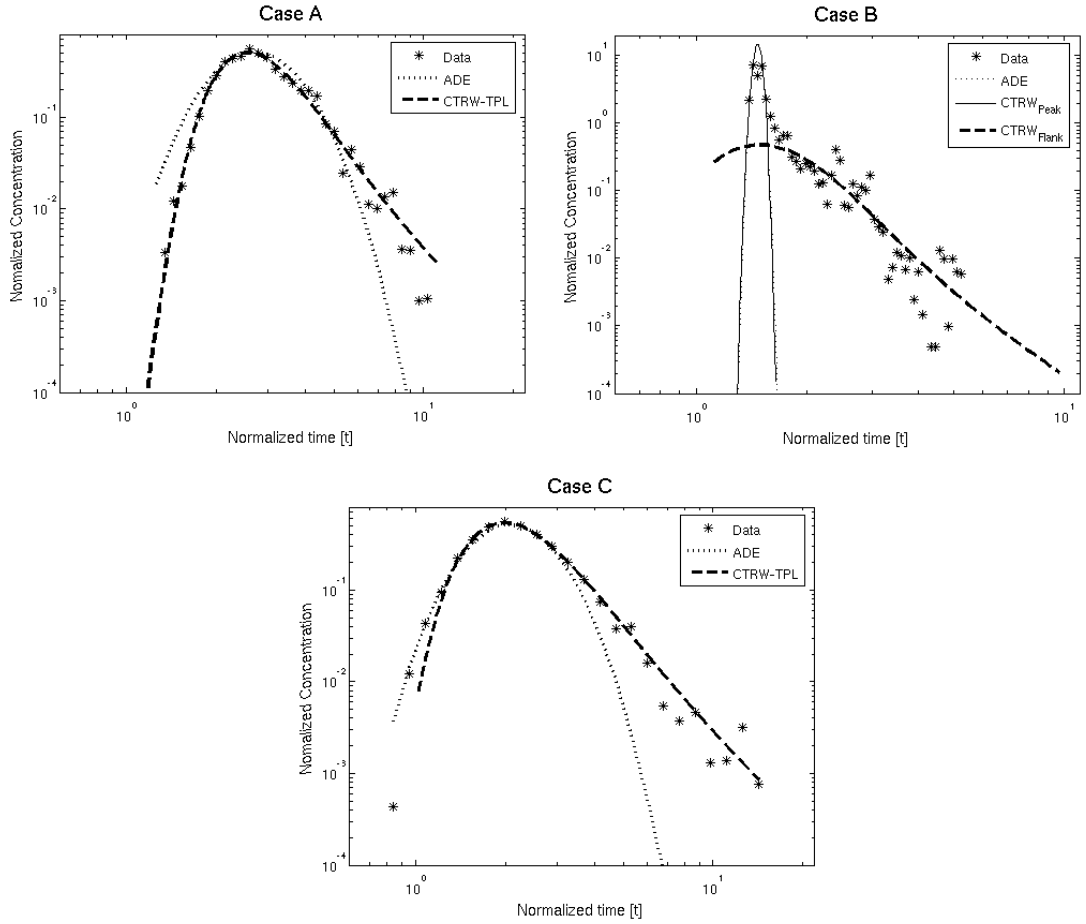

Figure 8: *Breakthrough curves, and best fits with ADE and CTRW for the three particle tracker models. Note that the CTRW solution can account for the late arrival tailing, whereas the ADE solution can only fit the peak of each curve.*

5.2. Advective dispersive transport

Unlike the particle tracker models, where each particle is representative of a given quantum of tracer mass, the advective dispersive models performed with Geosys/Rockflow V4 use the value of concentration to describe tracer mass distribution within the model. As concentration is not only dependent on the amount of tracer mass, but also on the volume wherein the tracer is distributed, extracting meaningful breakthrough curves from the models involved an additional normalizing step.
Values for concentration are provided at nodes along the outflow edges of the models. From these values, concentrations on the outflow faces of the edge elements were calculated, and weighted by the corresponding area of the element face. Averaging these weighted concentrations over the total outflow face surface for the model provides a normalized and representative measure for tracer mass, which allows for comparisons between individual models with different outflow edge areas. In order to average the multiple realizations of each model run, the same procedure must be applied again.

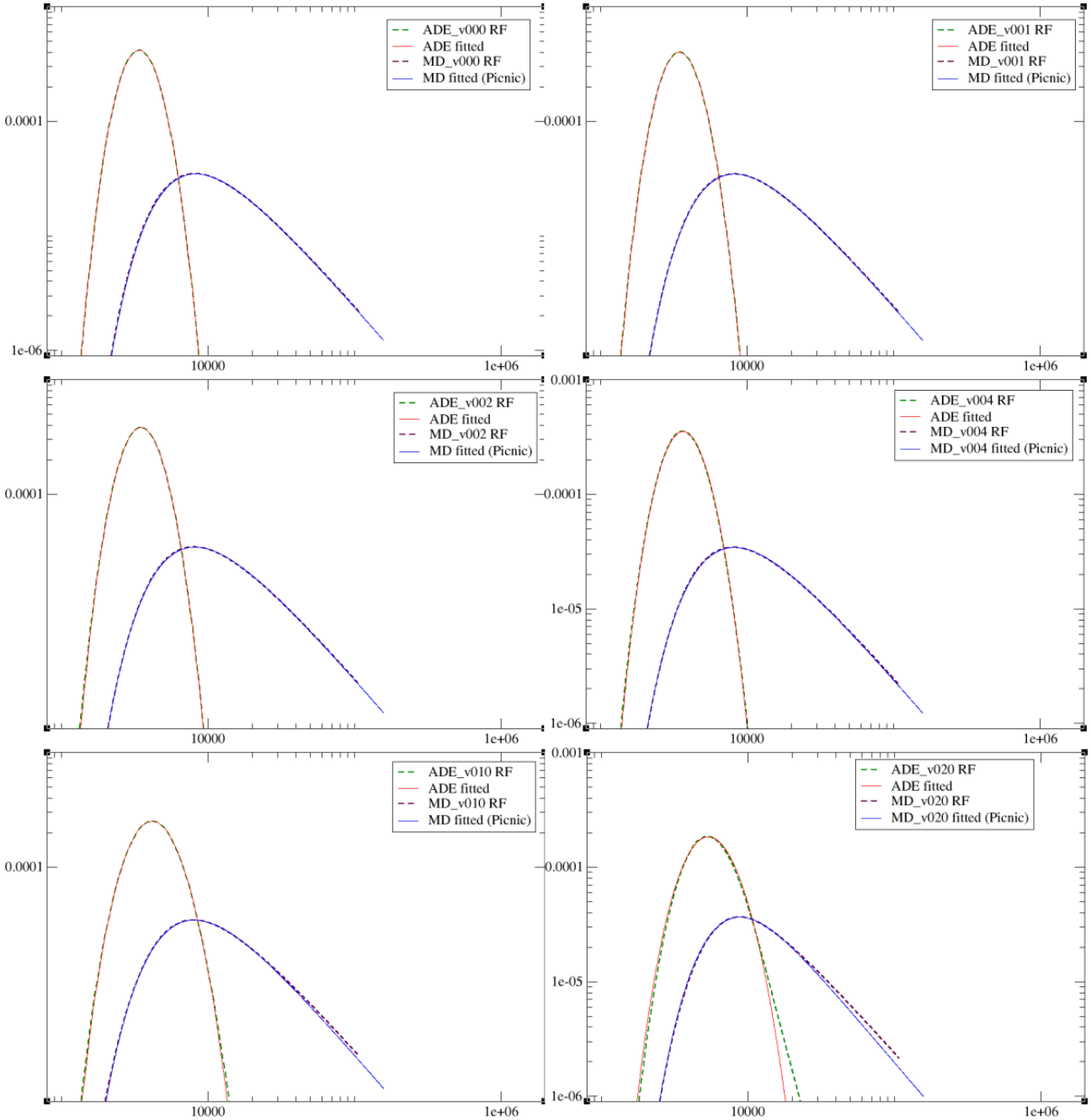

Figure 9: *Breakthrough curves at z=2.63 m, from the advective dispersive model, with and without matrix diffusion. Best fits with ADE, and Picnic are also shown*

5.2.1. Evaluating ADE and ADE+MD curves

Fitting the standard advection dispersion equation (ADE) to the obtained breakthrough curves was done by means of xmgrace, a free, open source mathematical fitting and plotting tool (http://plasma-gate.weizmann.ac.il/Grace/). Due to the complex choice of boundary conditions, a simple solution to ADE such as the usual Ogata-Banks solution was not applicable. A slightly modified version, documented in detail in McDermott et al. 2006 (third enclosed article) was used. The Quality of the fits was determined visually.
Fitting ADE with consideration for matrix diffusion is not so straightforward. In the picnic code (Barten & Robinson, 2001), there exists a known and confirmed solver for matrix diffusion influenced transport in 1D models which has been compared to the RF solution for a reference model by Kosakowski (2006). However, picnic only does forward modelling, so curve fitting was perform through iterative trial and error, by the use of a Matlab script for generating the picnic input files, while running through a range of parameters. Judging the fits visually was again chosen, due to the different importance of different 'parts' of the curve. Strong weight was placed i.e. on the tailing and peak regions and less on i.e. the early arrival flank.

5.2.2. Fitting parameters vs. model parameters

Fitting the ADE and ADE + MD curves returns a several characteristic parameters, among them flow velocity. The velocity at which the fluid moves through the studied system of fractures would appear to be a fairly straightforward parameter, easy to agree upon. Nonetheless, in this case we have no less than three approaches to the flow velocity. The parameter Vfit, obtained from the fitting of ADE, or ADE+MD, represents the velocity at which the fluid would be flowing in the hypothetical homogeneous single fracture, which would produce the best fitting breakthrough curves. Further, it is possible to determine a Vhyd parameters, representing the flow velocity that is to be expected from the hydraulic flux, and the average aperture of the model. Finally, the numerical models also provide flow velocity data for each element. Weighting these elements by the tracer mass which traversed each element and then taking the mean velocity, gives us a fairly realistic 'typical' velocity that is experienced my the fluid and the tracer in the model.
These three values for velocity may differ substantially from each other when compared. The same applies for other parameters, such as dispersivity or the diffusion coefficient in the case of ADE+MD models. The implications and consequences of these differences are discussed below. Detailed tables and discussion of these parameters can be found in McDermott et al. 2006 (third enclosed article).

6. Conclusions

The influence of small and large scale heterogeneities on processes involved in flow and transport through fracture crystalline rock was studied by analytical and numerical simulations of transport in fractures and fracture networks derived from an actual fracture network in the granodiorite of the Swiss Alps.

A range of models is presented which represent the relevant geometric characteristics of a natural fracture network across microscopic and macroscopic scales. Various degrees of complexity are used in the models, enabling the effects of microscopic heterogeneities such as variable apertures to be studied in contrast to, as well as combined with, matrix diffusion and the effect of macroscopic heterogeneities such as interconnections between the major fractures. Multiple methods of describing flow and transport in systems such as the studied fracture network, are applied, and both the results and the limitations of the various methods are compared and discussed.

It can be concluded that the effects of heterogeneities can cause significant deviations from the expected breakthrough curves in hydrogeological systems. It is thereby important to distinguish between heterogeneities which can be approximated statistically, such as the effect of the variable apertures on the local transit time distribution in the described particle tracker models (described in detail in Mettier et al., 2006, first enclosed article), and such which defy any meaningful statistical description, such as the large scale heterogeneities presented by the major fractures and their interconnections. The effect of a statistically describable heterogeneity can often be handled by using CTRW in place of common ADE theory to describe the system. Key to success with this method is obviously the problem of choosing a suitable probability density function. This need may appear as a disadvantage at first, but recent studies have shown that it is conceivably possible to obtain information about the actual velocity distribution in a hydrogeological system, through the use of non-invasive geophysical methods, such as radiological tracking of radioactive tracers, or through magnetic resonance or X-Ray tomography. Our experience with the particle tracking methods, and the excellent agreement between local transit time distributions show that is may well be possible to use these measured velocity distributions to tune the necessary probability density function for CTRW.

The influence of matrix diffusion can be accommodated by advanced numerical modelling approaches, such as the semi-analytical method presented in McDermott et al 2006 (third enclosed article).

In all but the simplest model examples, it could be shown that ADE cannot satisfyingly describe transport behaviour in complex hydrodynamic systems. Advectively dominated systems, without relevant heterogeneities, will often produce simple, peak-dominated breakthrough curves, which can be fitted by ADE, but any process that results in pronounced tailing in the breakthrough curve cannot be described or accounted for by simple ADE. Among these processes are large and small scale heterogeneities as well as matrix diffusion, and conceivably other processes which were not studied within this project, such as non-linear sorption in the rock matrix and on the fracture surface. This insight may conceivably reflect on large scale numerical models of hydrogeological systems, which principally solve ADE for small scale elements or distances, thus accumulating errors which distort the overall breakthrough curves.

With ADE + MD (Picnic) it was shown that models with significant small scale heterogeneities can still be fitted very well, with breakthrough curves from hypothetical homogeneous models. The good quality of the misleading ADE+MD fits may well break down for higher degrees of heterogeneity, but for the studied models the quality of the fits may blind the user to the fact that the resulting fitting parameters, such as flow velocity, dispersivity, mean aperture, etc. do not agree with the actual parameters chosen for the numerical models. It must therefore be mentioned that by fitting breakthrough curves measured in the field with ADE+MD, misleading parameters may well be obtained. This insight should especially be considered in field studies of contaminated ground water systems, where projections and hazard assessments are often based on measured breakthrough curves.

A further insight was reached with respect to limitations of data resolution, and the influences thereof on the quality of the final model results. The unavoidable resolution limits tend to limit the degree of detail and realism which can be incorporated into the basic model geometry. However, the limitations of other necessary techniques, such as meshing and the simplification of the underlying equations, necessary to numerically simulate flow and transport in such a geometrical model, would not allow for significantly increased complexity, even if such a model were available. At the current level, even with the unique nature of the data set, and the remarkable advances in preprocessing and modelling tools made during the last few years (Kalbacher et. al, 2006, second enclosed article), it would still be rather pretentious to speak of a truly realistic model.

7. Outlook

Smaller fractures, which may exist in large numbers in the studied volume, may have a large influence in the overall transport behaviour, partly as additional connections between major fractures, and partly as a retention device for the tracer material. Enhanced image resolution, and new, sophisticated software tools to build a complex three dimensional network from two dimensional cross section images are the main requirements for studying these assumed effects in similar future projects.

Further, it is known from in situ observations, and general geological knowledge, that many of the fractures in such a network may be partially or completely filled with fine grained material such as fault gouge. The porous nature of this material would obvious make it an important milieu for additional matrix diffusion, as well as slowing and disrupting advective-dispersive flow in the obstructed fracture. Unfortunately, information on the number, size and distribution of fault gouge deposits in the studied fracture network is not readily available, due to high pressure pumping tests carried out in situ, which flushed most of the porous material out of the system. Further studies of similar fracture networks may provide additional insights and the data necessary to study the influence of porous infill.

Finally, the advances in computational power, and sophistication of numerical methods and tools promise more detailed insights in this field. In particular, robust meshing algorithms will allow for more complex, and thus more realistic, model geometries to be used. Combined approaches of analytical, and numerical methods may allow for processes such as matrix diffusion and sorption to be directly integrated into a model of arbitrary complexity. In cases where complex geometry is essential, regardless of the difficulties involved with meshing, advanced particle trackers, capable of simulating advective and dispersive transport and matrix diffusion may be the solution. Bringing all these advanced methods together into a package which provides a certain minimum of usability will be another, and by no means lesser, challenge.

8. Acknowledgements

The author would like to thank Georg Kosakowski for his guidance, support and endless patience in his role as advisor during the project, often even in his personal free time. Further thanks must go to Andreas Jakob, Walter Heer, Jörg Hadermann and the entire LES team for additional support, many helpful discussions and hints, and also for providing a pleasant workplace and atmosphere.

Additional thanks must go to Olaf Kolditz, Thomas Kalbacher, and Chris McDermott for their help and collaboration during the work in Tübingen. Special thanks to Sebastian Bauer for his time, and his helpful comments on the original manuscript.

This work was enabled by the cooperation of the Waste Management Laboratory at Paul Scherrer Institut, Villigen, Switzerland, and the Center for Applied Geoscience at Eberhard Karls University of Tübingen, Germany. Further thanks go to Nagra, Wettingen, Switzerland, for providing the original EP data set, and to Bill Dershowitz of Golder Ass. for providing an academic license for their FracXP package.

Last, but by no means least, endless thanks go to my wife Monika Mettier, for her patience and support throughout the duration of the project, and simply for being there.

9. References

Agricultural Research Service, (1982), Analytical Solutions of the One-Dimensional Convective-Dispersive Equation, US Department of Agriculture, Technical Bulletin Nr. 1661, Issued June 1982.

Alexander W.R., Ota K., Frieg B., (2003a), The Nagra-JNC in situ study of safety relevant radionuclide retardation in fractured crystalline rock II,Nagra Technical Report 00-06, Nagra, Wettingen, Switzerland, ISSN 1015-2636.

Alexander W.R., Smith P.A., McKinley I.G., (2003b), Modelling radionuclide transport in the geological environment: a case study from the field of radioactive waste disposal. Ch.5, p.109-145 in E.M. Scott (ed), Modelling Radioactivity in the Environment, Elsevier, Amsterdam, The Netherlands.

Armstrong M., (1998), Basic Linear Geostatistics, Springer-Verlag, Berlin, Germany ISBN 3-540-61845-7

Bachmat Y., Bear J., (1986), Macroscopic modelling of transport phenomena in porous media. 1: The continuum approach, Transport in Porous Media, ISSN 0169-3913

Barten, W., Robinson P. C., (2001), Contaminant Transport in Fracture Networks with Heterogeneous Rock Matrices: The PICNIC code, 371 pp, PSI Report Nr. 01-02, February 2001, ISSN 1019-0643.

Bianchi L., Snow D.T., (1969), Permeability of crystalline rock interpreted from measured orientations and apertures of fractures, Annals of Arid Zone,8, 231-245

Biggin C., Möri A., Alexander W.R., Ota K., Frieg B., Kickmaier W., McKinley I.G., (2003), In situ radionuclide retardation in groundwater conducting systems: overview of the research carried out at Nagra's Grimsel Test site, central Switzerland. pp 207-228 in Environmental Radiochemical Analysis II (ed P. Warwick) RSC, London, UK

Bear J., (1972), Dynamics of Fluids in Porous Media,American Elsevier Publishing Company Inc., ISBN 0-486-65675-6

Berkowitz B., Scher H., (1997), Anomalous transport in random fracture networks, Physical Review Letters, 79, 4038-4041

Bossart P., Mazurek M., (1991), Grimsel Test Site: Structural geology and water flow-paths in the migration shear-zone - Nagra Technical Report, NTB 91-12, Nagra, Wettingen, Switzerland

Brown S.R.,(1987), Fluid flow through rock joints: The effect of surface roughness, J. Geophys. Res., Vol 92 Issue B2, 1337-1348

Cacas M.C., Ledoux E., De Marsily G., Tillie B., Barbreau A., Durand E., Feuga B., Peaudecerf P., (1990), Modeling fracture flow with a stochastic discrete fracture network: Calibration and Validation 1. The flow model, Water Resources Research, 26, 479-489

Cortis A., Berkowitz B., (2005), Computing "anomalous" contaminant transport in porous media: The CTRW Matlab toolbox, Ground Water, 43, 6, 947-950

de Dreuzy J., Davy P., Bour O., (2001), Hydraulic properties of two-dimensional random fracture networks following a power law length distribution 2. Permeability of networks based on log normal distribution of apertures Water Resources Research, 37 2079 –2095

Dentz M, Cortis A.,Scher H., Berkowitz B., (2004), Time behavior of solute transport in heterogeneous media: Transition from anomalous to normal transport, Advances in Water Resources, 27(2), 155-173).

Dershowitz, W., Lee, G., Geier, J., La Pointe, P., (1995), FracMan Interactive Discrete Feature Data

Dershowitz W.S., Fidelibus C., (1999), Derivation of equivalent pipe network analogues for three-dimensional discrete fracture networks by the boundary element method, Water Resources Research, 35, 2685-2692

Douglas J., Arbogast T., (1990), Dual Porosity Models for Flow in Naturally Fractured Reservoirs, Dynamics of Fluids in Hierarchical Porous Media. Acad. Pr., Inc., San Diego, California. 1990. p 177-221

Frick, U., Alexander, W.R., Baeyens, B., Bossart, P., Bradbury, M.H., Bühler, C., Eikenberg, J., Fierz, T., Heer, W., Hoehn, E., McKinley, I.G., Smith, P.A., (1992), The radionuclide migration experiment-overview of investigations 1985–1990, PSI-Bericht Nr. 120, Paul Scherrer Institut, Würenlingen und Villigen, Switzerland, and NAGRA NTB 91-04, NAGRA, Wettingen, Switzerland, 1992

Geckeis H., Schaefer T., Hauser W., Rabung Th., Missana T., Degueldre C., Möri A., Eikenberg J., Fierz T., Alexander W.R, (2004), Results of the Colloid and Radionuclide Retardation (CRR) experiment at the Grimsel Test Site (GTS) Switzerland – impact of reaction kinetics and speciation on radionuclide migration, Radiochim Acta 92, 9-21.

Hadermann, J., Heer, W., (1996), The Grimsel (Switzerland) migration experiment: integrating field experiments, laboratory investigations and modelling. J. Contam. Hydrol. 21, 87–100

Jakob, A., (2004), Matrix diffusion for performance assessment - experimental evidence, modelling assumptions and open issues., 75 pp, Paul Scherrer Institute.

Johns R.A., Roberts P.V., (1991), A solute transport model for channelized flow in a fracture, Water Resources Research, 27, 1797-1808

Johns R.A., Steude J.S., Castanier L.M., Roberts P.V., (1993), Nondestructive measurements of fracture aperture in crystalline rock cores using X ray computed tomography, J.Geophys. Res., Vol. 98, Issue B2, 1889–1900

Kalbacher T., Wang W., McDermott C., Kolditz O., Taniguchi T., (2005), Development and application of a CAD interface for fractured rock, Environmental Geology 47, 7

Kalbacher T., Mettier R., McDermott C., Wang W., Kosakowski G., Taniguchi T., Kolditz O., (2006), Geometric modelling and object-oriented software concepts applied to a heterogeneous fractured network from the Grimsel rock laboratory, Computational Geoscience 10, 4, ISSN 1420-0597

Keller A., (1998), High resolution, non-destructive measurement and characterization of fracture apertures, International Journal of Rock Mechanics and Mining Sciences and Geomechanics Abstracts, 35, 1037-1050

Kolditz O., Kaiser R., Habbar D., Rother T., Thorenz C., (1999), ROCKFLOW-Theory and Users Manual, Release 3.4, Groundwater Modeling Group, Institut für Strömungsmechanik und Elektronisches Rechnen im Bauwesen der Universität Hannover

Kosakowski, G., (1998). PTC - Particle Tracker für Rockflow, PTC-V11.05.98, NLfB-Report, Archiv-Nr. 117289, Hannover, Germany.

Kosakowski, G., (2004). Anomalous transport of colloids and solutes in a shear Zone. Journal of Contaminant Hydrology 72(1-4), 23-46, doi:10.1016/j.jconhyd.2003.10.005

Kosakowski, G. and Smith, P., (2005) Modelling the transport of solutes and colloids in the Grimsel Migration shear zone. PSI-Report, No. 05-03, Paul Scherrer Institut, Villigen, Switzerland, and Nagra Technical Report 04-01, Wettingen Switzerland.

Kosakowski, G., (2006). Testing a new solution for Matrix-Diffusion in Rockflow/Geosys: Comparison

with Picnic. PSI Internal Report, AN-44-06-06, Paul Scherrer Institut, Villigen Switzerland

Long J.C.S., Remer J.S., Wilson C.R., Witherspoon P.A., (1982), Porous media equivalents for networks of discontinuous fractures, Water Resources Research, 18, 645-658

Lunati I., Kinzelbach W., Sørensen I., (2003), Effects of pore volume-transmissivity correlation on transport phenomena, Journal of Contaminant Hydrology, 67, 195-217

Maryška J., Severýn O., Vohralík M., (2004), Numerical simulation of fracture flow with a mixed-hybrid FEM stochastic discrete fracture network model, Computational Geosciences 8: 217–234

Maloszewski P., Zuber A., (1993), Tracer Experiments in fractured Rocks: Matrix Diffusion and the Validity of Models, Water Resources Research, 29, 2723-2735

McDermott C., Mettier R., Kosakowski G., Kolditz O., (2006), Hybrid analytical and numerical modelling of mass and heat transport in fractured rocks, in preparation.

Mettier R., Kosakowski G., Kolditz O., (2006), Influence of small scale heterogeneities on contaminant transport in fractured crystalline rock, Ground Water, 44, 5, 687ff.

Moreno L., Neretnieks I., (1985), Analysis of some laboratory tracer runs in natural fissures, Water Resources Research, 21, 951-958

Moreno L., Tsang W., Tsang C.F., Hale F.V., Neretnieks I., (1988), Flow and tracer transport in a single fracture: A stochastic model and its relation to some field observations, Water Resources Research, 12, 2033-2048

Möri A., (2003), The CRR final project report series: 1. Description of the field phase – methodologies and raw data, Nagra Technical Report NTB 03-01, Nagra, Wettingen, Switzerland

Neuzil C.E., Tracy J.V., (1981), Flow Through Fractures, Water Resources Research Vol 17, 1, p 191-199

Oron A.P., Berkowitz B., (1998), Flow in rock fractures: The local cubic law assumption reexamined, Water Resources Research, 34, 2811-2825

Park J., Lee K., Kosakowski G., Berkowitz B., (2003), Transport behavior in three-dimensional fracture intersections, Water Resources Research, 39, 1215.

Pebesma E.J., (2004), Multivariable geostatistics in S: the gstat package. Computers & Geoscience, 30: 683-691.

Pfingsten W., Soler JM., (2003), Modelling of nonreactive tracer dipole tests in a shear zone at the Grimsel test site, J Contam Hydrol. 2003 Mar;61(1-4):387-403.

Smith P.A., Alexander, W.R., Heer W., Fierz T., Meier P.M., Baeyens B., Bradbury M.H., Mazurek M., McKinley I., (2001), The Nagra-JNC in situ study of safety relevant radionuclide retardation in fractured crystalline rock I: Radionuclide Migration Experiment – Overview 1990-1996, Nagra Technical Report NTB 00-09, Nagra, Wettingen, Switzerland

Tsang Y.W., Tsang C.F., (1987), Channel model of flow through fractured media, Water Resources Research, 23, 467-479

Vandersteen K., Carmeliet J., Feyen J., (2003), A Network Modelling Approach to Derive Unsaturated Hydraulic Properties of a Rough-Walled Fracture, Transport in Porous Media 50: 197–221

Wang J.S.Y., Narasimhan T.N., Scholz C.H., (1988), Aperture correlation of a fractal fracture, Journal of Geophysical Research, Volume 93, Issue B3, 2216-2224

ground water

Influence of Small-Scale Heterogeneities on Contaminant Transport in Fractured Crystalline Rock

by Ralph Mettier[1,2], Georg Kosakowski[3], and Olaf Kolditz[2]

Abstract

We present a sequence of purely advective transport models that demonstrate the influence of small-scale geometric inhomogeneities on contaminant transport in fractured crystalline rock. Special weight is placed on the role of statistically generated variable fracture apertures. The fracture network geometry and the aperture distribution are based on information from an in situ radionuclide retardation experiment performed at Grimsel test site (Swiss Alps). The obtained breakthrough curves are fitted with the advection dispersion equation and continuous-time random walks (CTRW). CTRW is found to provide superior fits to the late-arrival tailing and is also found to show a good correlation with the velocity distributions obtained from the hydraulic models. The impact of small-scale heterogeneities, both in fracture geometry and aperture, on transport is shown to be considerable.

Introduction

Flow and transport in crystalline rock mainly takes place within single or multiple fractures, or even complex networks of fractures. Due to the complexity and spatial inhomogeneity, flow and transport in fractured crystalline rock are much less well understood and modeled than in porous media. A good understanding of these processes is, however, key to a solid performance evaluation with regard to underground facilities, such as nuclear waste repositories (Heer and Smith 1998; Jakob et al. 2003). Several nations are planning on creating nuclear waste repositories in crystalline rock formations (e.g., Sweden [Backblom 1998], Finland [Enescu et al. 2004]). This provides a strong need for furthering the understanding of flow and transport processes in such media.

Several approaches to modeling flow and transport through single fractures (Moreno et al. 1988; Maloszewski and Zuber 1993; Oron and Berkowitz 1998; Lunati et al. 2003) and through more complex systems (Long et al. 1982; Hsieh et al. 1985; Geiger et al. 2004) of several, often interconnected, fractures have been used. Among these approaches are methods such as the use of equivalent porous media models (Endo et al. 1984), with single and dual/multiple porosities, representation of the fracture networks through networks of tubes of varying diameter (Dershowitz and Fidelibus 1999), reduction of the network to a single fracture or to several parallel fractures (Hadermann and Heer 1996), and also the use of statistically generated discrete fracture network models (Cacas et al. 1990; Berkowitz and Scher 1997; de Dreuzy et al. 2001a; Park et al. 2003). Common to all the mentioned approaches is that they are frequently used as a rather general representation of reality and are only rarely conditioned to represent a specific case, such as a fracture network. This is a consequence of the common absence of detailed data sets portraying the internal geometric structure of the studied rock volume. In most cases, "hard" data is limited to the breakthrough curves, with additional "soft" data coming from the borehole walls, surrounding geology, water chemistry, etc.

The excavation project (EP) provides us with a rare data set containing information not only of overall flow and transport characteristics but also on small- and medium-scale geometry and several geological properties of the studied rock volume (Alexander et al. 2003a). The data set was obtained by performing a number of transport tracer experiments through a section of a shear zone in the Grimsel test site in the Swiss Alps, followed by

[1]Corresponding author: Laboratory for Waste Management, Paul Scherrer Institute, Villigen, Switzerland; ralph.mettier@psi.ch
[2]Center for Applied Geoscience, Eberhard Karls University of Tübingen, Tübingen, Germany
[3]Laboratory for Waste Management, Paul Scherrer Institute, Villigen, Switzerland
Received October 2005, accepted April 2006.

doi: 10.1111/j.1745-6584.2006.00236.x

impregnation of the fracture network with fluorescent resin. Subsequent overcoring with two slightly overlapping 30-cm-diameter cores, parallel to the main flow direction, along the shear zone, and extraction of the resulting cores enabled a large percentage of the rock volume involved in the transport tests to be recovered intact and cut into slices of ~3-cm thickness. The surfaces of these slices were then photographed in visible and ultraviolet (UV) light. The resulting set of 304 digital images presents a unique view of the interior structure of such a fracture network.

Related to EP, further transport experiments with various tracers have been performed in other parts of the same shear zone within the framework of the Radionuclide Retardation Programme (RRP) project (Hadermann and Heer 1996; Smith et al. 2001; Alexander et al. 2003; Biggin et al. 2003) and Colloid Retention and Retardation (CRR) project (Möri 2003; Geckeis et al. 2004). The breakthrough curves obtained from CRR have recently been studied and fitted using the advection dispersion equation (ADE) and continuous-time random walks (CTRW) (Kosakowski 2004). It has therein been shown that neither uranine nor colloid tracers produce a breakthrough curve that can be adequately fitted using plain ADE. Both types of tracers show extended tailing, indicating some type of non-Fickian transport. Kosakowski (2004) showed that the introduction of matrix diffusion was sufficient to fit the breakthrough curves of uranine, but not those of the colloids, and suggested that colloids may not be party to matrix diffusion and that the prolonged tailing in the breakthrough curves stems from the influence of geometric small-scale heterogeneities. Similar observations concerning tailing effects in fractured media, which are not explainable by matrix diffusion, have been reported by Sidle et al. (1998), Kosakowski et al. (2000), and Becker and Shapiro (2000). Various related observations in other geological media are listed in Cortis et al. (2004). Based on this interpretation, one is led to suppose that factors such as matrix diffusion and geometric heterogeneities may be interchangeable to a degree in their role as tailing-producing retardation influences.

With this work, we attempt to study the impact of the small-scale geometric heterogeneity, including varying fracture apertures, upon the macroscopic advective transport. We base this on the geometric information from the EP project and do this with the following steps.

1. Create a simplified fracture network model, based on the geometric data obtained from EP
2. Quantify the spatial variability of fracture apertures and add this information to the fracture network model
3. Calculate purely advective transport in different conceptual models (different network geometries, with and without variable apertures) to see the influence of these fractures on the breakthrough curves
4. Compare the capability of fitting analytically obtained solutions to the modeled breakthrough curves by ADE and CTRW
5. Test the hypothesis that geometric heterogeneities can produce late-arrival tailing in purely advective transport, which may be mistaken for matrix diffusion or similar processes.

Model Geometry

Fracture Planes

The sequence of images provided by the EP data set allows us to identify three main fractures with a number of connections visible between them, in a model volume that encompasses two overlapping 30-cm-diameter cores in a rectangular prism box of 2.6-m length and 0.6-m width/depth. Of the interconnecting fractures, 18 were deemed significant for the flow and transport in the model. It must be noted that these main fractures are not always simple, continuous open fractures as normally imagined. In some areas, a single large aperture fracture dominates the structure; in other areas, the structures consist of many individual fractures of various sizes forming a continuous network of roughly planar shape. This type of fracture is typical of shear zone geometries. As Figure 1 illustrates, connecting fractures are much more like individual fractures in the classical geological sense, only rarely branching out into small network-like areas.

The possibility of further interconnections between these main fractures on a scale too small to be identified in the images cannot be excluded. The resolution of the images limits the size of recognizable fractures to one pixel, or ~0.6 mm. Based on visual inspection of a few select samples, and also from a qualitative, geological point of view, there is little doubt that smaller fractures of sizes possibly orders of magnitude smaller exist and function as connections between the main fractures. However, due to their small apertures, their influence on the overall fluid flow is minor. Further, the possibility of additional flow field–relevant fractures and intersections

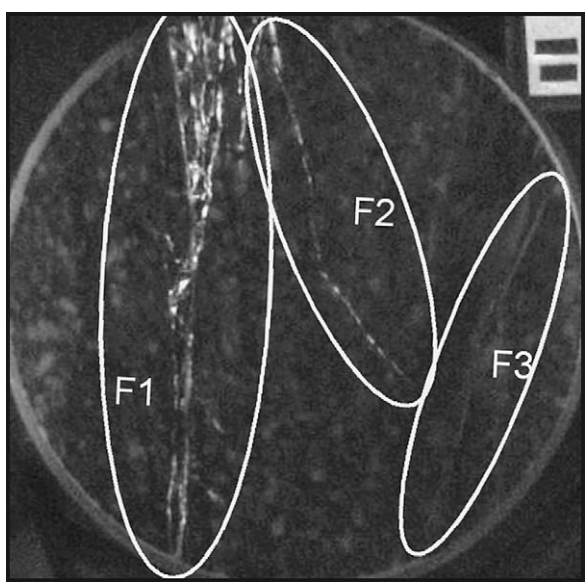

Figure 1. UV photography of one of the ~30-cm-diameter core slices obtained from the EP experiment. Resin-filled fractures show up well in the UV lighting. F1 is a main fracture, consisting of a large number of individual small fractures strongly interconnected and interspersed with mylonitic substance. F2 is a connecting fracture. F3 marks the beginning of a second main fracture.

outside the extracted rock volume can also not be excluded. Consideration of the full complexity of the fracture network is beyond our numerical capabilities, as well as beyond the level of detail that can be extracted from the data set. Therefore, our models shall be limited to the main fractures of the fracture network. As mentioned previously, we consider 18 connections between the three main fractures to be significant. These coincide with structures that are clearly identifiable in the images.

The main fractures are represented as single planes, extended to intersect the model borders on all sides. The connections between them are also portrayed as planar single fractures; however, their planes terminate where they intersect a main fracture or where they are no longer visible in the data.

As for degrees of complexity, we choose three variations. In case A, a single fracture with varying apertures represents the modeled volume, whereas the connections between the main fractures are ignored. In case B, the model consists of three parallel fractures and the connections between them. All fractures have a constant aperture of 1.3×10^{-4} m. The variation with the highest degree of complexity, and also the strongest resemblance to the actual system, is case C, a model consisting of three parallel main fractures, with connections and varying apertures on all fractures. Further possible geometric refinements of the model with regard to realism would consist of adding additional classes of fractures, smaller than the connecting fractures.

Apertures

All the planar representations of fractures, including main fractures and connections, are modeled as two-dimensional (2D) objects in three-dimensional space. As a first approximation, a unit aperture can be assigned. From RRP, an average transport aperture on the order of 10^{-4} m for each of the three parallel fractures was calculated. This is roughly equal to the constant aperture of 1.3×10^{-4} m in case B. As the average aperture is much smaller than the other dimensions of the fractures (0.3 to 0.6 m), the simplification as a 2D object appears justified, not only with regard to the massive reduction in the number of necessary mesh elements and thus computational power but also as such a model was suggested by Bossart and Mazurek (1991) in their original study of the geological structure of this shear zone.

Image resolution does not allow for a conclusive study of fracture apertures. Nonetheless, a study of some large fractures can yield some information toward correlation length and reasonable aperture distribution. The apertures of a section with fairly constant large apertures (>5 mm) over a vertical distance of 20 images were measured by a simple line counting method: horizontal rows of pixels across the open fracture are considered, and the pixels that are clearly part of the fracture are counted. Each image has a size of ~500 × 500 pixels, and the studied section shows a length between 0.5 and 1 core diameter (30 cm) in the images. This gives us a statistical data set of 8315 samples, large enough for a geostatistical analysis. The measured apertures were observed to have a distribution strongly reminiscent of a lognormal distribution; the histogram is shown in Figure 2. This appears credible as lognormally distributed apertures are known to commonly exist in fractured rock systems (see, e.g., Bianchi and Snow 1969; Keller 1998; de Dreuzy et al. 2001b; Vandersteen et al. 2003). Our working hypothesis is therefore that this observed lognormal distribution shall also be valid for smaller fractures.

As part of a geostatistical analysis, a variogram for the measured large fracture apertures was calculated. As shown in Figure 2, a theoretical variogram model is fitted to the data, allowing us to generate any number of aperture distributions, not only with the same statistical distribution but also with the same average rate of change in aperture over a given distance.

A satisfactory fit was found to be a combination of two spherical models (nugget: 0.005; sill 1: 0.014, range 1: 0.05 m; sill 2: 0.015, range 2: 0.25 m). The two spherical models incorporated into our model variogram cannot without a doubt be connected to specific directions or fractures. The first model, with a range of 5 cm may reflect an artifact, caused by the uncertainty of the image positions along the core axis. In spite of the uncertainties, this distribution, along with the given mean of 1.3×10^{-4} m, sufficiently fixes the parameters needed to generate suitable apertures. Using sequential Gaussian simulation, we generated 50 realizations of aperture distributions for model cases A and C, one of which is illustrated in Figure 3. Apertures are binned into 100 logarithmically spaced bins, varying from a low-end cutoff of 10^{-5} m to an upper-end cutoff of 2×10^{-2} m. The upper cutoff was determined by the largest fracture aperture to be identifiable in the images, while the lower cutoff was chosen rather arbitrarily to reduce the number of sparsely filled material bins. The resulting distributions show a standard deviation of 0.80 ± 0.02 for the decadic logarithms of the

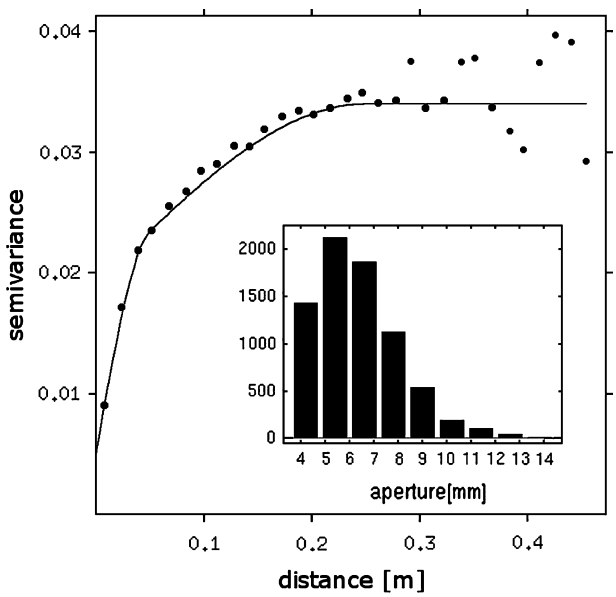

Figure 2. The variogram calculated from the sampled aperture data (circles), and the fitted theoretical variogram (solid line). Inset is a histogram of the aperture values determined from a large aperture section of a main fracture in the images.

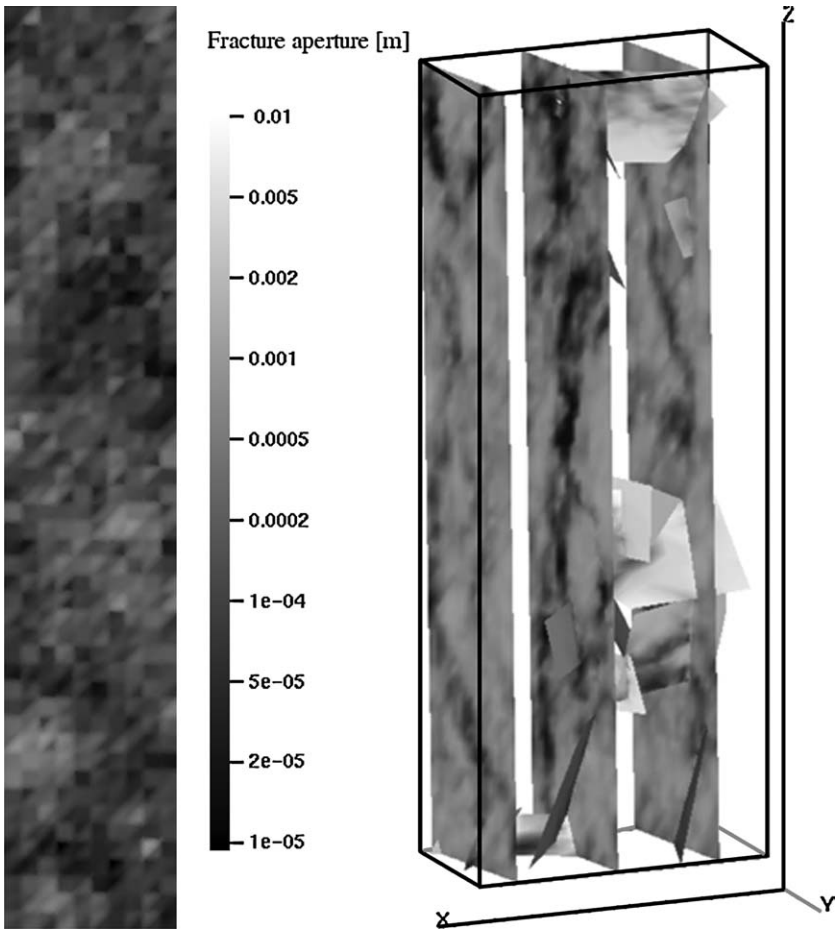

Figure 3. A realization of aperture distribution for a single main fracture (left). Gray scale represents aperture size, with light for large and dark for small apertures. The right half of the figure shows a realization of flow calculations for case C. Gray scale depicts the flow velocity in each element. Dark shades represent high velocities. It must be noted that the gray scale is overlayed by a shading effect and therefore should not be taken as an absolute measure of velocities.

apertures. It should be noted that, unlike a natural fracture, there are no elements with zero aperture. However, due to the use of a particle tracking method, a flow volume below a certain amount results in zero particles, which is equivalent to a closure point.

All geostatistical calculations were performed using R, particularly the gstat library for R (Pebesma 2004, http://www.gstat.org).

Calculations

Flow Calculations

We used Rockflow (Kolditz et al. 1999), a standard Finite Element Galerkin Solver, to solve the hydraulic equation for flow Q_f in a fracture:

$$Q_f = - T_f \nabla \tilde{\varphi} \tag{1}$$

where $\tilde{\varphi}$ is the average piezometric head across a fracture's width and T_f is the transmissivity of the fracture, determined via the cubic law (Equation 2), and thereby calculate the static flow field before turning to transport calculations.

$$T_f = \frac{\rho g}{\mu} \frac{b^3}{12} \tag{2}$$

where ρ is fluid density, g is gravitational acceleration, b is half the fracture aperture, and μ is the fluids coefficient of dynamic viscosity.

At the upper end of the models ($z = 2.8$ m), a Dirichlet boundary with constant zero hydraulic head was set as the outflow boundary. Intersections of all fractures with outside boundaries except the top and bottom were set as no-flow boundaries. The bottom boundary ($z = 0.2$ m) was set as an inflow boundary, by using a Neumann constant flow boundary (note: due to our choice of axis orientation, flow is from bottom to top). To determine a suitable flow rate at the inflow boundary, the models were first run with a Dirichlet inflow boundary of 1, representing a head difference of 1 m between inflow and outflow boundary. The total resulting influx volume was then distributed evenly among the number of vertices on the inflow boundary for the Neumann condition. This provides us with a constant and equal flux volume at each inflow node, without taking into account the variability of the apertures along the inflow boundary.

Transport Calculations

We employed a flow line following particle tracking algorithm, running on top of the hydraulic solutions, to model purely advective transport. Diffusion processes are not considered. This may lessen the degree of realism in the model as it is not equivalent to slow solute transport. It more closely resembles the fast transport of large particles with a relatively low diffusion constant. This facilitates the investigation into the mechanism of advective transport. Due to the use of a Neumann boundary with equal inflow at each node at the inflow edge, regardless of aperture, we can set the number of particles released at each inflow element edge proportional to the volume flux at that edge to achieve an equal release rate across the inflow boundary. As we also record particle arrivals at any point along the outflow edge, our transport calculations can be considered as pseudo–one dimensional (1D) even though the model geometries are not. Breakthrough curves for cases A and C were obtained by concatenating the arrival time lists of particles at the outflow boundary from the 50 realizations, and then binning them into 30 logarithmically spaced time windows. As case B has no varying aperture, a single realization was used.

Boundary Conditions

Our choice of the inflow boundary conditions may lessen the degree of realism in the model, but it also avoids some computational problems that can arise if the boundary is set using constant hydraulic heads. Foremost among these problems is the possibility of backflow due to the contrast in aperture between elements, which runs over several orders of magnitude.

In the case of elements with small apertures, this approach will cause a larger number of particles to be forced into the elements than is to be expected with a Dirichlet boundary setting. However, the velocity in these elements will also be higher than normal, causing these particles to quickly move into adjacent elements with larger apertures.

After short distances (and times), ~5% to 10% of the overall model length, the flow field has recovered from the disturbance of the flux boundary and a flow regime equivalent to one caused by a Dirichlet boundary condition has been reached. After these distances, particles are mainly contained in a number of channels. As can be seen in Figure 3, the heterogeneous velocity field has indeed normalized, and channels of higher velocities are visible, after ~15 cm.

Continuous-Time Random Walks

CTRW is an approach to modeling transport processes by representing them with a series of particle movements on a regular grid. Mathematically, CTRW performs this by numerically solving the 1D Fokker-Plank Equation with Memory for the Laplace transformed concentration $\tilde{c} = (x, u)$ in one dimension (Cortis and Berkowitz 2005):

$$u\tilde{c}(x,u) - c_0 = \tilde{M}(u)\left[v_\psi \frac{\partial}{\partial x}\tilde{c}(x,u) - D_\psi \frac{\partial^2}{\partial x^2}\tilde{c}(x,u)\right] \quad (3)$$

where

$$\tilde{M}(u) \equiv \bar{t}u\frac{\tilde{\psi}(u)}{1-\tilde{\psi}(u)} \quad (4)$$

is a memory function that accounts for the contained unknown heterogeneities. $\bar{t}$ is some characteristic time. v_ψ and D_ψ are the center of mass velocity and generalized dispersion coefficient, respectively, the details of which are discussed extensively in Dentz et al. (2004) and Cortis et al. (2004). The variable u is the Laplace variable.

The function $\tilde{M}(u)$ can take on several expressions depending on the form for $\tilde{\psi}(u)$. For the case of

$$\tilde{\psi}(u) \equiv \frac{1}{1+u} \quad (5)$$

Equation 3 reduces to the classical ADE, whereas for

$$\tilde{\psi}(u) \equiv (1+\tau_2 u t_1)^\beta \exp(t_1 u)\Gamma(-\beta, \tau_2^{-1} + t_1 u)/\Gamma(-\beta, \tau_2^{-1}), \quad 0<\beta<2 \quad (6)$$

we get a truncated power law (TPL) model, which requires the three input parameters β, t_1, and t_2 where $\tau_2 = t_1/t_2$.

The parameters t_1 and t_2 determine the upper and lower limits of the linear (on a log-log scale) or power law section of $\tilde{\psi}(u)$, whereas β determines the slope of the linear section. In addition, β determines if the flow type is Fickian ($\beta > 2$), non-Fickian ($1 < \beta < 2$), or strongly non-Fickian ($\beta < 1$).

All CTRW calculations for this project were performed using the CTRW Matlab toolbox (Cortis and Berkowitz 2005).

Advection Dispersion Equation

The ADE fits were calculated using the Matlab curve fitting tool, with the Ogata-Banks solution of the transport equation (Bear 1972)

$$C(x,t;t') = \frac{\mathrm{dM}}{[4\pi D(t-t')]^{1/2}}\exp\left\{-\frac{[x-q(t-t')/n]^2}{4D(t-t')}\right\} \quad (7)$$

where q is Darcy velocity and n is porosity, which is 1 in our case of unobstructed fractures. The total injected tracer mass dM is set as 1 to reflect our normalized breakthrough curves. This leaves us with a simplified version of

$$C(x,t) = \frac{1}{[4\pi Dt]^{1/2}}\exp\left\{-\frac{[x-Vt]^2}{4Dt}\right\} \quad (8)$$

where velocity V is q/n and $t = t'$. V and dispersion coefficient D are then obtained by fitting this equation to our breakthrough curves.

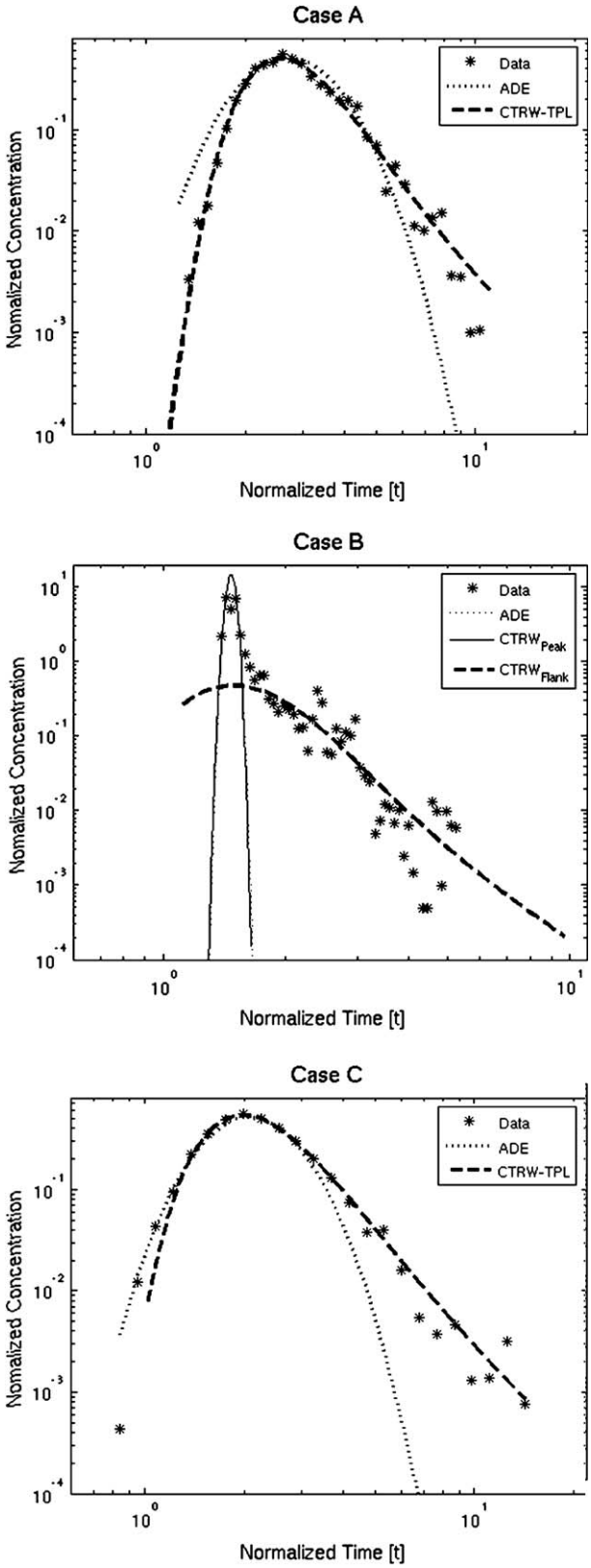

Figure 4. Comparison of fits by CTRW and ADE to the breakthrough curves. Case A shows the better fit provided by CTRW, especially for the late arrivals. Case B can be fitted only fairly well with CTRW if the whole breakthrough curve is addressed. ADE can only adequately fit the peak of case B. The CTRW fit for the peak is practically identical to the ADE fit. In case C, ADE again fits the peak well, but the tailing is represented much better with CTRW.

Results and Discussion

An important observation to be made in the results of the numerical models is the predominance of particle transport through a complex network of well-defined channels. This is in agreement with the findings of Moreno and Neretnieks (1985), Tsang and Tsang (1987), and Johns and Roberts (1991), who postulated that fluid flow should be unevenly distributed in a fracture plane with rough surfaces.

The breakthrough curves obtained via particle tracking can be observed in Figure 4, together with the fits from ADE and CTRW. All three curves show late-time tailing, which is usually considered to be typical of non-Fickian transport, and cannot be characterized by plain ADE. In order to directly compare the breakthrough curves, they must be normalized for a common Darcy flux of 1×10^{-8} m/s (fluid volume per area, where area is the fracture aperture multiplied by the width of the fracture). This is easily possible as it is evident from Equations 1 and 2 that flux, velocity, and head gradient are linearly related. To facilitate fitting by ADE and CTRW, the breakthrough curves were normalized to ensure that the peak of the case A breakthrough curve was located at $t = 2.6$ s, which gives us an average peak velocity of 1 m/s over the 2.6-m length of the models. It is evident that this normalization gives unrealistic high velocities, but due to the linear relationship in Equation 1, it is easily possible to backtransform all parameters to realistic values. In addition, the particle concentrations were normalized with the injected amount of particles to have an integral area of 1 for each curve.

For all three cases, ADE is unable to provide a satisfying fit over the whole lengths of the curves. The ADE fits to the peak regions of the curves, presented in Table 1, are good, but they cannot reproduce the late-arrival tailing. CTRW can produce a fit that takes both peak and tailing into account. Besides the difference in tailing, the CTRW fits also represent the general shape of the curves much better, especially for cases A and C. Case B proves harder to fit than cases A and C as the breakthrough curve of case B is markedly different from that of the other two. It consists of a narrow peak with

Table 1
The Values for Velocity *V* and Diffusion Coefficient *D* Obtained from the ADE Fits to the Breakthrough Curves of Cases A and C as Seen in Figure 4

	V (m/s)	*D* (m²/s)
Case A (single fracture, variable aperture)	0.93	1.1×10^{-1}
Case B (network, constant aperture)—peak	1.77	3.1×10^{-3}
Case C (network, variable aperture)	1.20	1.4×10^{-1}

only a small amount of tailing visible. We attempted to fit the peak region of case B with CTRW, and also with ADE. It is important to note that for the cases where transport is Fickian, CTRW and ADE are equivalent (Dentz et al. 2004). Further, the late-arrival flank, where non-Fickian transport is dominant, was also fitted by CTRW. However, all three fits to case B are fair at best.

In order to compare the breakthrough curves and their fits, it is necessary to consider the reasons and implications of the differences. As can be seen in Figure 3, the fracture network geometry consists mainly of three large parallel fractures, with two regions where the interconnection is substantially denser. These two "connected" regions mainly influence two of the major fractures, while flow and transport in the third major fracture is undisturbed after the initial intersection. A simple case of three parallel fractures without any interconnections would obviously result in a pulse arrival with only very little numerical diffusion. Fracture geometries consisting of multiple interconnected fractures are known to exhibit a retardation effect that also causes late-arrival tailing (Berkowitz and Scher 1998; Becker and Shapiro 2000). It stands to reason that, if isolated, the small networked region would show an answer function to a pulse tracer injection that also shows substantial tailing. The result in case B is a superposition of a typical pulse breakthrough and a breakthrough with some tailing from the geometrically complex region. As the majority of tracer particles is transported directly through the major fractures, and only a small portion enters the complex network region, the influence of the tailing is smaller than the influence of the direct pulse-like breakthrough. This larger-scale heterogeneity with regard to geometric complexity makes it impossible to find a "representative elementary volume" in this model, with all the known consequences (Berkowitz and Scher 1995); thus, a single curve cannot produce a suitable fit. Fitting two CTRW curves, as shown in Figure 4, can be interpreted as fitting either the influence of the strongly networked region (flank) or that of the regions without any strong influences from the interconnected main fractures (peak).

The introduction of variable fracture apertures has a strong impact, as can be seen when comparing case B to case C and also when considering that case A would show a simple pulse breakthrough without the varying apertures. Case C (Figure 4) shares the underlying geometry with case B, but the effect of this large-scale heterogeneity is essentially invisible due to the much stronger influence of the variable apertures. This shows that the retardation effects stemming from lengthened flow paths and/or local decreases of flow velocity, while basically comparable in function, are not present in a sufficient magnitude to present a visible impact in these models.

The fitting parameters obtained from ADE are shown in Table 1, and those from CTRW in Table 2. When comparing the values for V and D for the two approaches, it is apparent that CTRW delivers consistently higher values for V and lower values for D. This is consistent with similar cases where both types of fit have been compared (Jiménez-Hornero et al. 2005) and therefore does not seem to be an artifact of these particular two cases. The lower D returned by CTRW seems expectable, considering that in ADE, dispersion is the only component contributing to widening the breakthrough curve, whereas in CTRW, the effects of small-scale heterogeneity are also considered and incorporated in the memory term. The V parameters from CTRW and from ADE are directly comparable. Both values for V describe the average velocity, in the sense of the velocity of the center of mass of the increasingly spread out tracer cloud respectively the first spatial moment of the tracer distribution (Cortis et al. 2004).

The β parameters obtained from our fits to cases A and C (Table 2) are below 2, thus indicating non-Fickian transport. In case B, CTRW can fit either the peak, using a high value for β, thus representing Fickian transport as the ADE fit does, or the late-arrival flank, using a β below 2, representing non-Fickian transport.

When we consider our models to be "black boxes" between the two planes of inflow and outflow boundaries, the breakthrough curves are transit time distributions on a global or macroscopic scale: the distance between the boundaries. The applied finite-element method provides each model element with a fixed velocity vector. These vectors represent a velocity distribution on the scale of an individual element. By weighting the inverse of this velocity distribution with the corresponding element sizes, and with the number of particles that traversed each element, we obtained a local or microscopic transit time distribution. This distribution describe the probability of a given particle to transverse a standard element in a given time and is thus equivalent to the $\psi(t)$ function in CTRW. The local transit time distributions of all three models, shown in Figure 5, are fairly similar. On a

Table 2
The Values for Velocity V, Diffusion Coefficient D, and Fitting Parameters from the CTRW-TPL Fits to the Breakthrough Curves Seen in Figure 4. In the Case of the Peak CTRW Fit to Case B, a Non-TPL Was Used, Resulting in No Applicable Values for $t1$ and $t2$

	V (m/s)	D (m²/s)	β	$t1$ (s)	$t2$ (s)
Case A	1.34	1.19×10^{-2}	1.54	3.16×10^{-2}	1.01×10^{6}
Case B_{peak}	1.85	1.51×10^{-3}	2.0	—	—
Case B_{full}	1.72	8.30×10^{-3}	1.8	9.54×10^{-5}	3.05×10^{1}
Case C	1.24	2.45×10^{-2}	1.71	8.81×10^{-2}	9.45×10^{4}

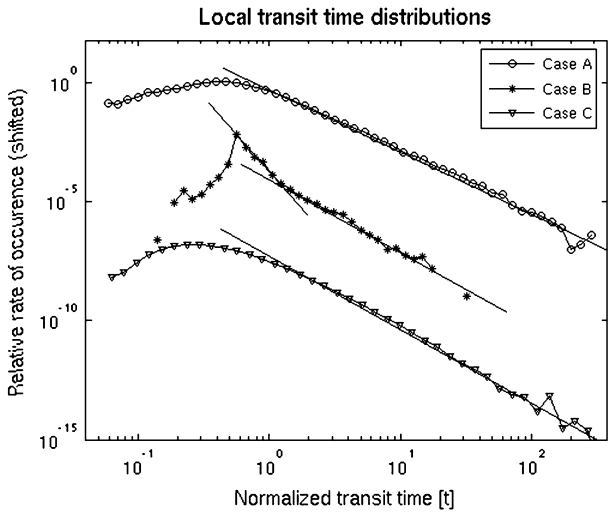

Figure 5. Microscopic or local transit time distributions of the three models. Straight lines fitted to the transit time distributions indicate the log-log slopes, with parameters presented in Table 3. Case B represents one realization, and cases A and C are stacks of 50 realizations each of which explains the smoother appearance of cases A and C. Cases B and C have been shifted along the y-axis by three and six decades, respectively, to allow for better viewing. Case B shows two linear segments, with differing slopes.

log-log scale they all have a strongly asymmetric shape; for small times they show approximately lognormal behavior, whereas for larger times, they show pronounced power law behavior. The power law slopes of the local transit time distributions as shown on a log-log scale in Figure 5 are presented in Table 3. The comparison between the slopes of the local transit distributions and the β parameters obtained from the CTRW fits provide additional evidence that an approximation of the observed transport behavior by CTRW with a TPL-determined $\psi(t)$ function is suitable in these cases. As for the TPL fits, the lower limiting time $t1$ is small and the upper limiting time $t2$ is larger by many orders of magnitude, and the fits essentially approximate the transit time distribution with a non-TPL. This is equivalent to the method using a non–TPL based $\psi(t)$ in Berkowitz et al. (2001). A $\psi(t)$ that also fits the lognormal section of the transit time distributions would be ideal; however, this approximation is considered sufficient for our purposes and is clearly superior to ADE, which is limited to exponential distributions of local transit times.

Table 3
CTRW Fitting Parameter β Compared to the Slopes of the $1/v$ Distributions Shown in Figure 5

	β	$-1-\beta$	Slope of $1/v$
Case A	1.54	−2.54	−2.53
Case B_{peak}	2.0	−3.0	−6.03
Case B_{full}	1.8	−2.8	−3.08
Case C	1.71	−2.71	−2.86

Table 4
Comparison of the Various Values for Velocity V, Which Are Obtained from the Two Fitting Procedures and from the Hydraulic Boundary Condition at the Inflow Boundary of the Models

	$V_{hydraulics}$	V_{CTRW}	V_{ADE}
Case A	1.64	1.34	0.93
Case B_{peak}	1.63	1.85	1.77
Case B_{full}	1.63	1.72	—
Case C	1.62	1.24	1.20

Besides the fitting parameters for V from CTRW and ADE, we can also calculate a flow velocity from the hydraulic boundary conditions, by simply dividing normalized flux Q by the cross-sectional area of the inflow edges. For case B, with a constant aperture of 1.3×10^{-4} m, this gives a precise calculation of the flow velocity at the inflow edge. For cases A and C, ergodicity dictates that we could also use an aperture of 1.3×10^{-4} m as this is the mean forced on the generated aperture distribution. In fact, however, the actual mean apertures over all 50 realizations of cases A and C were used (1.32×10^{-4} and 1.29×10^{-4} m, respectively). As the flux was normalized to be equal over equal inflow edge lengths, all models have a near-identical theoretical hydraulic velocity, which is compared to the velocities obtained from CTRW and ADE in Table 4.

Conclusions and Summary

We present a group of flow and transport models of varying geometric complexity, all based on the data extracted from EP.

These models all produce breakthrough curves with steep early-arrival flanks; wide, rounded peaks; and strong late-arrival tailing. Overall, these are comparable to curves obtained by transport experiments performed in situ on the rock volume described by EP.

These breakthrough curves cannot be fitted satisfactorily by the classical transport equation; they can, however, be fitted very well by CTRW. The fact that the breakthrough curve from case B cannot be fitted even with CTRW stems from the larger-scale geometric heterogeneity. A larger model, taking into account the statistical relevance of such "networked" areas, or a similar-sized model with additional smaller-scale geometric heterogeneities may provide a better approach for this case.

CTRW can be linked with the numeric transport models via the relationship between local transit time distributions, which directly portray the heterogeneity in fracture aperture and geometry, and $\psi(t)$, which describes the duration of the CTRW "hops." This indicates that it is conceivable to make limited predictions about transport behavior for a model case where nothing more than the local velocity distribution is known.

Comparison of our three models shows that the impact of varying fracture apertures on transport behavior is larger than that of the network geometry. However, a more

complex fracture network geometry would also have a larger impact on the velocity distribution, also leading to a widening of the breakthrough curves. Additional models, incorporating another "layer" of geometric complexity, on a smaller scale remain as a future task that promises better quantification of the role of network geometry.

Compared to the actual network structure studied in EP, our results are based on oversimplified fracture network geometries. Especially, the low complexity of the macroscopic heterogeneity presented by the network structure of the model does not allow us to fully quantify the possible influence of this characteristic on the breakthrough curves. They can offer no quantitative information about the roles of fracture aperture and network complexity in the EP transport experiments. It does, however, seem clear that both factors have the potential to enhance tailing in breakthrough curves. In the light of these results, the hypothesis presented by Kosakowski (2004) that certain tracers may show long late-arrival tailing caused by geometric complexity and small-scale heterogeneities, and not by matrix diffusion, seems very credible.

The main drawback of our scenarios is the lack of representation of diffusion processes. In a follow-up project, it is intended to include and investigate the influence of both chemical diffusion (from one flowpath to another) and diffusion into an adjacent porous rock (matrix diffusion).

Acknowledgments

Thanks to NAGRA (CH) and JAEA (J) for providing the initial data set. Further thanks to Walter Heer, Andreas Jakob, Wilfried Pfingsten, and Jörg Hadermann for helpful hints and discussion throughout the project, and to Brian Berkowitz and Andrea Cortis for help concerning CTRW theory. Also, the authors would like to thank Alan Shapiro, Gennady Margolin, and two anonymous reviewers for helpful critique and suggestions. Last but not least, many thanks to Bill Dershowitz and Golder Inc. for providing us with an academic license for their FracXP software package.

References

Alexander, W.R., K. Ota, and B. Frieg. 2003a. The Nagra-JNC in situ study of safety relevant radionuclide retardation in fractured crystalline rock II. Nagra Technical Report 00-06. Wettingen, Switzerland: Nagra.

Alexander, W.R., P.A. Smith, and I.G. McKinley. 2003b. Modeling radionuclide transport in the geological environment: A case study from the field of radioactive waste disposal. In *Modelling Radioactivity in the Environment*, ed. E.M. Scott, chap. 5, 109–145. Amsterdam, The Netherlands: Elsevier.

Backblom, G. 1998. Progress towards a deep repository for spent nuclear fuel in Sweden. *Journal of Nuclear Science and Technology* 35, 623–630.

Bear, J. 1972. *Dynamics of Fluids in Porous Media*. New York: American Elsevier Publishing Company Inc.

Becker, M.W., and A.M. Shapiro. 2000. Tracer transport in fractured crystalline rock: Evidence of nondiffusive breakthrough tailing. *Water Resources Research* 36, no. 7: 1677–1686.

Berkowitz, B., G. Kosakowski, G. Margolin, and H. Scher. 2001. Application of continuous time random walk theory to tracer test measurements in fractured and heterogeneous porous media. *Ground Water* 39, no. 4: 593–604.

Berkowitz, B., and H. Scher. 1998. Theory of anomalous chemical transport in random fracture networks. *Physical Review E* 57, no. 5: 5858–5869.

Berkowitz, B., and H. Scher. 1997. Anomalous transport in random fracture networks. *Physical Review Letters* 79, no. 20: 4038–4041.

Berkowitz, B., and H. Scher. 1995. On characterization of anomalous dispersion in porous and fractured media. *Water Resources Research* 31, no. 6: 1461–1466.

Bianchi, L., and D.T. Snow. 1969. Permeability of crystalline rock interpreted from measured orientations and apertures of fractures. *Annals of Arid Zone* 8, no. 2: 231–245.

Biggin, C., A. Möri, W.R. Alexander, K. Ota, B. Frieg, W. Kickmaier, and I.G. McKinley. 2003. In situ radionuclide retardation in groundwater conducting systems: Overview of the research carried out at Nagra's Grimsel test site, central Switzerland. In *Environmental Radiochemical Analysis II*, ed. P. Warwick, 207–228. London, UK: RSC.

Bossart, P., and M. Mazurek. 1991. Structural geology and water flow-paths in the migration shear zone. NAGRA Technical Report 91-12. Wettingen, Switzerland: NAGRA.

Cacas, M.C., E. Ledoux, G. De Marsily, B. Tillie, A. Barbreau, E. Durand, B. Feuga, and P. Peaudecerf. 1990. Modeling fracture flow with a stochastic discrete fracture network: Calibration and validation 1. The flow model. *Water Resources Research* 26, no. 3: 479–489.

Cortis, A., and B. Berkowitz. 2005. Computing "anomalous" contaminant transport in porous media: The CTRW Matlab toolbox. *Ground Water* 43, no. 6: 947–950.

Cortis, A., C. Gallo, H. Scher, and B. Berkowitz. 2004. Numerical simulation of non-Fickian transport in geological formations with multiple-scale heterogeneities. *Water Resources Research* 40, no. 3: W04209.

de Dreuzy, J., P. Davy, and O. Bour. 2001a. Hydraulic properties of two-dimensional random fracture networks following a power law length distribution, 1. Effective connectivity. *Water Resources Research* 37, no. 8: 2065–2078.

de Dreuzy, J., P. Davy, and O. Bour. 2001b. Hydraulic properties of two-dimensional random fracture networks following a power law length distribution, 2. Permeability of networks based on lognormal distribution of apertures. *Water Resources Research* 37, no. 8: 2079–2095.

Dentz, M., A. Cortis, H. Scher, and B. Berkowitz. 2004. Time behavior of solute transport in heterogeneous media: Transition from anomalous to normal transport. *Advances in Water Resources* 27, no. 2: 155–173.

Dershowitz, W.S., and C. Fidelibus. 1999. Derivation of equivalent pipe network analogues for three-dimensional discrete fracture networks by the boundary element method. *Water Resources Research* 35, no. 9: 2685–2692.

Endo, H.K., J.C.S. Long, C.R. Wilson, and P.A. Witherspoon. 1984. Model for investigating mechanical transport in fracture networks. *Water Resources Research* 20, no. 10: 1390–1400.

Enescu, N., T. Ahokas, E. Heikkinen, and C. Cosma. 2004. Integrated geophysical characterization of a hard rock site for nuclear waste disposal. In *EAGE 66th Conference & Exhibition*, EAGE, Paris, France, CD-ROM.

Geckeis, H., T. Schaefer, W. Hauser, Th. Rabung, T. Missana, C. Degueldre, A. Möri, J. Eikenberg, T. Fierz, and W.R. Alexander. 2004. Results of the colloid and radionuclide retardation (CRR) experiment at the Grimsel Test Site (GTS), Switzerland—Impact of reaction kinetics and speciation on radionuclide migration. *Radiochim Acta* 92, no. 9: 9–21.

Geiger, S., S. Roberts, S.K. Matthäi, C. Zoppou, and A. Burri. 2004. Combining finite element and finite volume methods for efficient multiphase flow simulations in highly heterogeneous and structurally complex geologic media. *Geofluid* 4, no. 4: 284–299.

Hadermann, J., and W. Heer. 1996. The Grimsel (Switzerland) migration experiment: integrating field experiments, laboratory

investigations and modeling. *Journal of Contaminant Hydrology* 33, no. 8: 87–100.

Heer, W., and P.A. Smith. 1998. Modeling the radionuclide migration experiments at Grimsel. What have we learned? In *Materials Research Society Symposium Proceedings* 506, 663–670. Pittsburgh, Pennsylvania.

Hsieh, P., S.P. Neuman, G.K. Stiles, and E.S. Simpson. 1985. Field determination of the three-dimensional hydraulic conductivity tensor of anisotropic media, 2. Methodology and application to fractured rocks. *Water Resources Research* 21, no. 11: 1667–1676.

Jakob, A., M. Mazurek, and W. Heer. 2003. Solute transport in crystalline rocks at Äspö—II: Blind predictions, inverse modeling and lessons learnt from test STT1. *Journal of Contaminant Hydrology* 61, no. 2: 175–190.

Jiménez-Hornero, F.J., J.V. Giráldez, A. Laguna, and Y. Pachepsky. 2005. Continuous time random walks for analyzing the transport of a passive tracer in a single fissure. *Water Resources Research* 41, no. 10: W04009.

Johns, R.A., and P.V. Roberts. 1991. A solute transport model for channelized flow in a fracture. *Water Resources Research* 27, no. 8: 1797–1808.

Keller, A. 1998. High resolution, non-destructive measurement and characterization of fracture apertures. *International Journal of Rock Mechanics and Mining Sciences and Geomechanics Abstracts* 35, no. 8: 1037–1050.

Kolditz, O., R. Kaiser, D. Habbar, T. Rother, and C. Thorenz. 1999. *ROCKFLOW—Theory and Users Manual, Release 3.4*, Groundwater Modeling Group, Institut für Strömungsmechanik und Elektronisches Rechnen im Bauwesen der Universität Hannover. Hannover, Germany: University of Hannover.

Kosakowski, G. 2004. Anomalous transport of colloids and solutes in a shear zone. *Journal of Contaminant Hydrology* 72, no. 1–4: 23–46.

Kosakowski, G., B. Berkowitz, and H. Scher. 2000. Analysis of field observations of tracer transport in a fractured till. *Journal of Contaminant Hydrology* 47, no. 2: 29–51.

Long, J.C.S., J.S. Remer, C.R. Wilson, and P.A. Witherspoon. 1982. Porous media equivalents for networks of discontinuous fractures. *Water Resources Research* 18, no. 3: 645–658.

Lunati, I., W. Kinzelbach, and I. Sørensen. 2003. Effects of pore volume-transmissivity correlation on transport phenomena. *Journal of Contaminant Hydrology* 67, no. 1–4: 195–217.

Maloszewski, P., and A. Zuber. 1993. Tracer experiments in fractured rocks: Matrix diffusion and the validity of models. *Water Resources Research* 29, no. 8: 2723–2735.

Moreno, L., and I. Neretnieks. 1985. Analysis of some laboratory tracer runs in natural fissures. *Water Resources Research* 21, no. 7: 951–958.

Moreno, L., W. Tsang, C.F. Tsang, F.V. Hale, and I. Neretnieks. 1988. Flow and tracer transport in a single fracture: A stochastic model and its relation to some field observations. *Water Resources Research* 24, no. 12: 2033–2048.

Möri, A. 2003. The CRR final project report series: 1. Description of the field phase—Methodologies and raw data. Nagra Technical Report NTB 03-01. Wettingen, Switzerland: Nagra.

Oron, A.P., and B. Berkowitz. 1998. Flow in rock fractures: The local cubic law assumption reexamined. *Water Resources Research* 34, no. 11: 2811–2825.

Ota, K., A. Möri, W.R. Alexander, B. Frieg, and M. Schild. 2003. Influence of the mode of matrix porosity determination on matrix diffusion calculations. *Journal of Contaminant Hydrology* 61, no. 1–4: 131–145.

Park, J., K. Lee, G. Kosakowski, and B. Berkowitz. 2003. Transport behavior in three-dimensional fracture intersections. *Water Resources Research* 39, no. 8: 1215.

Pebesma, E.J. 2004. Multivariable geostatistics in S: The gstat package. *Computers & Geoscience* 30, 683–691.

Sidle, R.C., B. Nilsson, M. Hansen, and J. Frederica. 1998. Spatially varying hydraulic and solute transport characteristics of a fractured till determined by field tracer tests, Funen, Denmark. *Water Resources Research* 34, no. 10: 2515–2527.

Smith, P.A., W.R. Alexander, W. Heer, T. Fierz, P.M. Meier, B. Baeyens, M.H. Bradbury, M. Mazurek, and I. McKinley. 2001. The Nagra-JNC in situ study of safety relevant radionuclide retardation in fractured crystalline rock, I: Radionuclide Migration Experiment—Overview 1990-1996. Nagra Technical Report NTB 00-09. Wettingen, Switzerland: Nagra.

Tsang, Y.W., and C.F. Tsang. 1987. Channel model of flow through fractured media. *Water Resources Research* 23, no. 3: 467–479.

Vandersteen, K., J. Carmeliet, and J. Feyen. 2003. A network modeling approach to derive unsaturated hydraulic properties of a rough-walled fracture. *Transport in Porous Media* 50, no. 3: 197–221.

Comput Geosci
DOI 10.1007/s10596-006-9032-8

ORIGINAL PAPER

Geometric modelling and object-oriented software concepts applied to a heterogeneous fractured network from the Grimsel rock laboratory

Thomas Kalbacher · Ralph Mettier · Chris McDermott · Wenqing Wang · Georg Kosakowski · Takeo Taniguchi · Olaf Kolditz

Received: 3 April 2006 / Accepted: 21 September 2006

Abstract Discrete fracture network simulations are computationally intensive and usually time-consuming to construct and configure. This paper presents a case study with techniques for building a 3D finite element model of an inhomogeneous fracture network for modelling flow and tracer transport, combining deterministic and stochastic information on fracture aperture distributions. The complex intersected fractures represent a challenge for geometrical model design, mesh quality requirements and property allocations. For the integrated and holistic modelling approach, including the application of numerical and analytical simulation techniques, new object-oriented concepts in software engineering are implemented to ensure a resourceful and practicable software environment.

Keywords fracture apertures · fractured network · geometric modelling · geostatistics · mesh quality · object orientation

T. Kalbacher · C. McDermott · W. Wang · O. Kolditz
Center for Applied Geoscience, University of Tübingen, Tübingen, Germany

R. Mettier · G. Kosakowski
Paul Scherrer Institut, Villigen PSI, Switzerland

T. Taniguchi
Graduate School of Environmental Science, Okayama University, Japan

T. Kalbacher (✉)
Center for Applied Geoscience (ZAG), Sigwartstr. 10, D-72076 Tübingen, Germany
e-mail: thomas.kalbacher@uni-tuebingen.de

1 Introduction

After long-standing research, understanding flow and transport processes in natural fractured rocks remains a challenging task. This is mainly due to the geometric complexity, the scale dependence, strongly varying fracture properties and the interaction of multiple-scale features and processes that influence the flow and transport characteristics of fractured rocks. Fields of applications include the oil industry, deep geological repositories for toxic or radioactive waste, utilisation of geothermal energy and CO_2 sequestration. Predictive modelling of flow and transport in fracture networks is vital for realistic long-term management of the systems in question.

A major step for fracture network development and application includes the conceptualisation and preprocessing of the input data. This comprises the design of the conceptual model, cleaning of the geometric data, meshing of the geometry in a quality that is adequate for the specific finite element (FE) model and methods to assign physical properties and parameters. The preprocessing is very often the most time-consuming task in the modelling chain, and the limited ability of specific software tools necessitates conceptual simplifications. In most applications, fracture network geometries must be strongly simplified, as only a limited amount of information about the actual network geometry is available. Determining the actual position of fractures in an *in situ* rock volume is possible only for major fractures on the scale of decameters and above [17], or otherwise for small laboratory-scale rock samples. Geological evidence, however, constantly reminds us that natural fracture networks do not show much similarity to simplified models, and are often dominated by millimeter aperture fractures running over lengths of centimeter to tens

of meters [43]. The increasing demand of more detailed, more complex, and therefore more realistic conceptual models for fractured networks requires the development of new methods to design and discretise the geometric model.

In general, two basic "end" concepts exist for the numerical modelling of fractured rocks: discrete fracture models and continuum models. Different types of discrete fracture models are described and applied first, e.g. by Brown and Scholz [8], Moreno et al. [41] and Tsang [50]. Some of the standard methods include simplifying the fracture network geometry to either an equivalent porous medium or a single fracture [34, 36, 41, 45]. Others combine the fracture network geometries to a network of tubes [4, 9, 16, 14], or as an ensemble of a few clearly determined and well-defined fractures [31, 37]. A holistic approach combining the benefits of discrete and continuum models is to use a hybrid approach [23] based on the architectural elements of the deposits being modelled, for instance the definition of geomechanical facies [39].

The influence of small-scale heterogeneities, like fracture surface roughness or fracture aperture variations, has been shown to be a significant factor affecting the flow and transport within fractures. In fracture network models, the individual fracture apertures may be considered as constant [12], or described with a geostatistical distribution, e.g. a lognormal distribution or fractal-based distribution [38, 42]. Such realistic-seeming fracture networks can be generated with statistical approaches, such as are applied by 'FracXP' software package from Golder Associates [15]. They can be conditioned to previously known information, such as fracture traces on the boundary surfaces of the studied rock volume, or borehole logs. Often, these generated fracture networks avoid sharp angles at fracture intersections, multiple intersections with small separations and generally numerically difficult geometries. This provides an advantage for the domain discretisation, but maybe oversimplifies the conceptualisation.

Most often, discrete FE models are used to deal with complex fractured network geometries. Some recent approaches include 2D fractures in 3D volume with power-law distributed fracture sizes [30, 42], or 2D fracture networks with power-law distributed fracture lengths [14]. Also, a combination of 1, 2 and 3D elements to model 2D fractures in 3D porous media can be applied [47]. The complexity of the conceptual model depends on the content and quality of the base dataset, the requirements of the modelling code, the actual requirements and constraints of chemical and/or physical processes and features under investigation. Additionally, the accuracy of the conceptual model depends on the quantity and quality of the computer-aided methods for the model design. A synchronized development of all these components is required to increase the potential geometric complexity and ensure the applicability of the FE model. A clearly structured and object-oriented software environment supports the task of such coordinated and balanced software developments. Here the procedures to set up a realistic and complex fracture network model for mass transport calculations taking into account processes on several scales is presented. This requires the following:

- Measurements of discrete fracture data and the model concept for application-oriented conceptualisation (Section 2).
- A well-organized code structure is needed which enables a transparent administration of the source code for a group of natural scientists and/or engineers (Section 3).
- Geometric model design: Robust calculations of the intersections between multiple fractures are used but the reliability of the results varies. Analyzing and cleaning of geometry is needed to ensure the suitability of the conceptual model (Section 4).
- Dedicated mesh generation techniques, which must take the fracture intersections as well as topologic and geometric relationships into account (Section 5).
- Physical assignments: The increasing demand for more detailed three-dimensional fracture network models as well as the permanent extension of models by introduction of new physical processes can lead to large mesh constructs, which are no longer visually controllable for manual parameter and property allocation. We suggest performing the management of these datasets, e.g. boundary conditions, by use of geometric information from the initial conceptual model (section 6).
- Information about the fracture aperture distribution: Fracture apertures can vary, and measured distributions are often not or only insufficient available for geostatistical procedures. However, the fracture aperture distribution needs direct linking to the finite element mesh (Section 6).

2 Dataset and model concept

The procedures described in this paper are demonstrated by using detailed experimental information gained from the excavation project at Nagra's Grimsel Test Site (Switzerland) [2]. In this project, comprehensive data has been gained on the fracture geometry and the flow and transport characteristics of a 2-m-long *in situ* section of a shear zone. Initially, a number of radionuclide transport tracer experiments were performed on the shear zone followed by impregnation of the fracture network with fluorescent resin. Subsequent overcoring parallel to the main flow direction, and extraction of the resulting large diameter cores enabled a

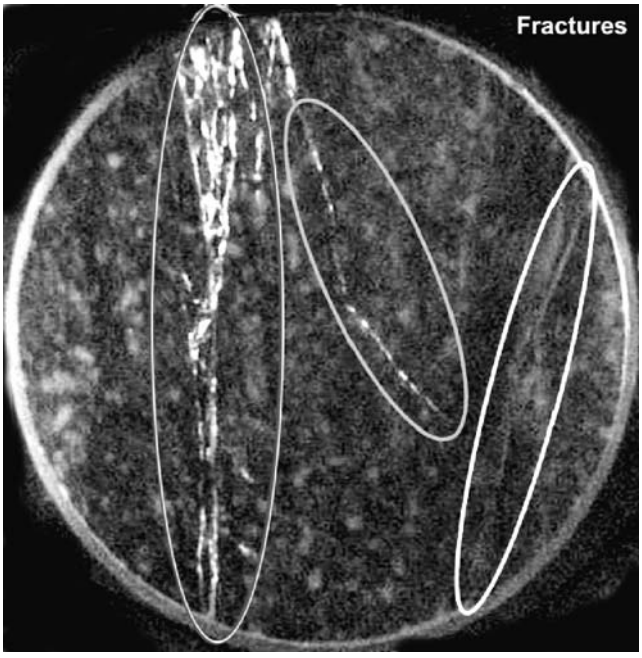

Figure 1 Ultraviolet photography of a core slices obtained from the excavation project (Ø ~ 30 cm). Located fractures are circled [40].

significant percentage of the rock volume involved in the flow and transport tests to be sliced and photographed in visible and ultraviolet light (figure 1). The resulting set of digital images presents a unique view of the interior structure of such a fracture network. From this dataset, a geometric model of the fracture network can be reconstructed. Although this is still a simplification, such a model shows a strong similarity to the actual fracture network, as far as positioning and dimensions of major fractures is concerned. Further small heterogeneities, such as fracture apertures, may also be extracted from the images, and adapted to the geometric model by geostatistical methods [40]. The appeal of performing numerical flow and transport calculations on such a model is obvious, but the near-realistic geometric properties also create significant difficulties as far as pre-processing is concerned.

2.1 Dataset: determination of fracture geometry

Sequential viewing of the cross-section images allows the three-dimensional geometry of the fractures to be determined [3]. The fractures were designed by the use of all images and the definition of 3–10 points for each visible fracture section. The best-fitting planar surfaces through each fracture point cloud define the spatial fracture geometry. In the studied rock volume, three major fractures can be identified, approximately parallel to the extracted core axis. Nineteen further large fractures can be extracted, providing a degree of interconnection between the three main fractures. Additionally, a large number of very small fractures and other small features (e.g. fracture-filling fault gouge) can be identified. These are, however, neglected in the model geometry because their extent and shape are not clearly identifiable due to the limited image resolution.

2.2 Overview of the geometric and physical model concepts

All modelling studies rely on a logical simplification of the system. Numerical methods can be used to predict the interaction of various physical processes. However, the more detailed the system is modelled, the more complex the solution procedure becomes and the more time-consuming are the calculations. Based on fracture network geometry measurements and aperture distributions [40], two scales of fracture network modelling are addressed.

1. The macro scale provides the three-dimensional representation of the 2D planes in 3D space. The fractures are approximated by triangular finite elements. In this way, the large-scale features of geometry and the interconnectivity of the fractures in the fracture network can be represented.
2. At the micro scale, different fracture apertures are mapped to material properties of individual triangular finite elements. Thereby, according to a certain estimated fracture aperture at a certain locality, the element representing that locality is mapped with a material property (in this case, permeability). At the micro scale, the relationship between the fracture aperture and the intrinsic permeability is given over the cubic law [55]. Using the value of hydraulic conductivity K (m s^{-1}), for the fracture elements, and groundwater head h (m), allows the hydraulic mass balance equation to be written as

$$S\frac{\partial h}{\partial t} - \mathrm{div}(K\,\mathrm{grad}\,h) = Q \tag{1}$$

where S is the storage (m), t is time and Q is the volume flux (m^3 s^{-1}). The solution of this equation using the finite element technique is covered in standard works such as [24, 26, 56]. Solving Eq. (1) provides the fluid head at each discrete node in the FE model, which then can be interpolated for the elements and converted into flow velocities v (m s^{-1}) in the elements.

The flow velocities are then used to derive the solution of the mass transport Eq. (2) [10].

$$\frac{\partial C}{\partial t} - \mathrm{div}(\mathbf{D}\,\mathrm{grad}C) + v\cdot\mathrm{grad}\,C = C_s \tag{2}$$

Here, C is the concentration of the compound (kg m^{-3}) under investigation and D represents the effective diffusion

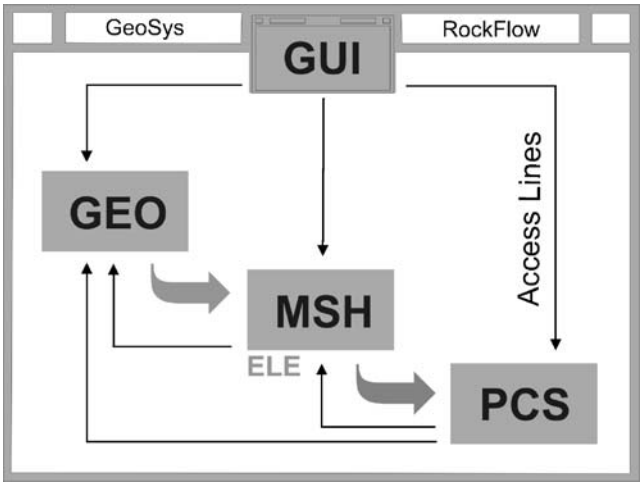

Figure 2 General concept of the object-oriented structure of GeoSys shows the four main object libraries and their access permission.

coefficient depending on the media ($m^2\ s^{-1}$) [21]. The term C_s refers to a source term (kg $m^{-3}\ s^{-1}$).

The transport of tracers in fractured media is governed by advective, diffusive, and dispersive mechanisms [18]. All these transport phenomena occur in the fractures and in the rock matrix. Several approaches allow the calculation of contaminant and heat transport in fractured media involving the diffusive exchange processes between water flowing through fractures and the rock matrix, known as matrix diffusion [44]. Analytical solutions can be applied to simple geometries such as single fractures or parallel fracture arrays [10, 32]. An excellent overview on analytical solutions for mass and heat transport analysis of porous media is given by Häfner et al. [22]. For the more complicated systems, analytical models can help to understand the interaction of the various processes, but numerical models are necessary for predictive modelling. For numerical analysis, stability criteria play an important role in ensuring the accuracy of the solution of the mass balance equations. One method for increasing the time efficiency and avoiding some stability problems is to include analytical solutions to describe diffusion-dominated processes.

Here, a hybrid approach to matrix diffusion is applied to remove the need to discretise the rock mass between the fractures. This significantly increases the efficiency of the modelling technique. The matrix diffusion of the tracer material is represented by an analytical source term, which takes into account the history of the concentration of the tracer passing the element in the fracture. Deriving from [22] the source term can be shown to be given by

$$C_s = \left[\sum_2^n \left[erfc\left(\frac{x}{2\sqrt{D_{app}(t_0 - t_{n-1})}}\right) - erfc\left(\frac{x}{2\sqrt{D_{app}(t_0 - t_n)}}\right) + erfc\left(\frac{x}{2\sqrt{D_{app}(t_0 - t_1)}}\right)\right]\right] 2AD_e \tag{3}$$

where n is the number of time steps prior to the current time step to be taken into account, A is the area of the fracture surface represented by the finite element node to which the source term is applied, D_e is the effective diffusion coefficient and D_{app} the apparent diffusion coefficient of the tracer in the matrix [21]. Using this approach, the matrix diffusion for non-sorbing and linear sorbing species can be calculated and is formulated here for a single-phase system. Details of the derivation and application of this solution will be given in a forthcoming report.

3 Software concept

This article gives a brief overview of the object-oriented procedures and implementations of the different objects. The illustrated methods and procedures of the next articles exemplify the need of a robust software concept to manage the use of new or improved software developments for FE modelling and preprocessing.

With the increasing requirements for the model design, comprehensive spatial data density with detailed property assignments and improved numerical approximations, object-oriented programming becomes increasingly important, especially in the context of complex natural environmental systems. A continual well-organized development of new methods for the fractured network model design, mesh generation and process data administration requires an efficient object-oriented code structure, which makes a transparent management of the source code for a group of natural scientists and/or engineers possible.

The concept of the GeoSys/RockFlow software development is based on object-oriented methods [26, 53] (figure 2) to achieve these aims. This guarantees a maximum reusability of all program components, helps to maintain the code structure, and enables continuous program development as well as an easy implementation of new functions.

3.1 Libraries

The object-oriented concept of GeoSys/RockFlow is the fundamental base for a stable interaction between geometric model design, meshing tools, visualisation, model admin-

istration and simulation. This assures flexibility and agility of the software development and allows fast rearrangement and optimisation, when new methods or processes are to be included. Four main object libraries, with geometric objects (GEO), mesh objects (MSH), process objects (PCS) and the graphical user interface (GUI), form the GeoSys/RockFlow software (figure 2). Unambiguous rules for the interacting data access of all four main object libraries are required to maintain these advantages.

The graphical user interface (GUI) is needed for 3D visualisation methods as well as for interactive control of geometric model design, meshing, physical assignments and process related administrations. Therefore, it is the only object, which can access to all object information.

The GEO has an internal topologic arrangement [11, 25] and includes data and methods for geometric points, polylines, surfaces, and volumes of the model domain. The geometric methods assign the options for the model design and its complexity. The GEO object is completely independent in its functionality and forbids the access to the other objects but allows unrestricted external access.

The mesh object (MSH) contains several mesh generators, mesh improvement methods, the mesh quality analyzing functions and uses GEO data structures as input. Consequently, it needs the full access to GEO data structures. The core component of the mesh object is the element object (ELE), described in the next section. The element data, such as geometrical and topological properties, as well as numerical operations of elements, like element matrix calculations and treatment of boundary conditions, are universally structured. The element object is also a fundamental entity for solving partial differential equations (PDE).

The process object (PCS) contains the numerical solvers, the equation system object, time step schemes, and all other process related methods. PCS can also be classified as the kernel of the simulator and it shows an internal object-oriented order [27]. The PCS needs access to MSH and to GEO. The central idea behind object orientation of processes is that the basic steps of the solution procedure – calculation of element contributions, assembly of equation system, solution of the equations system, linearisation methods and calculation of secondary variables – are independent of the specific problem [27, 28].

3.2 Element concept

The first step of finite element analysis is the domain discretisation and the construction of element meshes. The geometric element objects, one for each geometric element type (e.g. tetrahedra, cube, prism, etc.), are the basis of the element concept and their entities form the meshes. The finite element matrices for different PDEs are computed and the corresponding shape function is automatically selected according to its geometric element type. Finally, PCS objects assemble the equation systems for the problem type, in the case study presented here, the transport problems for fractured networks. The idea of the concept [53] is that specific, process-related information are introduced as late as possible to keep the software concept as clear and as flexible as possible.

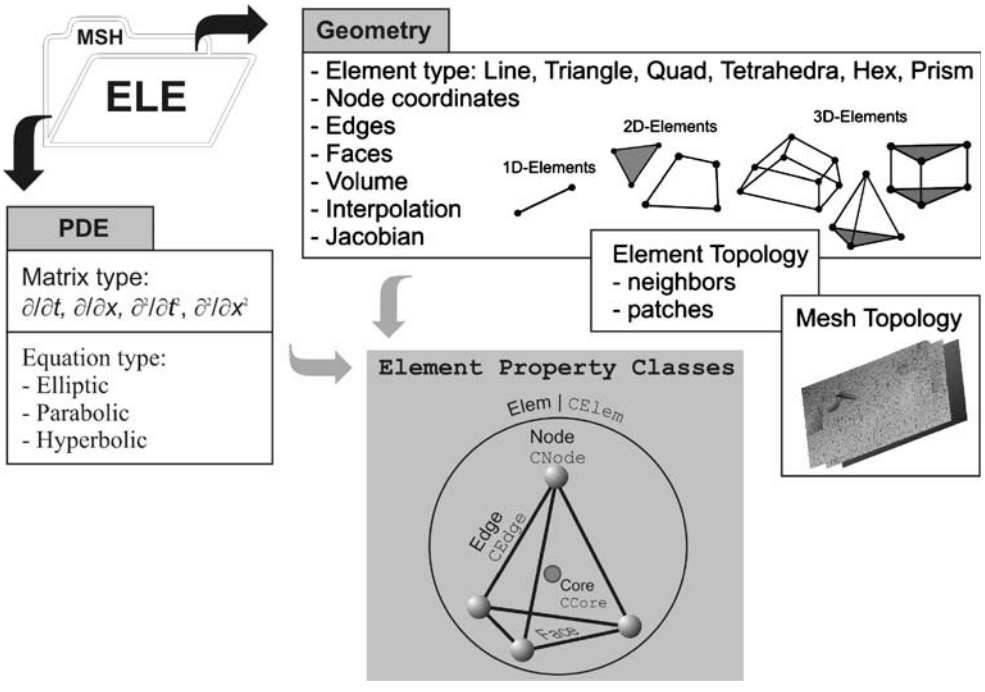

Figure 3 Geometry and PDE relation of the ELE object with the element property classes.

Figure 3 illustrates the concept of the element object. The element geometry includes the type specification (line, triangle, quad, tetrahedron, prism and hexahedron), the node coordinates, topological information of edges and faces, as well as volume quantification. Coordinate transformation functionalities are defined as geometric element properties, and neighbourhood relations of the elements define the element topologies, which are a function of the mesh topology.

The following four element property classes (figure 3) are designed to encapsulate all geometric and topological element information.

- The *CCore* class is abstracted as the base class of *CNode*, *CEdge* and *CElem*, and it contains common required data and methods.
- The *CNode* class is derived from the CCore class. The *CEdge* and *CElem* class are set as friend classes of *CNode* so that they can access to *CNode* private members directly. The *CNode* class provides the geometrical position of an element in real space and keeps the information which and how many elements use the particular mesh nodes. This node–element relationship contains very important information of the mesh topology, which is required, e.g. for mesh quality inspection, for extrapolation of Gauss point values to node values or for projecting element properties to nodes. It is organized as an own vector construct and the direct accessibility accelerates the topological methods.
- The *CElem* class represents an individual element of a mesh and it is derived from the *CCore* class. The node and edge class construct the element class. The *CElem* class is designed for the different geometric element types of lines, triangles, quadrilaterals, triangle-based prisms, tetrahedrons and hexahedrons.
- The *CEdge* class is derived from the CCore class. The edges construct the frame of a geometric element object and are frequently used as basic properties for mesh generation or mesh improvement methods. It is sufficient to use two nodes to form a geometric edge, but for higher-order finite elements, more points are required along an edge. In particular, the higher-order finite elements require edges through all computations. Therefore, we use a vector construct of *CNode* pointers as class member for all edge nodes. However, for node-based finite elements (i.e., linear interpolation), edges are only used to compute topological mesh structure and need not to be stored for later computations.

Element property numbers (element patch indices) are available for physical assignments and flux calculations. Depending on PDE type (elliptic, parabolic, hyperbolic,

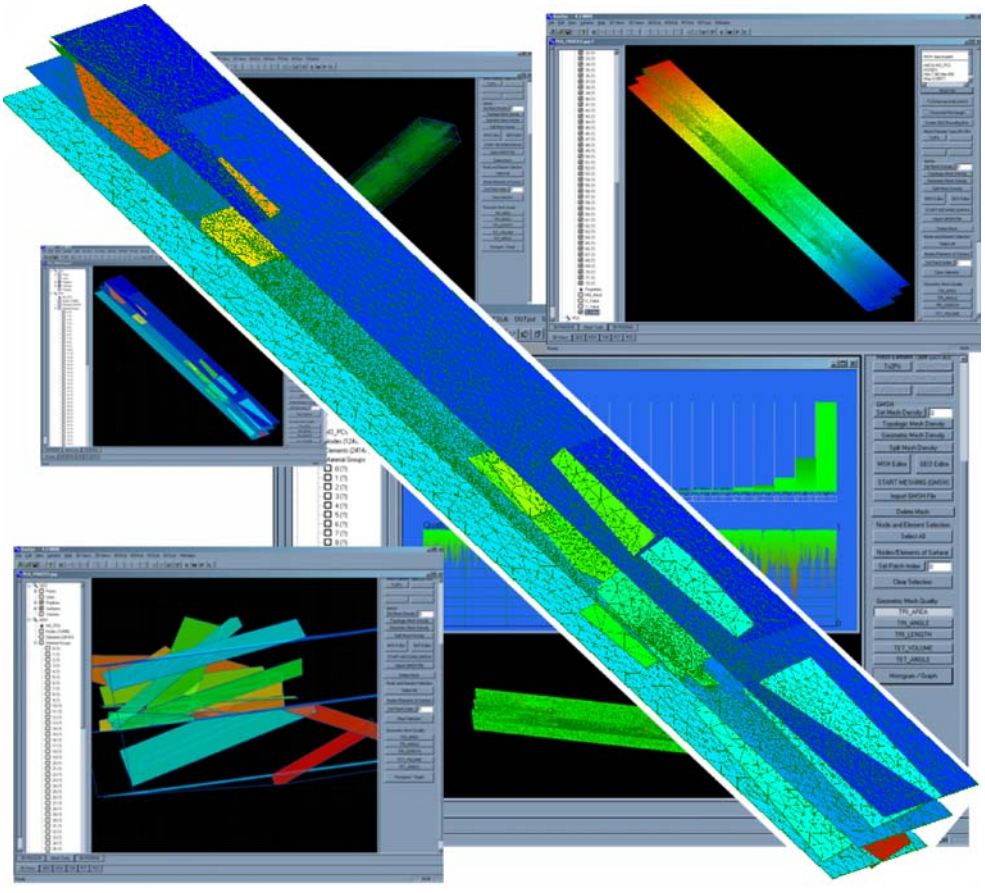

Figure 4 Visualization of the fracture network. Left: geometric input data visualization of polygons and surfaces. Top: view of mesh and result of a test run. Right: mesh quality analysis. Middle: triangulated network with patch index distribution.

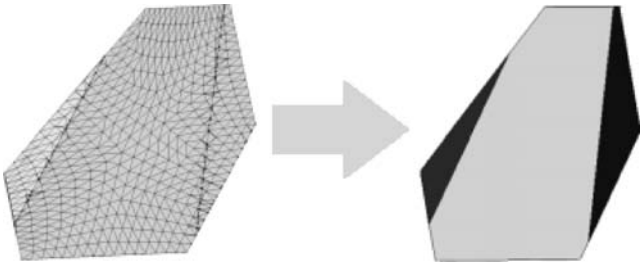

Figure 5 The original fracture plane is split into three polygons, which are then imported in GeoSys.

mixed), different first- or second-order differential terms can be evaluated ($\partial/\partial t$, $\partial/\partial x$; $\partial^2/\partial^2 t$; $\partial^3/\partial^3 x$). These differential terms are categorized in corresponding finite element matrix types: mass matrix, advection, dynamic, Laplacian matrix, tangential matrix and coupling matrixes. The major advantage of this approach is that element operations such as interpolations (shape functions) and derivations as well as tensor operations and Gaussian integrations can be conducted by considering the geometric element types only.

The presented object-oriented concept provides an efficient coding environment for geometric methods, mesh generation, mesh inspection and property assignment techniques. The following sections illustrate such procedures, which were essentially developed for the construction of the fracture network model.

4 Geometric modelling

The fractures extracted from the rock cores (see Section 2.1) provide the first geometric input data concerning fracture orientation and intersections. Subsequently, all fractures are approximated as planar surfaces. Next, intersections are calculated, followed by the segmentation of the surfaces into interconnected polygons. When dealing with a number of intersecting planar fractures, it is necessary to ensure a consistent geometry by checking the geometric and topological relationships of all geometric objects, such as points, polylines and surfaces, and to eliminate geometric conflicts. Modifications and extensions of the geometric input data are needed to make the data conform for mesh generation and available for the FE modelling (figure 4).

The following sections describe the procedures to build geometric model based on the simplified fracture geometry. Polygons have to be prepared to describe the model geometry, because these polygons describe the surface boundaries, which are required for mesh generation. The geometry of the conceptual model must be analysed and be

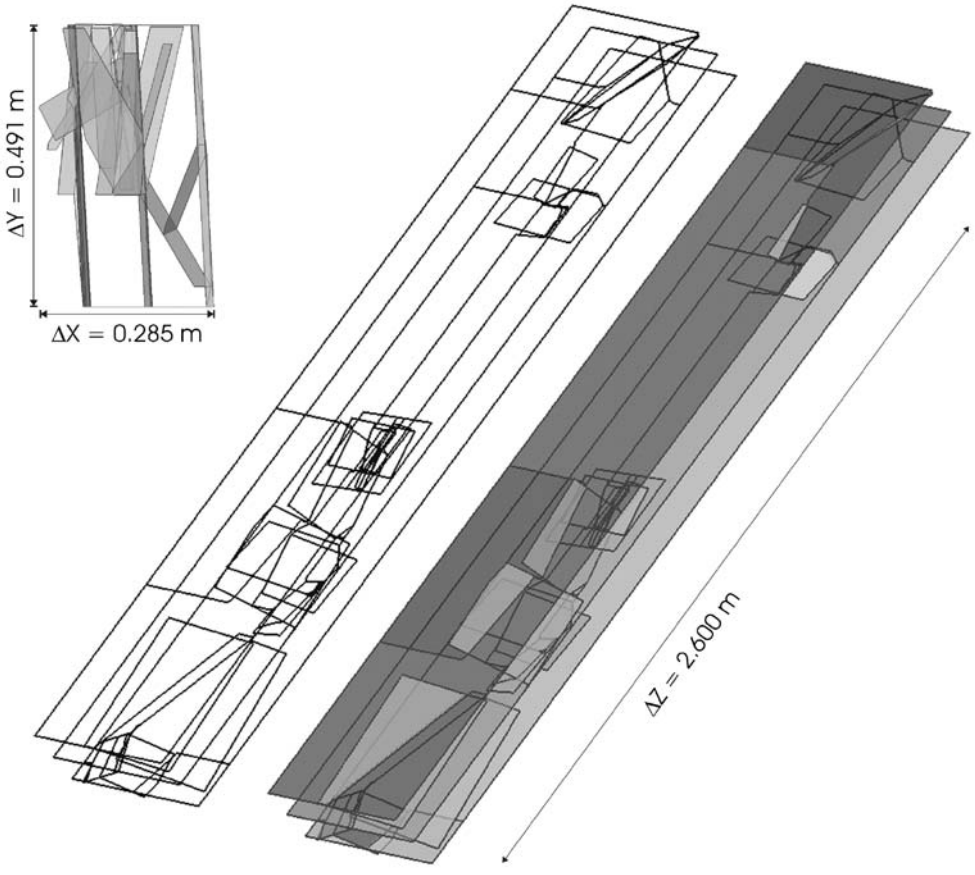

Figure 6 Geometric polylines and surfaces, which are needed to construct the fracture network model. Top left: *x*/*y* top view of the fracture network.

improved (cleaning) if necessary to ensure the applicability for mesh generation and the FE model simulation.

4.1 Intersections and polygon decomposition

Each plane surface of the fractures has to be subdivided into smaller units under consideration of its intersections with other surfaces. Some preprocessing of the dataset, e.g. the calculation of the intersection lines between the fractures, was done within the matrix and fracture interaction code MAFIC "Mesh" [35]. To apply further improvement techniques for the conceptual model, the intersection lines and segments of the planar fractures had to be reconstructed and combined to single polygons (figure 5). After all fracture planes have been split in this manner, the collected polygons are exported as a GeoSys geometry file.

4.2 Geometric data analysis and data cleaning

Geometric model quality problems are rooted in a variety of contributing factors that range from bugs in the preprocessing modelling system to errors of the data translation code. Data control and cleaning up of structure and precision are always needed to make the data functional for mesh generation and FE modelling. Consequently, complex fracture network models cannot be built without any user-controlled corrections and simplification to avoid errors in structure, precision and representation of reality. Structural problems include incoherent polyline orientation, fragmentary geometric input and non-defined or incorrect intersections. Structural errors can produce finite element meshes with intersected or not connected elements. This results in an unusable mesh for the numerical finite element model. Undesired effects are not attached fractures or fracture parts and consequent program crashes while solving the FE method problem. Precision requirements place limits on gaps between neighbouring geometric entities. Identical points should therefore be defined once by coordinates and the higher geometric entities by the point identification number. The model designer must balance the accuracy of numerical models with the amount of geometric information required. Precise fracture network models require complex and large data structures to define them, and simplifications are necessary to administrate and ensure the accuracy. Errors of reality representation can allow a model to run but the results are unrealistic due to physical limitations. Manual simplifications as well as automatic modulation procedures can cause such errors in the intersected areas of fracture network models.

4.2.1 Analysis of geometry

The fracture network of the case study presented consists of 233 points, 74 polygons and, consequently, 74 surfaces,

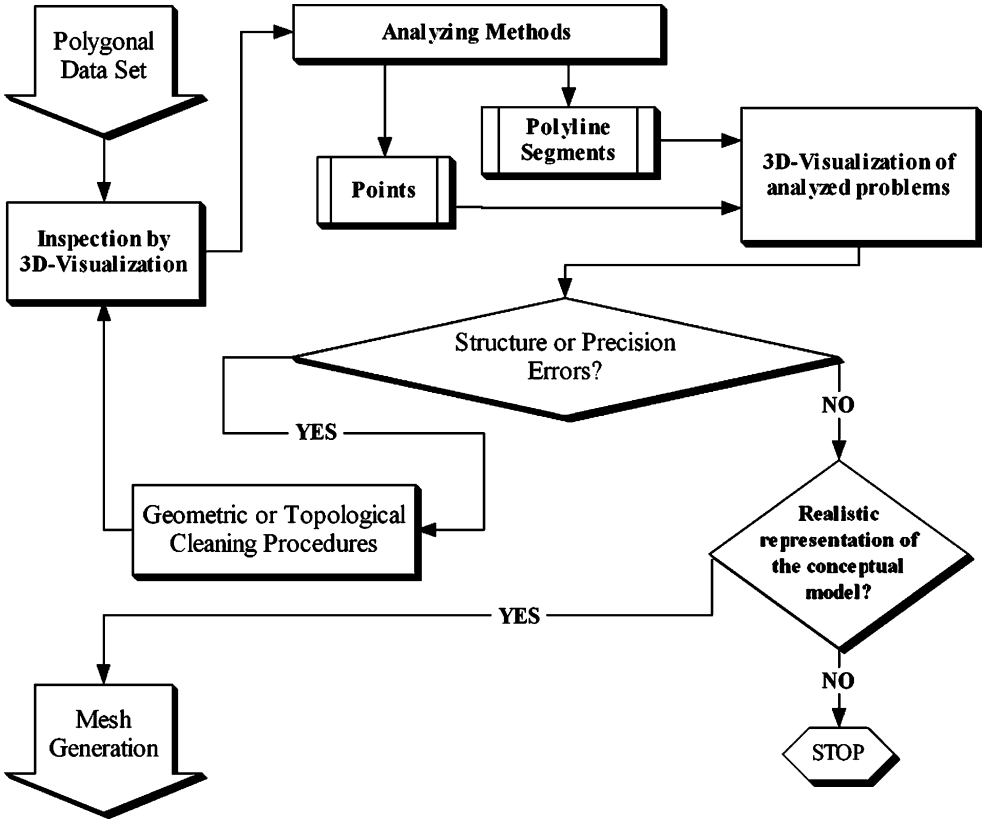

Figure 7 Procedure to prepare the conceptual model for mesh generation and FE model application. It is an iterative procedure with interaction of cleaning processes, data analysis and 3D visualization.

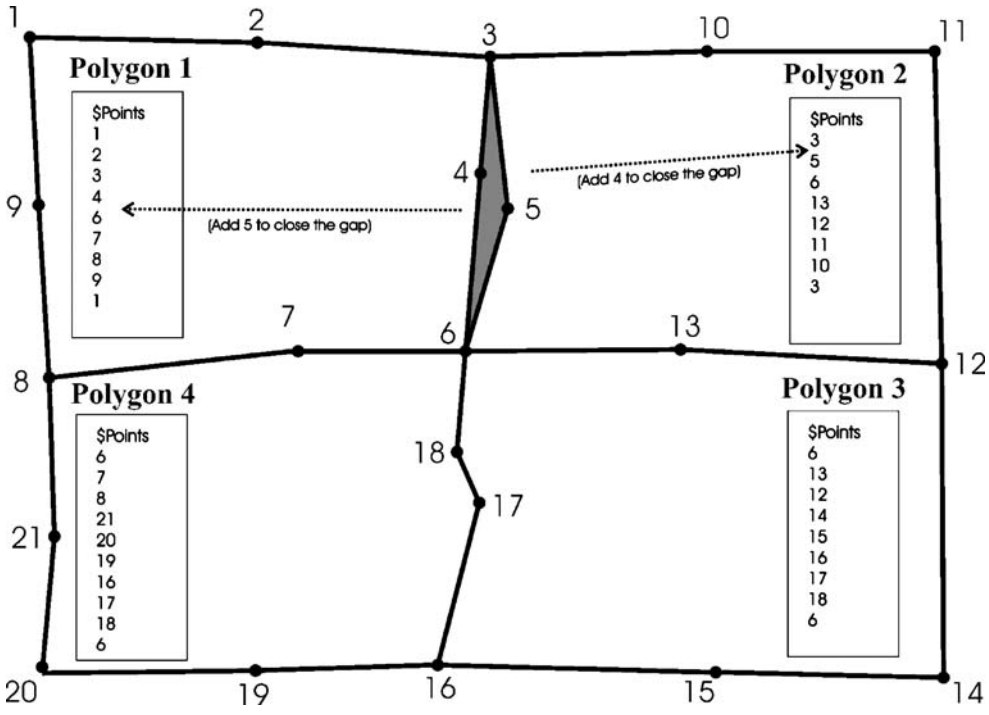

Figure 8 Example of an inconsistent polyline definition: Polygon 1 uses only Point 4 and Polygon 2 only Point 5. Both polygons must be corrected to close the gap (grey triangle.) The correction of only one polygon definition would produce another structural error by an undefined intersection.

which illustrate the 21 plane fractures (figure 7). The graphical user interface of GeoSys offers several tools for the geometric data analysis, and provides an OpenGL-based 3D visualisation (figure 4) of the fractured network data (geometry, mesh, properties, results) from any angle and position and allows image processing.

The 3D visualisation of geometric objects is an important tool to analyse the geometric input data (figure 6) and assists to localize accuracy and structural problems like missing geometry, gaps in polylines and gaps between polylines or surfaces. After analysing the consistency of the geometric data, it is necessary to prepare the geometry for the mesh generation. The user should have a clear idea how the mesh density distribution should look like, and which minimum and maximum element sizes are needed. The minimum is limited by the maximum of usable mesh size and mesh refinement. This defines the maximal geometric precision. The improvement of the geometric model is mostly an iterative procedure of geometric analysis and cleaning. Figure 7 illustrates the importance of efficient working analysis tools and cleaning procedures in combination with visualisation.

4.2.2 Data cleaning

A geometric searching algorithm examines the distances between points. This is important because small geometric point distances need local mesh refinement to ensure a certain mesh quality. This can increase the mesh size (number of nodes/elements) in a way that matrices for FE model simulation cannot be built up on standard computers or that the robustness limit of mesh generators is exceeded. In such cases, further geometric cleaning and simplifications are required. Should points be identified which are to close to one another, a merging tool can mark, display and combine those points that have smaller Euclidean distances than the user-defined tolerance. A further cleaning method is founded on geometric and topological techniques using the segment length of the polylines. Important information is the minimum and maximum length of all segments. The automatic "set length" function adds and removes points along the polyline segments with reference to the min/max length setting. This automatic function can distort the model domain as well as the automatic merging method, because curvature tests and other shape analysing methods are not implemented yet. However, both methods together are a useful tool to localize accuracy problems and help to improve the geometric data for mesh generation.

The GUI enables automatic cleanups as well as direct geometric data control using editors. In the case of this fracture network model, the GUI was needed to analyse the geometric input and to make some corrections to fix inconsistent polyline definitions (figure 8), to close gaps between polylines or surfaces, to modify or delete surfaces with acute angles (figure 9), and to merge points for a larger minimum distance of neighbouring points.

After cleaning the geometry, it is possible to add further geometric entities, e.g. to position boundary conditions or source and sink terms. Such extended geometries are usually transmitted geometric parts of the conceptual model

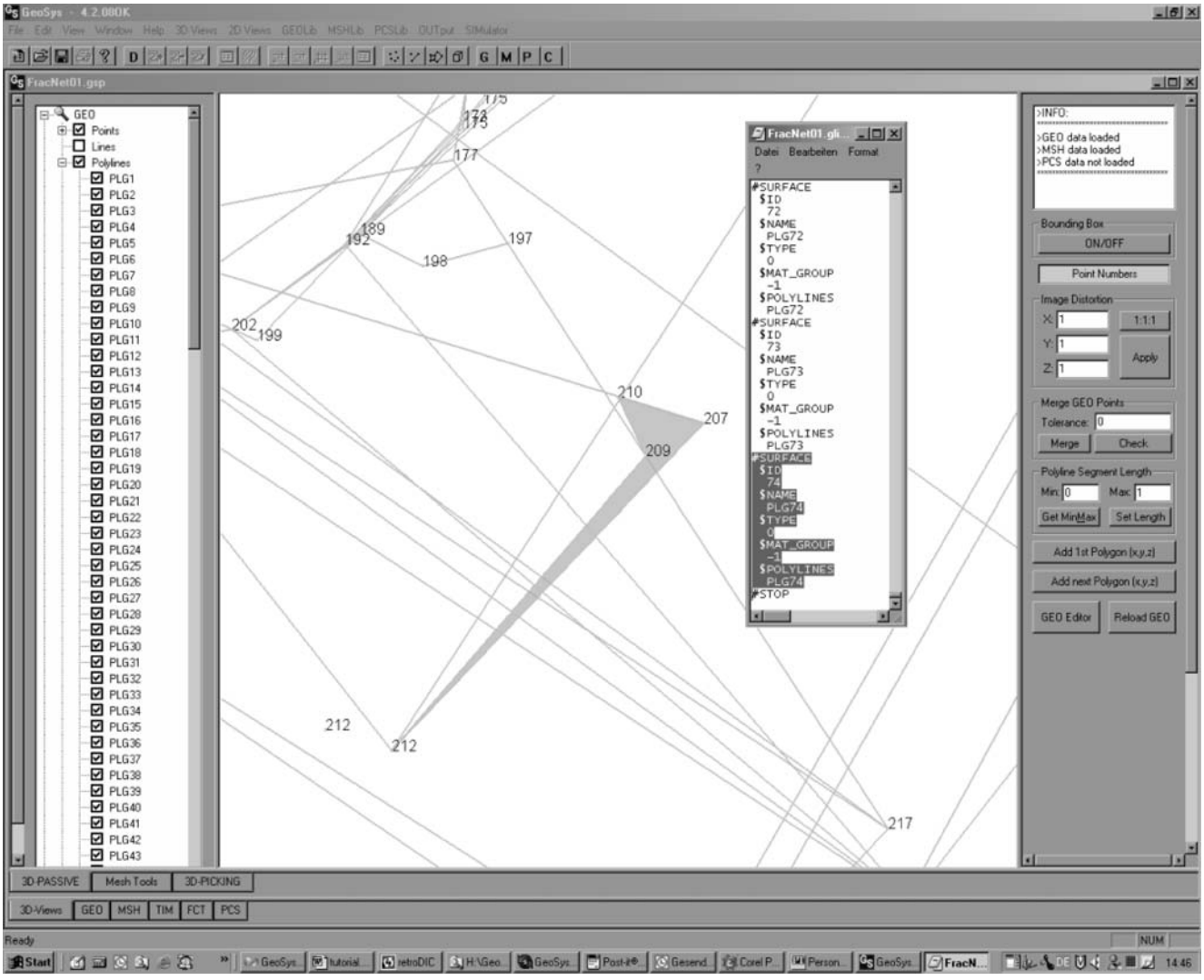

Figure 9 Surface with acute angle – This surface was deleted because of its shape and small relevance (small size and marginal position) for the model.

and should be included as late as possible. The insertion would be possible before cleaning as well, but this produces additional work for analyzing and modifying of these geometric entities after each cleaning procedure. In Section 6, more surfaces are introduced for boundary conditions using the point, polyline and surface editors together with the 3D visualisation for visual support and control.

5 Mesh generation

Meshing is an integral part of the FE model analysis process. The quantity and quality of the finite elements influences the accuracy, convergence and speed of the fractured network model solution. More importantly, the time it takes to create a mesh model is often a significant portion of the time it takes to get results from an FE method solution. Therefore, the more user-friendly and automated the meshing tools, the less time consuming is the evaluation of the appropriate settings for an optimal mesh density distribution.

The MSH includes objects of fundamental algorithms and mathematics for meshing and remeshing, independently usable but specifically designed for the class of geometric data. It provides structured and unstructured tetrahedra-, hexahedra-, prism-, rectangle- and triangle-mesh generators and quality analyzing tools. Structured meshes would offer a more direct control of size and shape of elements but are less flexible in fitting the domain along complex fracture intersections than unstructured mesh generation. The used mesh generator is based on Delaunay Triangulation [49] performed by GMSH [20]. The procedure can be classified in the following steps:

- First, meshing of a box defined by boundary nodes resulting from the discretisation of the surfaces is undertaken.

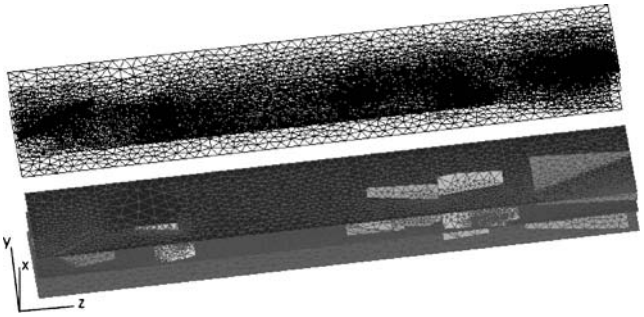

Figure 10 Triangulated fracture network (top) and patch indices (bottom). Elements of the same single surface have the same patch index and therefore the 73 surfaces created 73 different patch indices.

- Second, insertion of all the nodes on the surfaces based on the Bowyer–Watson algorithm [7, 54] for an initial triangulation, and a boundary reinstallation to keep all the edges of the surfaces to be present in the initial mesh.
- Third, the displacement of all the objectionable triangles and finally the insertion of new nodes by the Bowyer–Watson algorithm until the characteristic size of all triangles correspond with the mesh density description.

5.1 Mesh density

The density of the created mesh follows specific element size definitions (edge length of triangles) at points of the bounding segments. An element size definition at each geometric point is essential before starting the mesh generation. The element size allocation must take user-defined density distribution as well as the geometric required element sizes into account. A very small segment in the boundary needs a region of small elements in the surrounding area of the segment to ensure an appropriate mesh quality.

The user specifies at first a global maximum element size for all points and starts an automatic mesh density adaptation. The smaller the predefined specific element sizes, the less mesh refinements are necessary and the more homogeneous is the mesh of the fractured network model. GeoSys/RockFlow offers a topological and a geometrical optimisation technique. The geometric method takes only the Euclidian distance per point to all neighbouring GEO points into account and sets the minimum distance of the closest neighbour point as specific element size for the analysed point. The topological method calculates the Euclidian distance along topologically connected and neighbouring entities and sets the minimum distance as the specific element size. This might be critical if two or more not interconnected polyline segments are very close together. The specific element size is only changed when the calculated value is smaller than the predefined elements size value. Both optimisation techniques can lead to heterogeneous mesh constructs if the conceptual model shows alternating geometric complexity. Strong mesh refinements can be avoided by downscaling the global maximum element edge size, to achieve a more homogenous mesh and to prevent oscillating results for the mass transport modelling. Here, the needed process related element edge size is <0.10 m (numerical stability criteria) but the global defined maximum edge length is 0.05 m and produces in combination with the geometric optimisation method a less heterogeneous mesh with appropriate refinements around the fracture intersections of the $2.6\times0.5\times0.3$ m fracture network.

5.2 Meshing procedure

After mesh density definition and the selection of the applicable surfaces, the mesh generation can be started. The mesh consists now of 12,865 nodes and 24,840 triangular elements (figure 10). The minimum/maximum edge lengths are 7.96×10^{-5} and 0.085 m, and the average edge size is 0.2 m. The extreme minimum is the result of one intersected area where it was needed to place several points close to each other because of reality representation and structural uniqueness. In this case, fractures that were lying almost parallel would be incorrect connected.

The mesh is now refined in all areas where it is geometrically necessary. This should ensure an adequate mesh quality but must be analysed (see Section 5.3). The elements of each single meshed surface have the same element property numbers, which belong to the element object and which are mainly used for material group assignments and controllable within the GUI. Therefore, the 73 meshed surfaces, which construct the fractured network, produce 73 patch groups (figure 10).

5.3 Mesh quality

For the accurate calculation of the processes to be evaluated, the required mesh quality is actually also dependent on the process being considered. This makes it difficult to use geometric quality criteria alone before solution to evaluate the quality of the mesh for the process. There are available techniques that combine both the geometric quality of the mesh elements and the process solution procedure, the so-called solution-based computable error estimates (e.g. [6]). However, they are still under development for finite element analysis.

There are several ways to compute geometric quality of individual elements and to quantify the overall quality of a mesh [5]. In this paper, three elementary criterions for triangular elements have been applied. The fundamental principle is that equilateral triangles have the best possible

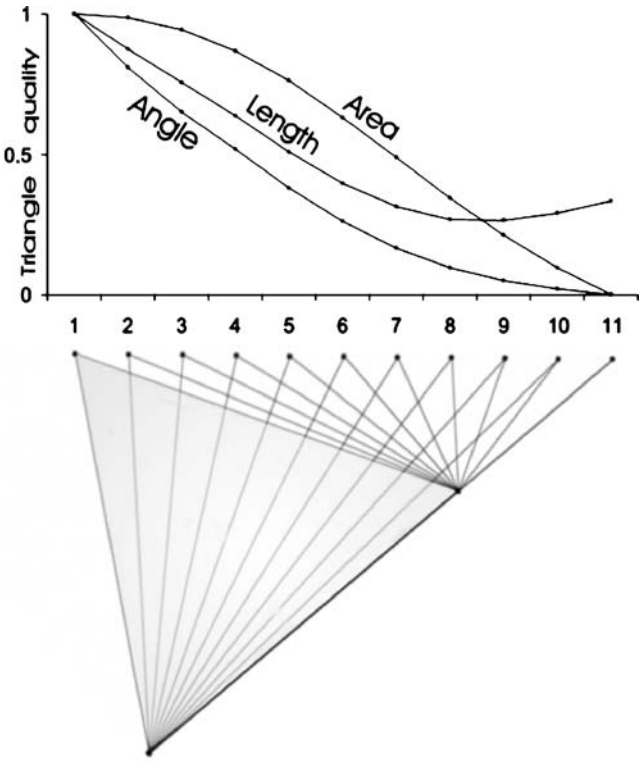

Figure 11 Length, angle and quality criteria for each triangle. The upper vertex of the grey equilateral triangle is moved by 10 steps horizontal to the right side.

element shape, and therefore the ideal number of elements linked to one node is six. The geometric quality can be expressed for triangular elements as

- LengthCriterion:

$$Quality_{\text{Lengh}} = \frac{\min\left(|\overrightarrow{e_1}|, |\overrightarrow{e_2}|, |\overrightarrow{e_3}|\right)}{\max\left(|\overrightarrow{e_1}|, |\overrightarrow{e_2}|, |\overrightarrow{e_3}|\right)} \tag{4}$$

- Angle Criteria:

$$Quality_{\text{Angle}} = \frac{\min(\alpha, \beta, \gamma)}{\max(\alpha, \beta, \gamma)} \tag{5}$$

- Area Criteria:

$$Quality_{\text{Area}} = \frac{4\sqrt{3}A}{|\overrightarrow{e_1}|^2 + |\overrightarrow{e_{21}}|^2 + |\overrightarrow{e_{31}}|^2} \tag{6}$$

The length criterion (4) is the relation of shortest and longest edge of the triangle $\left(|\overrightarrow{e_1}|, |\overrightarrow{e_2}|, |\overrightarrow{e_3}|\right)$, which is obviously one in the equilateral case just as well as the angle criterion (5), which is the ratio of the smallest to the largest angle (α, β, γ). Finally, the area criterion (6) compares the area A with the length of the edges $\left(|\overrightarrow{e_1}|, |\overrightarrow{e_2}|, |\overrightarrow{e_3}|\right)$, and is one for the equilateral triangles.

Figure 11 shows a comparison of the three triangle quality criterions. Starting with an equilateral triangle (grey triangle), the top left point with number 1 is moved along a horizontal line to the right side. Through this, we produce 11 triangles with decreasing quality until the triangle is completely distorted. For all 11 triangles, the quality criterions are calculated and displayed in a graph exactly over the moved top vertex of their corresponding triangles. The angle criterion is most sensitive for the upper quality range. Then the three graphs show nearly the same gradient. For the low quality range, the area criterion has the steepest gradient and therefore the most sensitive performance. The length criterion shows a divergent behaviour for triangles of lower quality (<0.35) where the quality factor starts increasing while the element quality is decreasing. These criteria are implemented within the GUI. The three-dimensional visualisation shows the spatial distribution of mesh quality (figure 4, right). This helps to localize critical areas of mesh quality (figure 12), but faces of completely distorted elements are invisible. Therefore, it is necessary to visualize the mesh quality of each element in a diagram (figure 12). An additional and maybe most important overview of the mesh quality distribution are given by histograms, which are displayed together with the element quality graph (figure 12).

Such geometric factors are not a guarantee for sufficient mesh quality for any physical processes. However, in combination with rule-based adaptive time step calculations they assist in appraising the usability of the mesh for the FE model application. Due to the sensitive performance in the low quality range of the fracture network mesh, we choose the area criterion to analyse triangles with a quality below 0.5 to extract and locate potential critical areas. First, we located poor elements along intersections (figure 12), and improved the mesh by manual geometric input corrections and refined remeshing. After the improvement, the mesh of the fractured network shows an adequate quality distribution but still some single poor elements (figure 12, minimum of lower diagram). These elements are due to acute angles of surface boundaries at fracture intersections, since the fracture geometry was not more simplified to avoid unwanted fracture linkage.

6 Physical assignments

The demand for more detailed and complex fracture network models as well as the task to extend the model by introducing new physical processes can lead to complex mesh constructs, which are no longer visually controllable for manual parameter and property assignments. User-defined management of these datasets has to be performed within a geometric environment, which excludes the finite

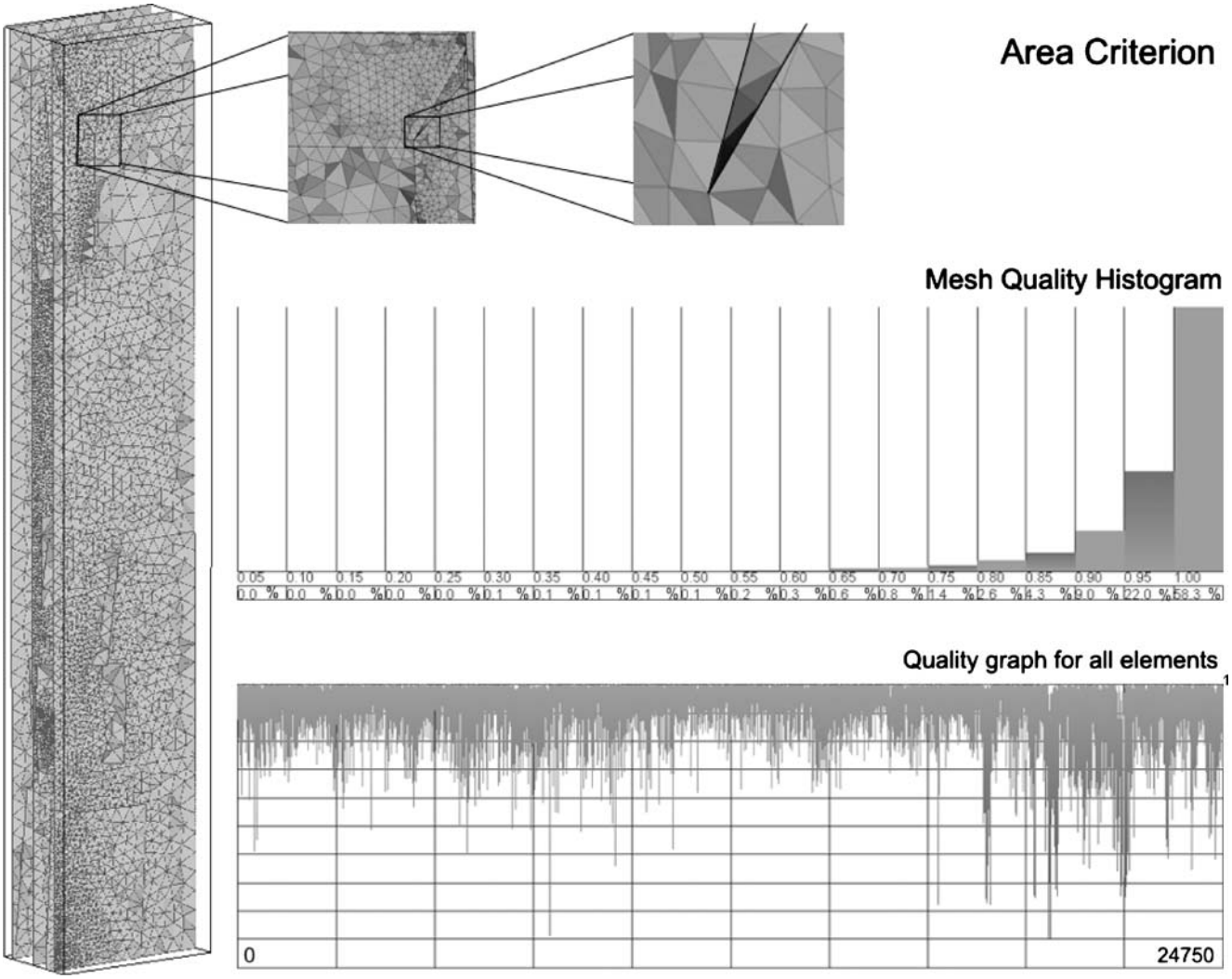

Figure 12 Spatial distribution of the area criterion (left) and an example of typical poor element quality (zoomed dark grey/black triangles) along fracture intersections (top). Histogram (middle) and graph (bottom) of the area criterion.

element mesh. Physical assignments are declared in the PCS object and are linked with the appropriate entities of the GEO object. Automated functions connect the information of MSH and PCS by using the geometric input data.

6.1 Node properties

The boundary conditions for the groundwater flow and mass transport model need specifications of hydraulic heads and concentrations, static or time-dependent, as well as the geometric locations for these conditions. Numerically, all locations for boundary conditions consist of a set of mesh nodes. As the complexity of the model increases, it may often become impossible for the user to visualize and assign node properties correctly. Therefore, the boundary conditions can be geometrically defined by the basic and initial geometric entities, e.g. points, polylines and surfaces. Here, the user simply selects the surfaces (figure 13) and defines the physical parameters, such as concentrations or hydraulic heads. A searching and allocation algorithm selects the appropriate mesh nodes and links them with the boundary condition object (figure 13). The following three major steps describe the applied procedure:

- Triangulation of the surfaces for the boundary conditions, with less (the more elements, the more time-consuming) but not distorted elements (because of robustness and reliability).
- Calculation of the geometric accuracy to calibrate the search algorithm. Only with a correct calibration is it possible to find exactly all points along the surface.
- Searching all nodes, which lie inside or on the edge of the triangulated surface. This is carried out via an angle sum calculation and/or area comparison: Connecting the point with the edges of a triangle produces three extra

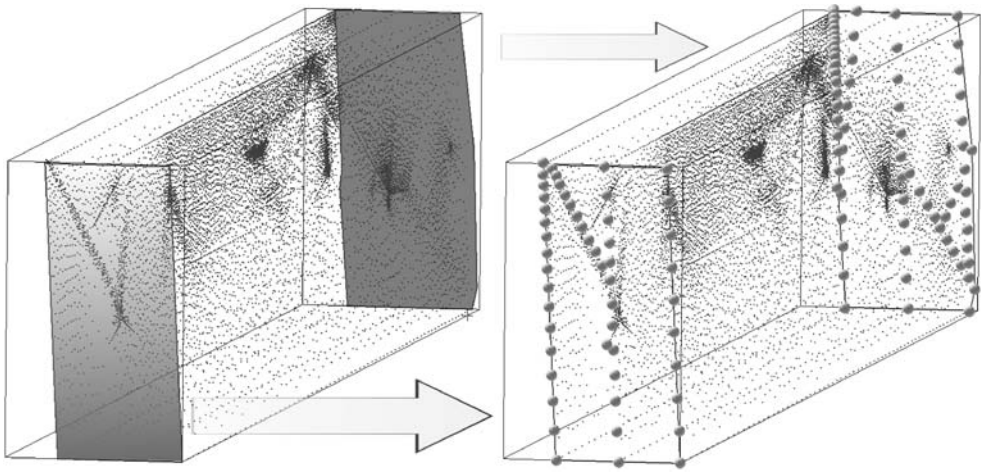

Figure 13 Surfaces (grey planes) are used to place boundary conditions (left). A search locates the mesh nodes for boundary condition setup (right).

triangles. If the point is inside, these three triangles altogether should have the same area as the base triangle, and the sum of their interior angles (angle of the common point) is 360°.

The advantage of physical assignment by basic and mesh-independent geometric entities is their fast creation. However, visual control is still very important to ensure the reliability.

6.2 Element properties

The assignment of heterogeneous material properties for fractures is done by directly connecting the material property parameters with the individual elements. In this case study, the fractures have variable apertures which are coupled with the transmissivity by the cubic law.

Several authors investigated the detailed structure of fracture surfaces, e.g. Brown and Scholz [8]. To reproduce the fracture roughness, i.e. the topography of fracture surfaces, different methods have been employed such as stochastic and fractal approaches [1, 19, 29, 38, 41, 52]. Fracture roughness effects the hydraulic conductivity of the fractures [33]. Fracture flow is divided into parallel and non-parallel motion by a critical value of roughness. Consequently, the specific geometry of a fracture (i.e., the distribution of the fracture aperture) influences its hydro-mechanical characteristics. This phenomenon is called flow channelling [51], and is taken into account in this modelling approach.

Geological evidence shows that fracture apertures are often spatially correlated, with an underlying lognormal distribution [13], causing a significant tailing in the breakthrough of solutes [40]. Geostatistical analysis, foremost the use of variograms, can provide a perception of the spatial distribution observed. If any actual apertures have been measured, an experimental variogram can be calculated from the data. A model variogram can then be fitted to the experimental one. This model variogram can be used to simulate any number of equivalently distributed aperture patterns by, e.g. sequential Gaussian simulation [46]. The patterns can be additionally conditioned to other measurements. They can be used in a Monte Carlo approach to investigate the effect of varying apertures on transport [40], or to recreated plausible aperture distributions in other models where no measurements on the actual apertures are available.

A simple tool enables the user to generate geostatistically distributed aperture values for model geometries consisting of planar, or near planar, fractures, discretised in 2D triangular elements. It makes use of the statistical program R [48], and therein mainly of the geostatistics package gstat [46].

The following requirements must be met:

- The fracture network geometry must consist of separable individual fractures, which either are of planar nature, or can be transformed (projected, warped, etc.) to planar form.
- The finite element mesh should consist of triangular elements.
- R 2.0 for Linux and the corresponding gstat package for R.

After the polygonal model geometry is loaded, the following steps are performed:

- Obtain the parameters which define the model variogram.
- If necessary, separate the fracture network into individual planar fractures.
- Create three R input files for each fracture (nodes.dat: consisting of the mesh vertices for each element (2D); centers.dat: which contains the center of mass for each element; rvario.r: the R script tailored to the calculation for each fracture).

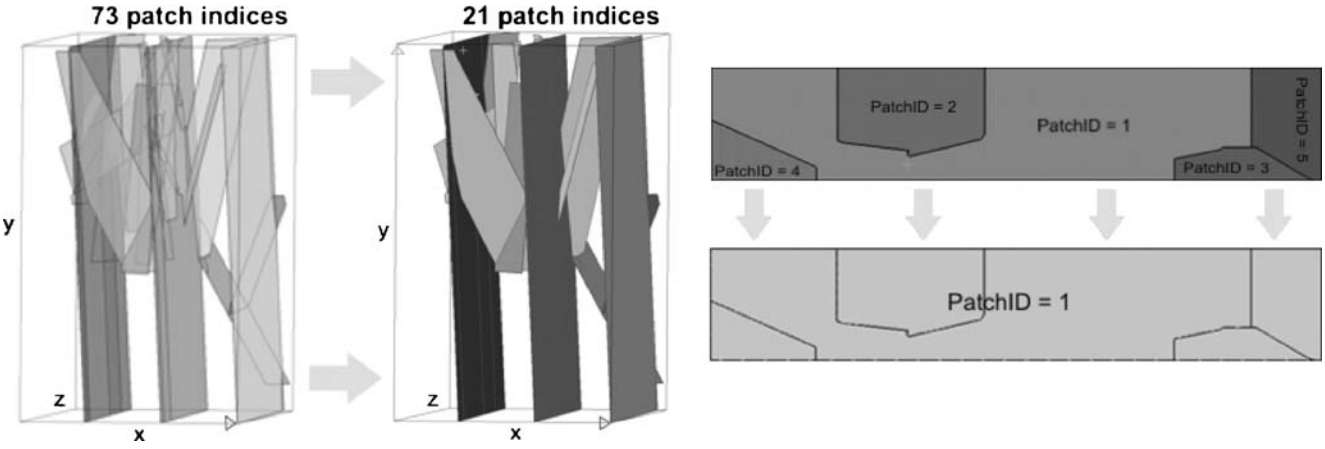

Figure 14 Merging of the patch indices for one fracture (right) and for the all fractures of the network (left).

- Call R, with the necessary options to execute rvario.r and return an output file, apert.dat, containing the aperture values at each of the element centers.
- Read apert.dat and assign each model element with the calculated aperture.
- Return the resulting model parameters to the patch object.
- Write the patch object out in a material file for distributed elements property data.

For the task of separating the individual fractures, element property indices are required to identify the element groups of each planar fracture (Section 6.3). The elements and vertices of each planar fracture are individually passed to the R input file generator together with the parameters, which characterize the variogram. This is done to ensure that intersecting fractures do not necessarily exhibit similar apertures near the intersection line, merely because their separation is small.

6.3 Simulation

The 73 patch groups (figure 6) represent the 73 surfaces, which were needed for the geometric discretisation of the fracture network model. The input is provided in form of a

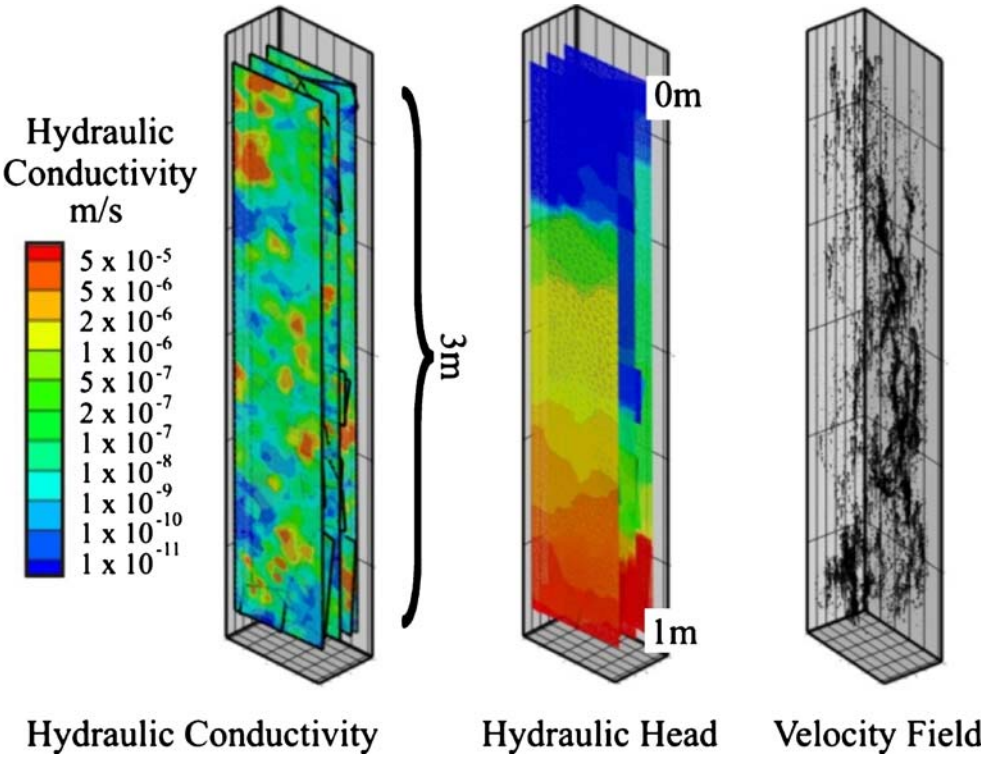

Figure 15 Permeability mapping and hydraulic results for the Grimsel shear zone.

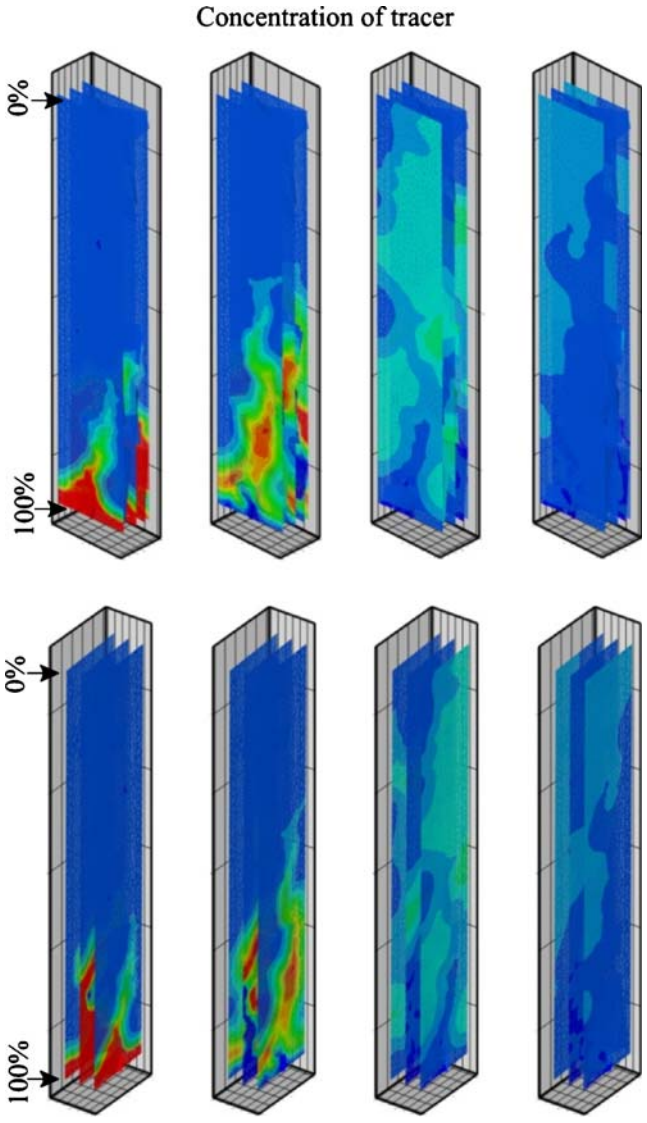

Figure 16 Tracer transport results with matrix diffusion for the Grimsel shear zone.

GeoSys MSH file, with a patch index for each element containing the element affiliation with a planar fracture. Therefore, it is necessary to merge all patch index groups, which belong to the same surfaces (figure 14).

After converting this arranged MSH file, now with 21 patch index groups (figure 14), to a GeoStatFrac file, the necessary parameters for the variogram model can be provided. The output is provided as a GeoSys material file (value per element), where additional material parameters such as aperture or transmissivity are related to element numbers. Figure 15 shows one realisation of a permeability distribution after such a geostatistical procedure.

Now, the geometric modelling – with model design, mesh generation, mesh analysis and the particular physical parameter assignments – is completed and the model can be applied for numerical simulations. Based on these results, experimental results can be analysed to determine the factors dominating the flow and transport characteristics of the shear zone material.

Using the procedure described above, figure 15 illustrates the mapping of the hydraulic conductivities onto a 3D representation of the investigated Grimsel shear zone, the solution of the heads according to Eq. (1) and the derivation of the velocity field. Figure 16 presents the solution of the transport equation with the inclusion of the matrix analytical solution Eq. (3) as a source term. Here, the initial transport results for four different time steps and from two different viewpoints are illustrated.

7 Conclusion

This paper presents necessary preprocessing steps to set up an FE model that allows calculation of advective and diffusive (dispersive) transport in realistic fractures, combined with slow diffusion of solutes into a porous rock matrix adjacent to the fractures and equilibrium sorption processes in the rock matrix. The methods and modelling assumptions can be tested on hand of a unique dataset comprising the internal geometry of a relatively large part of a shear zone in the Grimsel rock laboratory ($2.6 \times 0.5 \times 0.3$ m) and the results of real *in situ* transport experiments. To evaluate the results, numerous realisations of the fracture geometry based upon different geostatistical realisations of the measured fracture aperture distribution require a great deal of automation of the pre-processing tools. Due to the geometrical complexity of modelling fracture networks, it is necessary to have geometric and meshing tools capable of providing accurate geometric model design, domain discretisation and the spatial parameter assignments. The graphical user interface presented in this paper is able to show the user all required information (3D visualisation, diagrams, graphs, tables, etc.) and provides the interactive tools to administrate and revise the data. The complete object-oriented software concept must present a clear organized structure to maximize the reusability and flexibility of the source code for timesaving software engineering. In the case of the fractured network model presented, these capabilities are especially important because a large number of spatially and temporally, stochastic or deterministic distributed model properties are required.

Acknowledgements The authors want to particularly thank Nagra in Wettingen, Switzerland (http://nagra.ch, http://www.grimsel.com), and JAEA in Tokai, Japan (http://www.jaea.go.jp), which enabled the access to the cores themselves and provided the dataset from the excavation project as well as the images of the cores. Ralph Mettier

thanks Bill Dershowitz and Golder Inc. for providing him with an academic license for their FracXP software package. (http://fracman.golder.com/). The funding of the Deutsche Forschungsgemeinschaft (DFG) for further development of fracture network models under grant (MCD113/1-5) is gratefully acknowledged. Furthermore, we thank the BMBF for funding our developments of coupled numerical models for C:HM transport processes (02C1295)

References

1. Acuna, J.A., Yortsos, Y.C.: Application of fractal geometry to the study of networks of fractures and their pressure transient. Water Resour. Res. **31**(3), 527–540 (1995)
2. Alexander, W.R., Ota, K., Frieg, B.: The Nagra-JNC *in situ* study of safety relevant radionuclide retardation in fractured crystalline rock. Nagra Technical Report 00-06. Nagra, Wettingen, Switzerland (2003)
3. Baraka-Lokmane, S., Liedl, R., Teutsch, G.: Comparison of measured and modelled hydraulic conductivities of fractured sandstone cores. Pure Appl. Geophys. **160**, 909–927 (2003)
4. Berkowitz, B., Scher, H.: Anomalous transport in random fracture networks. Phys. Rev. Lett. **79**, 4038–4041 (1997)
5. Bern, M., Epstein, D.: Mesh Generation and Optimal Triangulation. Report CSL 92-1, Xerox Corporation, Palo Alto Research Center, Palo Alto, CA, 94304 (1992)
6. Berzins, M.: Solution-based mesh quality indicators for triangular and tetrahedral meshes. Int. J. Comput. Geom. Appl. **10**(3), 333–346 (2000)
7. Bowyer, A.: Computing Dirichlet tessellations. Comput. J. **24**(2), 162–166 (1981)
8. Brown, S.R., Scholz, C.H.: Broad bandwidth study of the topography of natural rock surfaces. JGR, J. Geophys. Res. B **90**(14), 12.575–12.582 (1985)
9. Cacas, M.C., Ledoux, E., De Marsily, G., Tillie, B., Barbreau, A., Durand, E., Feuga, B., Peaudecerf, P.: Modeling fracture flow with a stochastic discrete fracture network: calibration and validation 1. The flow model. Water Resour. Res. **26**, 479–489 (1990)
10. Carslaw, H.S., Jaeger, J.C.: Conduction of Heat in Solids. Oxford University Press Oxford, UK, (1959)
11. Chen, C.: Integrating GIS methods for the analysis of geosystems. PhD thesis, Center for Applied Geoscience, University of Tübingen (2006)
12. Cvetkovic, V., Painter, S., Outters, N., Selroos, J.O.: Stochastic simulation of radionuclide migration in discretely fractured rock near the Äspö Hard Rock Laboratory. Water Resour. Res. **40** (2004)
13. de Dreuzy, J-R., Davy, P., Bour, O.: Hydraulic properties of two dimensional random fracture networks following a power law length distribution, 2. Permeability of networks based on lognormal distribution of apertures. Water Resour. Res. **37**(8), 2079–2095 (2001)
14. de Dreuzy, J.-R., Darcel, C., Davy, P., Bour, O.: Influence of spatial correlation of fracture centers on the permeability of two-dimensional fracture networks following a power law length-distribution. Water Resour. Res. **40** (2004)
15. Dershowitz, W., Lee, G., Geier, J., La Pointe, P.: FracMan Interactive Discrete Feature Data Analysis Geometric Modelling and Exploration – User documentation (1995)
16. Dershowitz, W., Fidelibus, C.: Derivation of equivalent pipe network analogues for three-dimensional discrete fracture networks by the boundary element method. Water Resour. Res. **35**, 2685–2692 (1999)
17. Fisher, M.K., Wright, C.A., Davidson, B.M., Goodwin, A.K., Fielder, E.O., Buckler, W.S., Steinsberger, N.P.: Integrating fracture-mapping technologies to improve stimulations in the Barnett Shale. SPE Prod. Facil. 85–93 (2005)
18. Freeze, R.A., Cherry, J.A.: Groundwater. Prentice-Hall Englewood Cliffs, NJ (1979)
19. Glover, P.W.J., Matsuki, K., Hikima, R., Hayashi, K.: Characterising rock fractures using synthetic fractal analogues. Geotherm. Sci. Technol. **6** (1999)
20. GMSH website: http://www.geuz.org/gmsh/.
21. Grathwohl, P.: Diffusion in natural porous media: Contaminant Transport, Sorption/Desorption and Dissolution Kinetics. Kluwer Academic Publishers (2003)
22. Häfner, F., Sames, D., Voigt, H.-D.: Wärme- und Stofftransport – Mathematische Methoden. Springer, Berlin Heidelberg New York (1992)
23. Helmig, R., Braun, C., Manthey, S.: Upscaling of two-phase flow processes in heterogeneous porous media: determination of constitutive relationships. IAHS–AISH Publ. **277**, 28–36 (2002)
24. Istok, J.: Groundwater Modeling by the Finite Element Method. Water Resources Monograph. American Geophysical Union, Washington, DC (1989)
25. Kalbacher, T., Wang, W., McDermott, Ch., Kolditz, O., Taniguchi, T.: Development and application of a CAD interface for fractured rock. Environ. Geol. **47**, 1017–1027 (2005)
26. Kolditz, O.: Computational Methods in Environmental Fluid Mechanics. ISBN 3-540-42895-x. Berlin: Springer-Verlag, ss378 (2002).
27. Kolditz, O., Bauer, S.: A process-orientated approach to compute multi-field problems in porous media. Int. J. Hydroinf. **6**, 225–244 (2004)
28. Kolditz, O., Beinhorn, M., de Jonge, J., Xie, M., Kalbacher, T., Bauer, S.,Wang, W., Bauer, S., McDermott, C., Chen, C., Beyer, C., Gronewold, J., Kemmler, D., Legeida, D., Walsh, R., Du, Y.: GeoSys/RockFlow, open source software design. Technical Report, GeoSys-Preprint [2004-25] http://www.uni-tuebingen.de/zag/geohydrology. GeoSysResearch, Center for Applied Geosciences, University of Tübingen (2004)
29. Kosakowski, G.: Modellierung von Strömungs- und Transportprozessen in geklüfteten Medien: Vom natürlichen Kluftsystem zum numerischen Gitternetzwerk. VDI Fortschritt-Berichte **7**(304) (1996)
30. Kosakowski, G., Kasper, H., Taniguchi, T., Kolditz, O., Zielke, W.: Analysis of groundwater flow and transport in fractured rock – geometric complexity of numerical modelling. Z. Angew. Geol. **43**(2), 81–84 (1997)
31. Kosakowski, G., Berkowitz, B., Scher, H.: Analysis of field observations of tracer transport in a fractured till. J. Contam. Hydrol. **47**, 29–51 (2001)
32. Lauwerier, H.A.: The transport of heat in an oil layer caused by the injection of hot fluid. Appl. Sci. Res. **A5**, 145–150 (1955)
33. Louis, C.: Strömungsvorgänge in klüftigen Medien und ihre Wirkung aus die Standsicherheit von Bauwerken und Böschungen im Fels. Dissertation thesis, Universität Karlsruhe, Karlsruhe (1967)
34. Lunati, I., Kinzelbach, W., Sørensen, I.: Effects of pore volume–transmissivity correlation on transport phenomena. J. Contam. Hydrol. **67**, 195–217 (2003)
35. MAFIC (http://fracman.golder.com/software/mafic.asp).
36. Maloszewski, P., Zuber, A.: Tracer experiments in fractured rocks: matrix diffusion and the validity of models. Water Resour. Res. **29**, 2723–2735 (1993)
37. Maryška, J., Severýn, O., Vohralík, M.: Numerical simulation of fracture flow with a mixed-hybrid FEM stochastic discrete fracture network model. Comput. Geosci. **8**, 217–234 (2004)

38. McDermott, C.I., Kolditz, O.: Geomechanical model for fracture deformation under hydraulic, mechanical and thermal loads. Hydrogeol. J., Springer-Verlag, ISSN: 1431-2174 (Paper) 1435-0157 (Online) Doi: http://dx.doi.org/10.1007/s10040-005-0455-4 (2005)
39. McDermott, C.I., Lodemann, M., Ghergut, I., Tenzer, H., Sauter, M., Kolditz, O.: Investigation of coupled hydraulic–geomechanical processes at the KTB site: pressure dependent characteristics of a long term pump test and elastic interpretation using a geomechanical facies model. Geofluids **6**, 1–15 (2006)
40. Mettier, R., Kosakowski, G., Kolditz, O.: Influence of small scale heterogeneities on contaminant transport in fractured crystalline rock, Ground Water, submitted (2006)
41. Moreno, L., Tsang, Y.W., Tsang, C.F., Hale, F.V., Neretnieks, I.: Flow and tracer transport in a single fracture – a stochastic-model and its relation to some field observations. Water Resour. Res. **24** (12), 2033–2048 (1988)
42. Mourzenko, V.V., Thovert, J.-F., Adler, P.M.: Macroscopic permeability of three-dimensional networks with power-law size distribution. Phys. Rev. E **69** (2004)
43. National Research Council: Rock Fractures and Fluid Flow – Contemporary Understanding and Applications. Washington, DC: National Academy, 1996, ISBN:0-309-04996-2 (1996)
44. Neretnieks, I.: A Note on fracture flow dispersion mechanisms in the ground. Water Resour. Res. **19**(2), 364–370 (1983)
45. Oron, A.P., Berkowitz, B.: Flow in rock fractures: the local cubic law assumption reexamined. Water Resour. Res. **34**, 2811–2825 (1998)
46. Pebesma, E.J., Wesseling, C.G.: Gstat: a program for geostatistical modelling, prediction and simulation. Comput. Geosci. **24**(1), 17-31 (1998) http://www.gstat.org
47. Peratta, A., Popov, V.: A new scheme for numerical modelling of flow and transport processes in 3D fractured porous media. Adv. Water Resour. **29**, 42–61 (2005)
48. R Development Core Team: R: A Language and Environment for Statistical Computing. R Foundation for Statistical Computing, Vienna, Austria, ISBN 3-900051-07-0, http://www.R-project.org (2005)
49. Shewchuk, J.R.: Triangle: Engineering a 2D quality mesh generator and Delaunay triangulator. In: Ming, C., Manocha, L., Manocha, D.(eds.) Applied Computational Geometry: Towards Geometric Engineering, vol. 1148 of Lecture Notes in Computer Science, pp. 203–222. Springer, Berlin Heidelberg New York (1996)
50. Tsang, C.F.: Coupled hydromechanical–thermochemical processes in rock fractures. Rev. Geophys. **29**(4), 537–552 (1991)
51. Tsang, Y.W., Tsang, C.F.: Channel model of flow through fractured media. Water Resour. Res. **23**(3), 467–479 (1987)
52. Wang, J.S.Y., Narasimhan, T.N., Scholz, C.H.: Aperture correlation of a fractal fracture. J. Geophys. Res. **93**(B3), 2216–2224 (1988)
53. Wang, W., Kolditz, O.: Object-oriented finite element analysis of thermo-hydro-mechanical (THM) problems in porous media. Int. J. Numer. Methods Eng. (accepted) (2005)
54. Watson, D.F.: Computing the *n*-dimensional Delaunay tessellation with application to Voronoi polytopes. Comput. J. **24**(2), 167–172 (1981)
55. Witherspoon, P.A., Wang, J.S.Y., Iwai, K., Gale, J.E.: Validity of cubic law for fluid flow in a deformable rock fracture. Water Resour. Res. **16**(6), 1016–1024 (1980)
56. Zienkiewicz, O.C., Taylor, R.L.: The Finite Element Method, 1. Butterworth-Heinemann, 752 pp (2005)

Hybrid analytical and numerical modelling of mass and heat transport in fractured rocks.

Christopher I McDermott

Center for Applied Geoscience, University of Tübingen, 72076 Tübingen, Germany

Ralph Mettier

Paul Scherrer Institut, Villigen PSI, Switzerland

Georg Kosakowski

Paul Scherrer Institut, Villigen PSI, Switzerland

Olaf Kolditz

Center for Applied Geoscience, University of Tübingen, 72076 Tübingen, Germany

Abstract

Quantification of mass and heat transport in fractured porous rocks is important to areas such as contaminant transport, storage and release in fractured rock aquifers, the migration and sorption of radioactive nuclides from waste depositories and the characterisation of engineered heat exchangers in the context of enhanced geothermal systems. The large difference in flow and transport characteristics between fractures and the surrounding matrix rock mean models of such systems are forced to make a number of simplifications. Analytical approaches assume a homogeneous system, numerical approaches address the scale at which a process is operating, but may loose individual important processes due to averaging considerations. Numerical stability criteria limit the contrasts possible in defining material properties. Here a hybrid analytical numerical method to modelling diffusive transport in fractured media is presented using the advantages of both approaches. The methodology is developed, verified for simple geometries and applied to experimental field data obtained from a shear zone in the Grimsel rock laboratory. The influence of heterogeneities in the fractured surfaces on issues such as channelling and retardation due to matrix diffusion are addressed.

Key words: fractured rock, diffusion, contaminant transport, heat transport, numerical modelling.

1 Introduction

[1] The experimental and numerical modelling of mass transport in fractured rocks is an area of investigation that has drawn significant attention over the last 20 to 30 years. In the fields where the combination of advective dominated transport in the rock fractures with diffusive dominated transport in the rock matrix surrounding the fractures is of particular importance, a number of approaches to deal with the complexity of solving the coupled partial differential equations describing the processes operating have been developed. Fields where such processes are relevant include contaminant transport, storage and release in fractured rock aquifers, the migration and sorption of radioactive nuclides from waste depositories and the characterisation of engineered heat exchangers in the context of enhanced geothermal systems.

[2] Over the years several key processes have been identified as having a significant or less significant effect on the mass flow and transport properties [*Jakob*, 2004]. The processes investigated numerically and experimentally include the influence of roughness on the fracture flow, e.g. [*Jakob*, 2004], channel flow [*Cornet, et al.*, 2003; *Sisavath, et al.*, 2003; *Chen, et al.*, 2004; *Zhang, et al.*, 2006], matrix diffusion [*Cornet, et al.*, 2003; *Sisavath, et al.*, 2003; *Chen, et al.*, 2004; *Zhang, et al.*, 2006] and reactive transport, e.g. [*DiDonato and Blunt*, 2004] in the context of both a simplified one dimensional idealised model of the fractured system, to increasingly large scale three dimensional complex networks of different populations of fractures. In general, two basic “end” concepts exist for the numerical modelling of fractured rocks: discrete fracture models, and continuum models. A

holistic approach combining the benefits of both of these approaches is to use a hybrid scale approach [*Helmig, et al.*, 2002], for instance the definition of geomechancial facies [*McDermott, et al.*, 2006]. The hybrid analytical numerical approach presented here provides a means of describing processes normally requiring a continuum approach and still allowing the discrete geometry of the fractures to be represented.

[3] At the analytical level simplified models have provided much insight into the key parameters and processes involved in defining the mass and heat transfer processes. A key example is the work of [*Tang, et al*., 1981] who provided a standard work on the mathematical description of the transport of a solute in a single fracture with matrix diffusion. However due to geometrical constraints, analytical models are only valid for a simplified investigation of processes [*Carrera, et al.*, 1998].

[4] To simulate complex *in situ* geometrical conditions of fracture networks, and the coupling of several processes, numerical techniques have to be applied. Simulating heat and mass transport in a fractured may be undertaken by several approaches, current trends are discussed in [*Neuman*, 2004]. Fracture surface heterogeneity or roughness [*Glover, et al.*, 1997, 1998; *Lewis and Schrefler*, 1998], coupled thermal -hydro-mechanical behaviour [*Witherspoon, et al.*, 1980; *Matsuki, et al.*, 2001; *Heiland*, 2003; *Neuzil*, 2003; *Rutqvist, et al.*, 2005; *McDermott and Kolditz*, 2006] and complex 3D geometry make the meaningful solution of these systems using analytical solutions impossible.

[5] On the other hand numerical simulations are complicated by the mathematical stability of the solution techniques, especially where large differences in material parameters are to be accounted for. Time dependent solution of advective and diffusive processes are controlled by different stability criteria, outlined for instance in [*Kolditz*, 1997]. When discretely modelling flow in fractured media, often the time step control of the diffusive processes is several orders of magnitude greater that that required for the stable solution of the advective transport, unless intricate and complex mesh refinement has been undertaken. Such mesh refinement leads to significantly increasing computational requirements, and consideration of grid adaptation algorithms, e.g. [*Haefner and Boy*, 2003]

[6] In this paper we present a hybrid numerical and analytical model, which uses the advantages of both numerical and analytical techniques to analyse flow, transport and the effects of matrix diffusion in a fracture plane from the Grimsel shear zone. For simplified fracture geometries the approach is validated against the PICNIC code, [*Barten and Robinson*, 2001].

[7] The fracture plane was characterised using detailed experimental data and geostatistically represented in terms of log normal distributions of aperture. The geometry of the fracture surface was represented discretely in the model and the advective transport solved using the finite element solver, GeoSys/RockFlow, [*Kolditz*, 2002]. The effect of the matrix diffusion was represented by an analytical solution, which provided the flux into or out of the matrix as a result of the previous transport history of the fracture. The flux into or out of the matrix at each of the mesh nodes defining the elements representing the fracture surface was linked to the advective flow via a source term.

[8] The analytical solution allow species dependent geometrical and physical parameters to be accounted for and may include linear sorption. The discrete representation of the fracture surface allows the effects of different fracture surface profiles to be investigated, e.g. the effects of increased channelling. The hybrid numerical and analytical approach, requiring only the fracture to be discretely defined geometrically, allowed problems to be solved with significantly less computational power than standard approaches where both the matrix and the fracture require geometrical definition.

2 Modelling approach

[9] Fluid flow can be described by the mass balance equation (1), [*Freeze and Cherry*, 1979]. To evaluate the fluid flow in the fractures we approximate the permeability of the fracture as a function of the fracture aperture via the cubic law (2) [*Witherspoon, et al.*, 1980]. The fracture is discretised into individual elements, an aperture is mapped to each element depending on the statistical distribution and generation used (Figure 1). (1) is given in terms of the head of the fluid, and therefore the intrinsic permeability is converted into the hydraulic conductivity by (3)

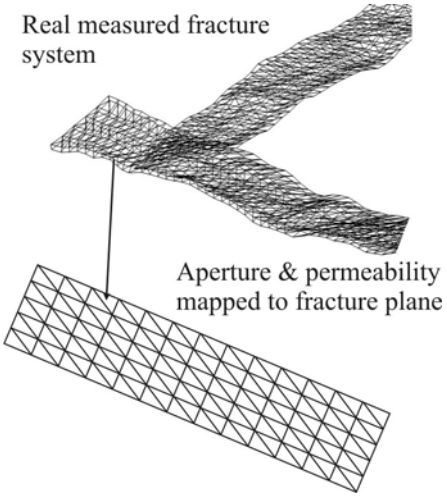

Figure 1. Geostatistical aperture distribution mapped to fracture plane.

$$S\frac{dh}{dt} - K\,\mathrm{grad}\,h = Q \tag{1}$$

$$k_f = \frac{e^2}{12} \tag{2}$$

$$K = \frac{k_f \mu}{\sigma g} \tag{3}$$

[10] The solution of (1) using the finite element technique is covered in standard works such as [*Istok*, 1989; *Lewis and Schrefler*, 1998; *Kolditz*, 2002; *Zienkiewicz and Taylor*, 2005]. Solving (1) provides the fluid head at each discrete node in the finite element model which then can be interpolated for the elements and converted into flow velocities v (m/s) via (4) in the elements.

$$v_{(x,y,z)} = K\,\mathrm{grad}\,h_{(x,y,z)} \tag{4}$$

[11] The flow velocities are then used to derive the solution of the mass transport equation (5) or heat transport equation (6) [*Istok*, 1989; *Lewis and Schrefler*, 1998; *Kolditz*, 2002; *Zienkiewicz and Taylor*, 2005].

$$\frac{dC}{dt} = D\nabla^2 C - v\cdot\nabla C - C_s \tag{5}$$

$$c\rho\frac{dT}{dt} = D\nabla^2 T - c^w\rho^w v\cdot\nabla T - T_s \tag{6}$$

[12] Flow in fractured rock is characterised by advective dominated transport in the fractures and diffusive dominated transport in the matrix. To ensure the stability of the numerical solution of (1) and (5) the Courant (7) and Neumann (8) mesh stability criteria have to be observed [*Kolditz*, 1997]. The velocity of advective transport dominates the courant number, and the diffusion coefficient dominates the Neumann number. In fractures the advective velocity is several orders of magnitude larger than the matrix diffusion coefficients for typical contaminants. To solve this problems the mesh can be refined parallel to the diffusive flow [*Kolditz and Clauser*, 1998], this however leads to intensive computational requirements. In this paper the advective transport is solved numerically allowing the complicated geometry of the fracture surfaces to be reproduced, but the matrix diffusion is solved analytically and included in (5) and (6) via the source term.

$$Cr = \left|\frac{v\Delta t}{\Delta l}\right| \le 1 \tag{7}$$

$$\frac{D}{\Delta l^2}\Delta t \le \frac{1}{2} \tag{8}$$

[13] Assuming that the diffusive flux from a fracture is normal to the direction of advective flow, the diffusion profile can be represented by the second order unsteady state diffusion equation, Fick's second law (9). Here the coordinate direction z is the normal to the irregular fracture plane at a node position (x,y) (Figure 2). The standard solution to this equation for a concentration at a time t and distance z from the source is (11) [*Fetter*, 1993]. Here note the similarity to heat transport (10). The formulation is developed for the diffusion of a material, however later the application to heat transport is presented.

$$\frac{dC}{dt} = \frac{d^2C}{dz^2} \tag{9}$$

$$\frac{dT}{dt} = \frac{d^2T}{dz^2} \tag{10}$$

$$C(z,t) = C_o erfc\left[\frac{z}{2\sqrt{Dt}}\right] \tag{11}$$

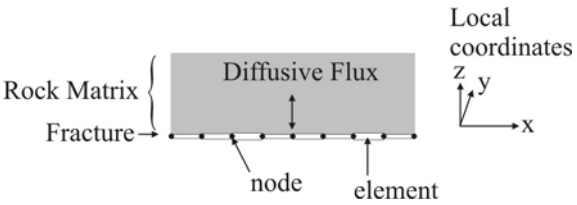

Figure 2. Local coordinate system for matrix diffusion.

[14] Following [*Häfner, et al.*, 1992] by superimposition of a time dependent pulses it is possible to write (12) which gives the concentration profile at the current time t, for a pulse of concentration C_{t0} starting at time t_0 and ending at a time t_1 where $t > t_1 > t_0$. Generalising this for n pulses gives (13)

$$C(z,t) = C_{t_0} erfc\left[\frac{z}{2\sqrt{D(t-t_0)}}\right] - C_{t1} erfc\left[\frac{z}{2\sqrt{\sqrt{D(t-t_1)}}}\right] \tag{12}$$

$$C(z,t) = \sum_{2}^{n}\left\{C_{t_n} erfc\left[\frac{z}{2\sqrt{D(t_0-t_n)}}\right] - C_{t_{n-1}} erfc\left[\frac{z}{2\sqrt{D(t_0-t_{n-1})}}\right]\right\} + C_{t_0} erfc\left[\frac{z}{2\sqrt{D(t-t_1)}}\right] \tag{13}$$

[15] The source term C_s represents a flux into or out of the rock matrix. The flux can be defined by Fick's first law of diffusion (14). The term $\frac{dC}{dz}$ is found first by partially differentiating (11) with respect to z, giving (15)

$$F = -D\frac{dC}{dz}A \tag{14}$$

$$\frac{\partial C(z,t)}{\partial z} = -C'\frac{2}{\sqrt{\pi}}\exp\left[\frac{z^2}{4D(t-t')}\right]\frac{1}{\sqrt{4D(t-t')}} \tag{15}$$

[16] The flux into and out of the matrix is governed by the gradient at the contact of the fluid in the fracture with the matrix. Therefore (15) can be simplified by considering the coordinate $z = 0$, i.e. the

contact. Substituting this result in (13) allows the term $\frac{dC}{dt}$ from (14) to be evaluated as (16) and so the source term C_s per node for the diffusive flux to be defined. Here n is the number of time steps prior to the current time step to be taken into account

$$\frac{\partial C(z=0,t)}{\partial z} = \frac{dC}{dz} = \sum_2^n \left\{ \frac{C_{n-1}}{\sqrt{\pi D\left(t_0 - t_{n-1}\right)}} - \frac{C_n}{\sqrt{\pi D\left(t_0 - t_n\right)}} \right\} + \frac{C_0}{\sqrt{\pi D\left(t_0 - t_1\right)}} \qquad (16)$$

[17] The definition of the diffusive term D and the transformation of the flux into a source term in the respective units of the balance equation being solved requires constitutive properties. For linear sorption (17) defines the apparent diffusion coefficient for transient conditions in the matrix [*Grathwohl*, 1998]. For non-sorbing species D becomes (19). For the calculation of non-linear sorption the depth dependent concentration of the required species in the wall required. This is possible deriving from (13) but beyond the current scope of this work, and combined with more intensive computational requirements.

$$D_a = \frac{D_{aq}\varepsilon_e}{\left(\varepsilon_e + K_d\rho\right)\tau_f} \qquad (17)$$

$$\tau_f = \frac{\varepsilon_e}{\left(\varepsilon_e\right)^{-2}} \qquad (18)$$

$$D_e = D_{aq}\varepsilon_e \qquad (19)$$

$$D = \frac{\kappa}{\rho c} \qquad (20)$$

[18] Following common notation, the term $\left(\varepsilon_e + K_d\rho\right)\tau_f$ can be described as a capacitance factor α. If no dead end or blind pores are assumed then a pore retardation factor can be defined as

$$R_p = \frac{\alpha}{\varepsilon_e} = 1 + K_d\frac{\rho}{\varepsilon_e} \qquad (21)$$

[19] In comparison the heat diffusion tensor is given by (20) and there is no sorptive consideration necessary. Substituting the appropriate value of D into (16), combining with (14) and assuming steady state conditions for the duration of the time step Δt gives (21) for mass transport. For heat transport (21) is multiplied by ρc of the porous media to give the energy sink or source.

$$C_s = \left[\begin{array}{l} \sum_2^n \left[C_{n-1}\,erfc\left(\frac{x}{2\sqrt{D_a\left(t_0 - t_{n-1}\right)}} \right) - C_n\,erfc\left(\frac{x}{2\sqrt{D_a\left(t_0 - t_n\right)}} \right) \right] \\ + C_0\,erfc\left(\frac{x}{2\sqrt{D_a\left(t_0 - t_1\right)}} \right) \end{array} \right] 2AD_e \qquad (22)$$

[20] As only the advective stability criteria dominates the solution of the fracture flow, the Neumann criteria in the matrix discussed above can be neglected. However, one further stability criteria needs to be taken into account, known as the “well criteria”. This is related to the source terms and expresses the fact that a source term may not take more mass, or energy from a node in the fracture than is present in a time step. Looking at (16), this conditions may occur when the concentration gradient at the wall of the fracture is large (particularly the case for sorbing species, where D is then of the order of 10-11m/s²). For the case where a fracture plane is represented by mapped permeability elements, the amount of mass assigned to the individual nodes is related to the aperture of the fracture elements surrounding it (volume) and the concentration present. The well

stability criteria can be expressed as (22) where the change in mass of a substance in a time step can not be greater than the amount of mass present. A similar expression can be derived for heat energy.

$$\frac{C_s \Delta t}{C \Delta z \Delta y \Delta x} = \frac{\Delta Mass}{Mass} \leq 1 \tag{23}$$

[21] For a fracture the volume represented by a node is dependent on the aperture of the fracture. The smaller the aperture of the fracture, the smaller the amount of mass actually present in that part of the fracture, and therefore the smaller the amount of mass is which is available to be removed in a certain time step. Based on (22) it is possible to calculate the time step stability limits as a function of the fracture aperture. From (21) allowing a slug of normalised concentration (most extreme gradient) to enter the fracture, we see that the flux for the first time step is given by (23). Therefore combining (22) and (23), noting that for the given example $\Delta y \Delta x = A$ and $C = 1$, the expression for the maximum allowable time step under the steepest concentration gradient conditions is given by

$$F_m = \frac{2AD_e}{\sqrt{\pi D_a \Delta t}} \tag{24}$$

$$c \Delta t_m \leq e^2 \tag{25}$$

where

$$c = \frac{4D_e^{\,2}}{\pi D_a} \tag{26}$$

[22] For conservative tracers $D_e = D_a$ and $c = \frac{4D_e}{\pi}$. Consequently (24) means the smaller the fracture aperture (less material) the smaller the time step can be. In our simulations we restricted the smallest aperture to $10 \mu m$ (RALPH?) of the same order of magnitude as what was measurable.

[23] Observing (21) one can see that information is required for the concentration (or temperature) for every single time step and node to derive the solution. For large fracture networks and long term tests several thousand time steps may be employed in modelling. As the time difference between the current time and the pulse history increases so the influence of the older pulses becomes less significant. Additionally the resolution of the pulse history does not necessarily have to be the same as the time step, rather the main features of the pulse need to be captured. To allow for increased computational efficiency it was found that time step history could be averaged over several time steps without effecting the integrity of the results, as long as the characteristics of the pulse were captured. In terms of implementation we introduced a resolution, indicting that the concentration at a node should only be sampled at every n^{th} time step.

3 Verification

[24] The transport of a diffusive substance through fractured rock has been the subject of many years of investigation. Much investment into research has been applied in the assement of radionuclide migration. For Swiss saftey assessment a transport code based on analytical solutions and tested against several standard litterature analytical solutions, PICNIC (PSI/QuantiSci Interactive Code for Networks of Interconnected Channels) [*Barten and Robinson*, 2001] was used to verify the results of the hybrid analytical and nummerical approach. Figure. 3 illustrates the comparison and agreement of the the two codes, for purely advective transport and for advective transport with matrix diffusion in each case for a simplified fracture based on the experimetnally investigated fracture at Grimsel. The input parameters are presented in table 1.

Table 1: Geometry and material properties for the simulations.

Symbol	Description	Value
L [m]	Distance between boundary and observation points	2.5
α_T [m]	trans. dispersion (Rockflow only)	-
ρ [kg m^{-3}]	bulk matrix density	2670
2b [m]	fracture aperture	0.55×10^{-3}
v [m s^{-1}]	fluid velocity	7.05×10^{-4}
α_L [m]	long. dispersion (Rockflow only)	0.1
Pe [-]	Peclet number (Picnic only)	25
ε_p [-]	matrix porosity	0.3
D_p [m^2 s^{-1}]	diffusion constant in rock matrix	7.4×10^{-11}

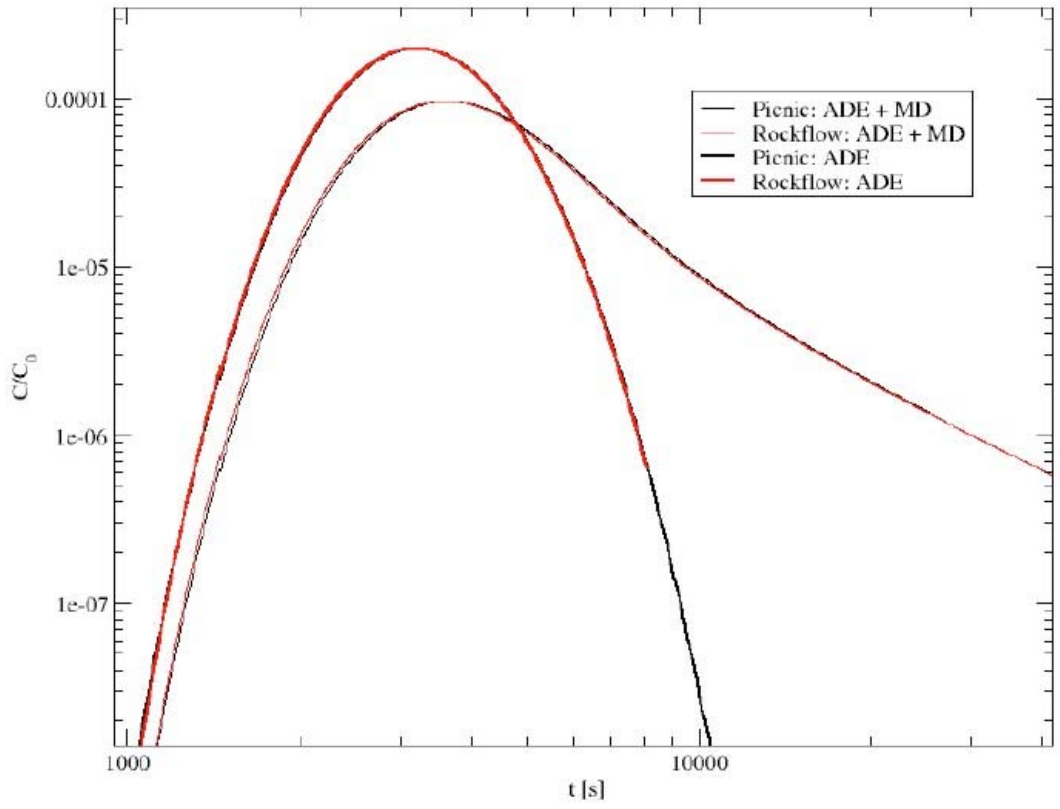

Figureure 3. Picnic vs GS/RF

4 Application

[25] The hybrid analytical numerical solution can now be applied to more complicated descrete fracture geometries than both analytical solutions and numerical codes can handle. Using a geostatistical representation of the fracture apertures based on real experimental data from a 5.2m

section of a shear zone at the Grimsel site [*Mettier, et al.*, 2005 submitted] (Mettier et al, 2006) the flow and mass transport of the fracture system can be analysed. The shear zone comprises several discretely identifiable fracture planes, the numerical meshing of which is discussed in [*Kalbacher, et al.*, 2006]. From a scale perspective, the macro scale provides the three dimensional representation of the 2D plane in 3D space (may include several interconnected fractures). Large scale features of geometry and the interconnectivity of the fractures in the fracture network can thus be easily represented. At the micro scale different fracture apertures are mapped to material properties of individual triangular finite elements. To demonstrate the current approach, a single fracture plane is selected from this data set, the basic geometry consists of a single planar, rectangular, two dimensional fracture of 5.2 meters length, and 0.5 meters width, located in three dimensional space with mapped appertures. The fracture is discretized into 5916 identical triangular elements, with 3150 nodes.

[26] The mapping of the element apertures is based on measurements performed on digital images of a fracture network in granodiorite, extracted from a shear zone in the Swiss Alps (Mettier et al, 2006). Overall, the apertures show a log-normal distribution, with a median aperture of 10^{-4} meters. The spatial distribution is determined by a geostatistical model variogram, consisting of two overlaying spherical models. The original model variogram was fitted to the aperture data and describes the underlying normal distribution of the log-apertures. Using the same model variogram, and sequential Gaussian simulation, any number of equivalent aperture distributions can be mapped to the triangular mesh of any studied fracture.

[27] The original parameters, obtained from the experimentally investigated rock fracture network show a variance of the underlying normal distribution of 0.9, which results in a considerable degree of small scale heterogeneity in the fracture. Representing such a high variance requires the inclusion of extreme end members, and therefore problems with the well criteria (25) were encountered for very small apertures. Here we note that the extremely small aperture fractures carry a minimum percentage of the total mass present, and therefore a range of smaller variances were chosen as the governing factor for the different model scenarios whereby the main features of the fracture plains could be investigated (0.01; 0.02; 0.04; 0.1; 0.2). Twenty realisations of the aperture distribution were generated and mapped to the discretised fracture for each variance. It is important to note that while the mean of the normal log-aperture distribution is constant at -4 and thus the median of the generated log-normal aperture distribution is also constant at 10^{-4}, the mean, or arithmetic medium of the apertures is not.

[28] The hydraulic boundary conditions were set so that flow occurred along the 5.2m length of the fracture. The upper boundary, deemed the “outflow edge” of the fracture, was set as constant zero hydraulic head, and the “inflow edge” of the fracture was given a combined constant hydraulic flow of 7e-8 m^3/s, as per field conditions. These simple boundary conditions ensure a static hydraulic flux from the bottom of the fracture to the top. Tracer mass is injected as a 50 sec pulse of constant mass flux at a line parallel to the hydraulic inflow boundary and 3 cm into the model. The hydraulic inflow edge is set to a constant zero mass tracer concentration. The hydraulic outflow edge was left to default as a zero gradient mass transport boundary. For the sake of demonstrating the modelling approach, the mass transport curves were recorded across a control plane in the middle of the fracture to ensure comparison to the analytical solutions in PICNIC where infinite fracture regimes are used in the solution of the differential equations.

[29] The possibility to stack and average breakthrough curves representing the same volume of total flux for the multiple realisations of a common variance is a prerequisite for a sound Monte Carlo approach to the investigation of the effects of the heterogeneous distribution of apertures. The combination of avoiding edge effects of the outflow boundaries, and equal flux at the inflow boundaries, allows for direct comparisons between the breakthrough curves obtained from the different statistical realisations with the analytical approximations from PICNIC, even allowing for the non-linear influence of MD. The numerically simpler method of setting a constant hydraulic head for all realisations leads to variations in total mass flux, as well as velocities. Due to the non-linear aspect of MD, rescaling to equal fluxes is not possible, thus invalidating any concept of mean velocity, or average breakthrough curve.

[30] In order to study the influence of the small scale heterogeneities in comparison to the known retarding effect of Matrix Diffusion [*Jakob*, 2004], we performed the exact same realisations twice,

once with and once without the analytical solution for Matrix Diffusion (MD) enabled in RF/GeoSys. The parameters used for MD are based on experimental data, obtained during the Colloid Retention and Retardation (CRR) project, also performed at the Grimsel Test Site, by Nagra. The same parameters were used previously to fit the breakthrough curves from CRR with Continuous Time Random Walks (CTRW) based models (Kosakowski & Smith, 2003), and are shown in table 2.

	Diffusion Constant in Rock Matrix (?-De, or Da)	Matrix Porosity	Sorption Coefficient in Rock matrix	Tortuosity	Rock Matrix Density
Value	7.4e-11	0.3	1.0	1.0	2760

Table 2: Parameters used to semi-analytically calculate the influence of Matrix Diffusion on the mass transport in the fracture.

[31] [*Zhang, et al.,* 2006] discuss the use of a single effective matrix diffusion coefficient to predict breakthrough curves in a fractured formation. Here we apply a similar approach and compare the breakthrough curves predicted by the hybrid model application with the analytical fitting of PICNIC, which assumes a single effective matrix diffusion coefficient. That is we generate numerically the breakthrough curves based on a discrete fracture geometry, and then fit these breakthrough curves with analytical solutions. To compare the breakthrough curves we use a flux weighted concentration across the control plane.

5 Results and discussion

[32] Figure. 4 illustrates a group of realisations, at the same timestep, with identical boundary conditions, but with differing underlying log-aperture variances. Generally high variance results in more pronounced channelling. High variance realisations which do not show preferential flow paths are conceivable, but are less probable than realisations with preferential flow paths. Fracture planes with the same underlying log-aperture variance can also show strong differences in channelling and spreading of the tracer cloud, depending on the underlying structure in the apperture distributions. The variation within a group is correlated with the log-aperture variance of the group.

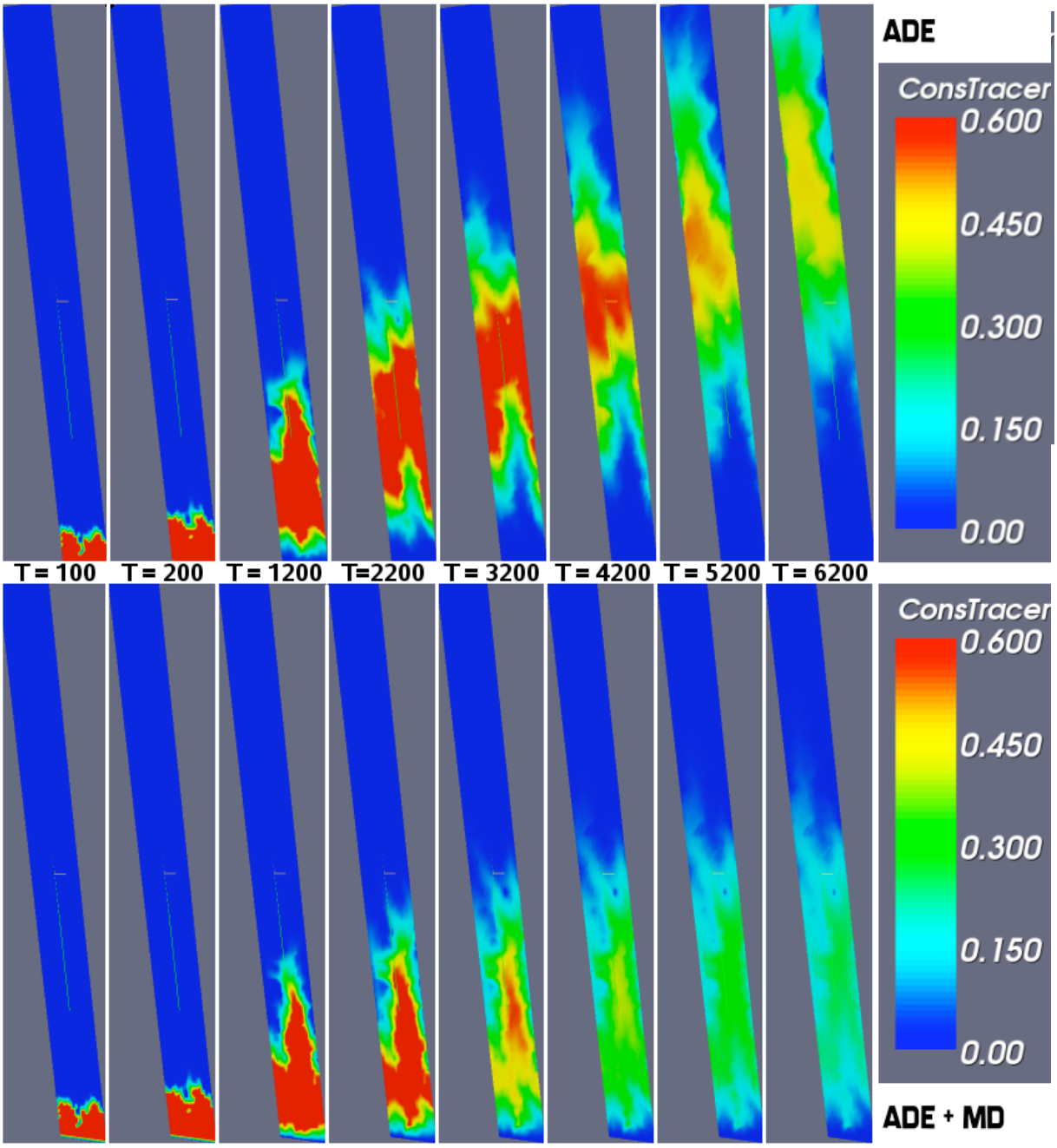

Figureure 4: Time series of a tracer cloud moving through one realisation of the fracture, without (top) and with (bottom) matrix diffusion. The retardation effect is clearly visible at later time steps, as is the overall lower amount of tracer mass in the fracture, due to some of the mass being held in the matrix.

[33] The diffusive flux into and out of the matrix is dependent on the area available to flux and volume of the local fracture aperture, the contact time and the concentration in the fracture. The cumulative effect of these factors is a non-linear retardation of the overall movement of the tracer cloud. Figure. 5 compares advective dispersive mass transport in the fracture against the same system with matrix diffusion.

[34] The resulting representative breakthrough curves were then fitted with analytical solutions. For the ADE cases, we used the Ogata-Banks solution (Bear, 1972). For the ADE+MD cases, the fits were determined using PICNIC. The resulting fitting parameters are displayed in table 2.

		var = 0.01	*var = 0.02*	*var = 0.04*	*var = 0.10*	*var = 0.20*
ADE	V_{fit} (m/s)	6.74e-4	6.63e-4	6.26e-4	5.17e-4	3.91e-4
	D_{fit} (m^2/s)	6.92e-5	7.34e-5	7.38e-5	8.93e-5	7.50e-5
	V_{mean} (m/s)	6.89e-4	6.79e-4	6.56e-4	5.75e-4	4.77e-4
ADE + MD	V_{fit} (m/s)	6.85e-4	6.75e-4	6.44e-4	5.55e-4	4.10e-4
	D_{fit} (m^2/s)	8.10e-5	8.80e-5	8.85e-5	9.50e-5	7.00e-5
	b_{fit} (m)	0.98e-4	0.99e-4	1.04e-4	1.24e-4	1.90e-4
	p	0.3	0.3	0.3	0.3	0.3
	dM (m^2/s)	7.4e-11	7.4e-11	7.4e-11	7.4e-11	7.4e-11
	V_{mean} (m/s)	6.96e-4	6.90e-4	6.78e-4	6.14e-4	5.09e-4
Geom	Aperture(m)	1.022e-4	1.048e-4	1.105e-4	1.290e-4	1.708e-4
	V_{hyd} (m/s)	6.85e-4	6.68e-4	6.33e-4	5.43e-4	4.10e-4

Table 2: The parameters for the analytical curves fit to the measured breakthrough curves for the heterogeneous models. For ADE, V_{fit} and D_{fit} are the velocity and dispersivity obtained by fitting with the Ogata-Banks solution, using xmgrace. V_{mean} is the mean element velocity weighted by mass.
For ADE + MD, V_{fit} is the velocity, D_{fit} is the dispersivity, and b the fitted fracture homogeneous fracture aperture. porosity p and diffusion constant into the matrix dM were held fixed at the shown values. V_{mean} is again the mean element velocity weighted for mass which transverse each element.
The Geom. section shows the actual mean apertures taken from the model files, and the hydraulic velocity calculated from this aperture and the known hydraulic flux.

[35] In order to further compare the velocities, actual mean element velocities from the model files were also calculated. In order to be comparable, they must be weighted by the traversed mass for each element. For this weighting to be meaningful, only the data from time steps prior to 4200seconds can be used, as this is the determined time where the earliest outflow from the model must be considered. After this time, mass from the fastest sections has already left the model, thus skewing the weighting.

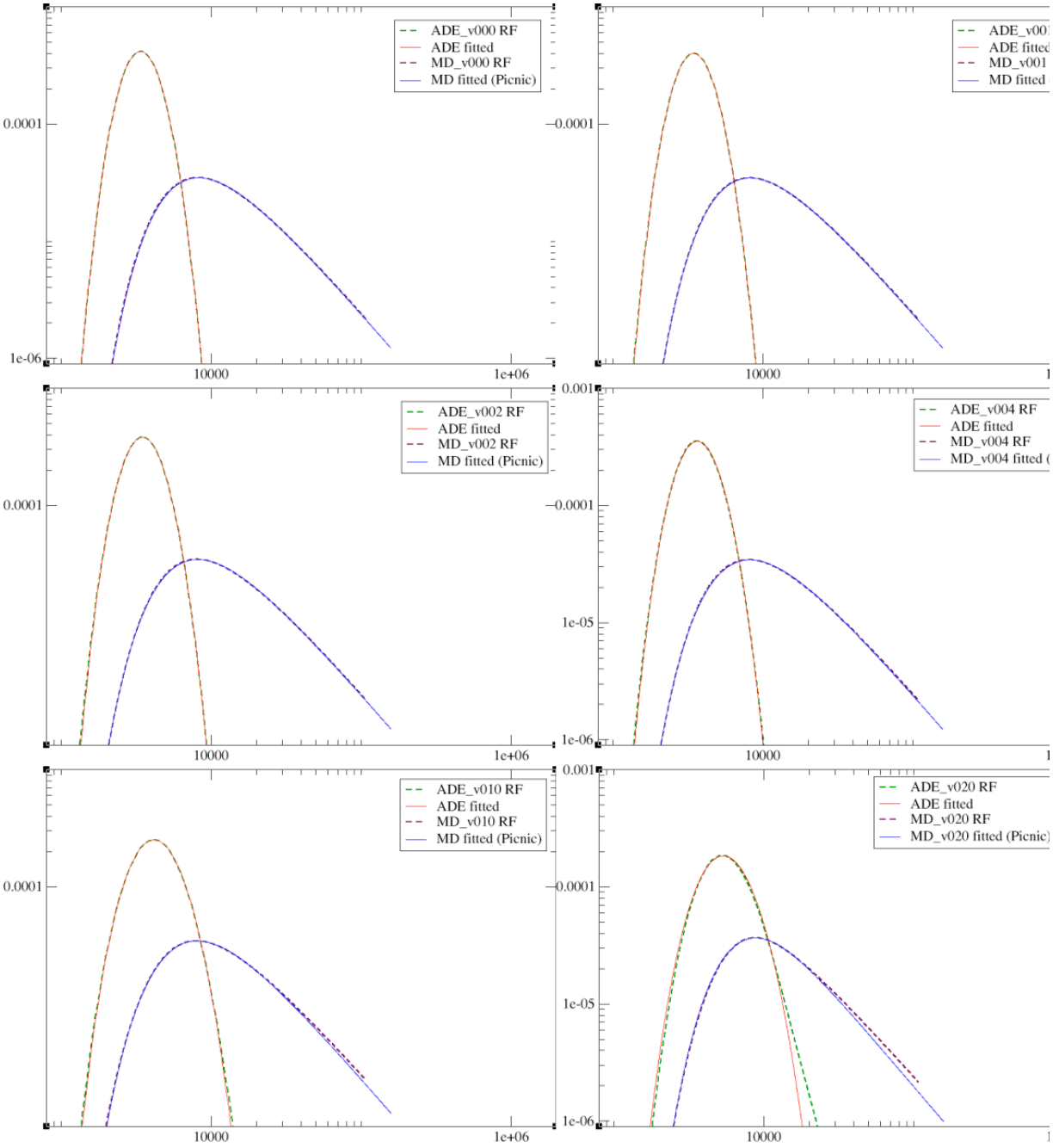

Figure 5: Breakthrough curves for the model groups with heterogeneous fracture apertures. Best fitting analytical curves are also shown. Log-log scales, time axis is in seconds, concentration axes normalized.

[36] The fits to the modelled breakthrough curves are excellent for the variance models (var = 0.01 – 0.04). As the variance increases so the use of effective parameters becomes less valid. The analytical solutions (assumption of a homogeneous fracture model) cannot adequately fit early arrivals due to channelling or late arrival tailing of the modelled curve, both interpreted as the influence of the heterogeneity. The obtained parameters will therefore not reflect the actual properties of the models and may lead to wrong long term predictions.

6 Conclusions

[37] A new hybrid analytical and numerical modelling technique is presented which combines the advantages of both approaches to modelling mass transport in complicated heterogeneous fracture

geometries. The numerical model solves discretely flow and mass transport in the fracture and the analytical model represents the continuum based matrix diffusion processes.

[38] The diffusive numerical Neumann stability criteria can be neglected, the advective flow in the fractured rock and a source term stability condition define the limits of the numerical solution. This allows the discrete features of the fractures to be represented numerically, and the diffusive flux in and out of the matrix to be included without the necessity of the three dimensional mesh representation of the matrix and the accompanying intensive computational demands.

[39] The analytical solution for matrix diffusion is developed for mass transport of contaminants, and can be applied to both conservative and linearly sorbing species. The application of the same solution to heat transport is also illustrated. The solution procedure is verified against standard analytical solutions for simple fracture matrix geometries.

[40] Applying real field data several geostatistical representations of a Grimsel shear zone are analysed for flow and mass transport. The effect of increasing variance (related to roughness) on the flow and mass transport are investigated, and the appropriateness of applying simple analytical solutions (homogenous fracture solutions) to real fracture systems and the analysis of experimental data. The results of the comparison of modelled fracture systems and fitted systems in terms of the effect of an assumption of a homogeneous fracture compare well with other recently published work.

[41] The discrete analysis of the fracture surfaces allows species and porosity variations to be modelled individually rather than requiring the introduction of unknown effective parameters. Currently the matrix diffusion term assumes an unlimited depth of penetration in the matrix blocks. However further development of the analytical solution will allow different scenarios to be addressed.

[42] The hybrid analytical numerical technique provides a powerful tool for this investigation of complicated fracture systems and the interaction of several coupled processes.

7 Acknowledgements

The authors gratefully acknowledge the German Science Foundation (Deutsche Forschungsgemeinschaft) for funding of this work (MC 113/1-5).

8 References

Barten, W., and P. C. Robinson (2001), Contaminant Transport in Fracture Networks with Heterogenous Rock Matrices: The PICNIC code, 371 pp, PSI Report Nr. 01-02, February 2001, ISSN 1019-0643.

Carrera, J., et al. (1998), On matrix diffusion: formulations, solution methods and qualitative effects., *Hydrogeology Journal*, *6*, 178-190.

Chen, C. Y., et al. (2004), Experimental study of liquid-gas flow structure effects on relative permeabilities in a fracture, *Water Resources Research*, *40*, W083011-W0830115.

Cornet, F. H., et al. (2003), The hydromechanical behaviour of a fracture; an in situ experimental case study, *International Journal of Rock Mechanics and Mining Sciences*, *40*, 1257-1270.

DiDonato, G., and M. J. Blunt (2004), Streamline-based dual-porosity simulation of reactive transport and flow in fractured reservoirs., *Water Resources Research*, *40*.

Fetter, C. W. (1993), *Contaminant hydrogeology*, 458 pp., Prentice-Hall International.

Freeze, R. A., and J. A. Cherry (1979), *Groundwater*, Prentice Hall, Englewood Cliffs, NJ 07632.

Glover, P. W. J., et al. (1997), Fluid flow in fractally rough synthetic fractures, *Geophys. Res. Lett.*, *24*, 1803 - 1806.

Glover, P. W. J., et al. (1998), Synthetic rough fractures in rocks, *J. Geophys. Res.*, *103*, 9609 - 9620.

Grathwohl, P. (1998), *Diffusion in natural porous media: Contaminant Transport, Sorption/Desorption and Dissolution Kinetics*, Kluwer Academic Publishers.

Haefner, F., and S. Boy (2003), Fast transport simulation with an adaptive grid refinement, *Ground Water*, *41*, 273-279.

Häfner, F., et al. (1992), *Wärme- und Stofftransport - Mathematische Methoden*, Springer Verlag, Berlin - Heidelberg - New York.

Heiland, J. (2003), Laboratory testing of coupled hydro-mechanical processes during rock deformation, *Hydrogeology Journal*, *11*, 122-141.

Helmig, R., et al. (2002), Upscaling of two-phase flow processes in heterogeneous porous media: Determination of constitutive relationships, *IAHS AISH Publication*, *277*, 28-36.

Istok, J. (1989), *Groundwater Modeling by the Finite Element Method*, American Geophysical Union, 2000 Florida Avenue, NW, Washington, DC 20009.

Jakob, A. (2004), Matrix diffusion for performance assessment - experimental evidence, modelling assumptions and open issues., 75 pp, Paul Scherrer Institute.

Kalbacher, T., et al. (2006), Geometric modelling and object orientated software concepts applied to a heterogeneous fractured network from the Grimsel rock laboratory., *Computational Geosciences, (accepted)*.

Kolditz, O. (1997), *Strömung, Stoff- und Wärmetransport im Kluftgestein*, Bortraeger Verlag, Berlin-Stuttgart.

Kolditz, O. (2002), *Computational Methods in Environmental Fluid Mechanics*, Springer-Verlag Berlin Heidelberg New York.

Kolditz, O., and C. Clauser (1998), Numerical simulation of flow and heat transfer in fractured crystalline rocks: Application to the hot dry rock site in Rosemanowes (U.K.), *Geothermics*, *27*, 1-23.

Lewis, R. W., and B. A. Schrefler (1998), *The Finite Element Method in the Static and Dynamic Deformation and Consolidation of Porous Media*, 2 ed., 508 pp., John Wiley & Sons.

Matsuki, K., et al. (2001), Time-dependent closure of a fracture with rough surfaces under constant normal stress, *International Journal of Rock Mechanics and Mining Sciences*, *38*, 607-619.

McDermott, C. I., and O. Kolditz (2006), Geomechanical model for fracture deformation under hydraulic, mechanical and thermal loads., *Hydrogeology Journal*, *14*, 487-498.

McDermott, C. I., et al. (2006), Investigation of Coupled Hydraulic-Geomechanical Processes at the KTB site: Pressure dependent characteristics of a long term pump test and elastic interpretation using a geomechanical facies model, *Geofluids*, *6*, 67-81.

Mettier, R., et al. (2005 submitted), Influence of small scale heterogenieties on contaminant transport in fractured crystalline rock, *Ground Water*.

Neuman, S. P. (2004), Trends, prospects and challenges in quantifying flow and transport through fractured rocks, *Hydrogeology Journal*, *13*, 124-147.

Neuzil, C. E. (2003), Hydromechanical coupling in geologic processes, *Hydrogeology Journal, 11*, 41-83.

Rutqvist, J., et al. (2005), A numerical study of THM effects on the near-field safety of a hypothetical nuclear waste repository--BMT1 of the DECOVALEX III project. Part 3: Effects of THM coupling in sparsely fractured rocks, *International Journal of Rock Mechanics and Mining Sciences, 42,* 745.

Sisavath, S., et al. (2003), A Simple Model for Deviations from the Cubic Law for a Fracture Undergoing Dilation or Closure, *Pure and Applied Geophysics, 160,* 1009 - 1022.

Tang, D. H., et al. (1981), Contaminant transport in fractured porous media; analytical solution for a single fracture, *Water Resources Research*, *17*, 555-564.

Witherspoon, P. A., et al. (1980), Validity of cubic law for fluid flow in deformable rock fracture., *Water Resour. Res.*, *16*, 1016-1024.

Zhang, Y., et al. (2006), Effects of diffusive property heterogeneity on effective matrix diffusion coefficient for fractured rock, *Water Resour. Res.*, *42*, 1-8.

Zienkiewicz, O. C., and R. L. Taylor (2005), *The Finite Element Method*, 6 ed., 752 pp., Butterworth Heinemann.